SSC–375

UNCERTAINTY IN STRENGTH MODELS FOR MARINE STRUCTURES
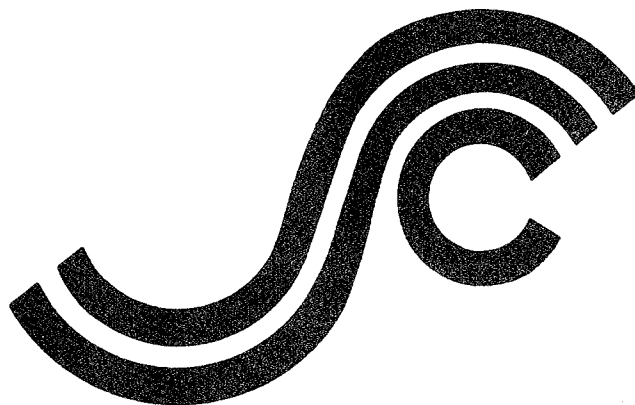
19950306 036

DTIC
ELECTE
MAR 0 9 1995
S   D
B
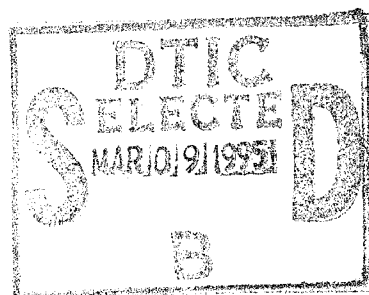
SHIP STRUCTURE COMMITTEE

1994

SHIP STRUCTURE COMMITTEE

The SHIP STRUCTURE COMMITTEE is constituted to prosecute a research program to improve the hull structures of ships and other marine structures by an extension of knowledge pertaining to design, materials, and methods of construction.

RADM J. C. Card, USCG (Chairman)
Chief, Office of Marine Safety, Security
 and Environmental Protection
U. S. Coast Guard

Mr. Thomas H. Peirce
Marine Research and Development
 Coordinator
Transportation Development Center
Transport Canada

Mr. H. T. Haller
Associate Administrator for Ship–
 building and Ship Operations
Maritime Administration

Dr. Donald Liu
Senior Vice President
American Bureau of Shipping

Mr. Alexander Malakhoff
Director, Structural Integrity
 Subgroup (SEA 03P)
Naval Sea Systems Command

Mr. Thomas W. Allen
Engineering Officer (N7)
Military Sealift Command

Mr. Warren Nethercote
Head, Hydronautics Section
Defence Research Establishment–Atlantic

EXECUTIVE DIRECTOR

CDR Stephen E. Sharpe, USCG
U. S. Coast Guard

CONTRACTING OFFICER TECHNICAL REPRESENTATIVE

Mr. William J. Siekierka
Naval Sea Systems Command

SHIP STRUCTURE SUBCOMMITTEE

The SHIP STRUCTURE SUBCOMMITTEE acts for the Ship Structure Committee on technical matters by providing technical coordination for determinating the goals and objectives of the program and by evaluating and interpreting the results in terms of structural design, construction, and operation.

MILITARY SEALIFT COMMAND

Mr. Robert E. Van Jones (Chairman)
Mr. Rickard A. Anderson
Mr. Michael W. Touma
Mr. Jeffrey E. Beach

MARITIME ADMINISTRATION

Mr. Frederick Seibold
Mr. Norman O. Hammer
Mr. Chao H. Lin
Dr. Walter M. Maclean

U. S. COAST GUARD

CAPT G. D. Marsh
CAPT W. E. Colburn, Jr.
Mr. Rubin Scheinberg
Mr. H. Paul Cojeen

AMERICAN BUREAU OF SHIPPING

Mr. Stephen G. Arntson
Mr. John F. Conlon
Mr. Phillip G. Rynn
Mr. William Hanzelek

NAVAL SEA SYSTEMS COMMAND

Mr. W. Thomas Packard
Mr. Charles L. Null
Mr. Edward Kadala
Mr. Allen H. Engle

TRANSPORT CANADA

Mr. John Grinstead
Mr. Ian Bayly
Mr. David L. Stocks
Mr. Peter Timonin

DEFENCE RESEARCH ESTABLISHMENT ATLANTIC

Dr. Neil Pegg
LCDR D. O'Reilly
Dr. Roger Hollingshead
Mr. John Porter

SHIP STRUCTURE SUBCOMMITTEE LIAISON MEMBERS

U. S. COAST GUARD ACADEMY

LCDR Bruce R. Mustain

U. S. MERCHANT MARINE ACADEMY

Dr. C. B. Kim

U. S. NAVAL ACADEMY

Dr. Ramswar Bhattacharyya

CANADA CENTRE FOR MINERALS AND ENERGY TECHNOLOGIES
Dr. William R. Tyson

SOCIETY OF NAVAL ARCHITECTS AND MARINE ENGINEERS
Dr. William Sandberg

U. S. TECHNICAL ADIVSORY GROUP TO THE INTERNATIONAL STANDARDS ORGANIZATION
CAPT Charles Piersall

NATIONAL ACADEMY OF SCIENCES – MARINE BOARD
Dr. Robert Sielski

NATIONAL ACADEMY OF SCIENCES – COMMITTEE ON MARINE STRUCTURES
Mr. Peter M. Palermo

WELDING RESEARCH COUNCIL

Dr. Martin Prager

AMERICAN IRON AND STEEL INSTITUTE

Mr. Alexander D. Wilson

OFFICE OF NAVAL RESEARCH

Dr. Yapa D. S. Rajapaske

STUDENT MEMBER

Mr. Trevor Butler
Memorial University of Newfoundland

**Ship
Structure
Committee**

An Interagency Advisory Committee

SSC-375
SR-1338

31 October, 1994

UNCERTAINTY IN STRENGTH MODELS FOR MARINE STRUCTURES

This project is the fourth of a continuing series of Ship Structure Committee projects directed towards developing probabilistic design strategies for ship structures. These methods provide a more rational basis for design than the current deterministic methods. In order to develop these reliability based methods the uncertainties in each portion of the design equation must be quantified. This project develops a method to quantify the uncertainties in strength capacities of structures. It closely complements the earlier work in SSC-363 "Uncertainties in Stress Analysis on Marine Structures" and SSC-373 "Probability Based Ship Design, Loads and Load Combinations".

J. C. CARD
Rear Admiral, U.S. Coast Guard
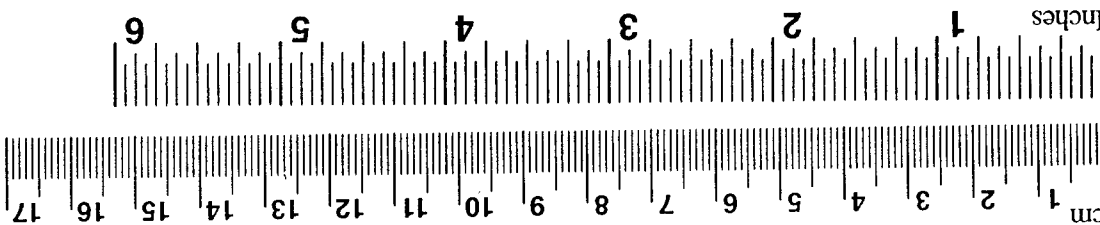Chairman, Ship Structure Committee

1. Report No. SSC–375	2. Government Accession No. PB95–126819	3. Recipient's Catalog No.		
4. Title and Subtitle **UNCERTAINTY IN STRENGTH MODELS FOR MARINE STRUCTURES**		5. Report Date **July 24, 1994**		
		6. Performing Organization Code		
7. Author(s) **O. Hughes, E. Nikolaidis, B. Ayyub, G. White, P. Hess**		8. Performing Organization Report No. **SR1338**		
9. Performing Organization Name and Address **Dr. Owen Hughes c/o Proteus Engineering 301 Pier One Road, Suite 200 Stevensville, MD 21666**		10. Work Unit No. (TRAIS)		
		11. Contract or Grant No. **DTCG23-92-C-E01089**		
12. Sponsoring Agency Name and Address **Ship Structure Committee c/o U.S. Coast Guard (G-MI/SSC) 2100 Second Street, S.W. Washington, D.C. 205393-0001**		13. Type of Report and Period Covered **Final Report**		
		14. Sponsoring Agency Code **G-M**		
15. Supplementary Notes **Sponsored by the Ship Structure Committee. Jointly funded by its member agencies.**				

16. Abstract

This project is a part of a long term effort to develop a reliability based method for the structural design of ship structures. The main task in the development of a reliability-based design method is the determination of the load factors and the strength (or resistance) factors. In order to achieve this task, it is necessary to have a quantitative measure of the various uncertainties that are inherent in both the loads and the strength models. Earlier SSC projects have examined the uncertainties related to loads. The objective of this project is to develop and demonstrate a method for quantifying the bias and uncertainty in structural strength algorithms (or computational models) in order to further the overall goal.

17. Key Words **Ship Structure, Reliability, Strength, Uncertainty, Failure, Collapse, Tripping**		18. Distribution Statement **Distribution Unlimited, Available From: National Technical Information Services Springfield, VA 22161**		
19. Security Classif. (of this report) **Unclassified**	20. Security Classif. (of this page) **Unclassified**	21. No. of Pages 130	22. Price	

Form DOT F 1700.7 (8-72) Reproduction of completed page authorized

NIST

METRIC CONVERSION CARD

Approximate Conversions to Metric Measures

Symbol	When You Know	Multiply by	To Find	Symbol
LENGTH				
in	inches	2.5	centimeters	cm
ft	feet	30	centimeters	cm
yd	yards	0.9	meters	m
mi	miles	1.6	kilometers	km
AREA				
in^2	square inches	6.5	square centimeters	cm^2
ft^2	square feet	0.09	square meters	m^2
yd^2	square yards	0.8	square meters	m^2
mi^2	square miles	2.6	square kilometers	km^2
	acres	0.4	hectares	ha
MASS (weight)				
oz	ounces	28	grams	g
lb	pounds	0.45	kilograms	kg
	short tons (2000 lb)	0.9	metric ton	t
VOLUME				
tsp	teaspoons	5	milliliters	mL
Tbsp	tablespoons	15	milliliters	mL
in^3	cubic inches	16	milliliters	mL
fl oz	fluid ounces	30	milliliters	mL
c	cups	0.24	liters	L
pt	pints	0.47	liters	L
qt	quarts	0.95	liters	L
gal	gallons	3.8	liters	L
ft^3	cubic feet	0.03	cubic meters	m^3
yd^3	cubic yards	0.76	cubic meters	m^3
TEMPERATURE (exact)				
°F	degrees Fahrenheit	subtract 32, multiply by 5/9	degrees Celsius	°C

Approximate Conversions from Metric Measures

Symbol	When You Know	Multiply by	To Find	Symbol
LENGTH				
mm	millimeters	0.04	inches	in
cm	centimeters	0.4	inches	in
m	meters	3.3	feet	ft
m	meters	1.1	yards	yd
km	kilometers	0.6	miles	mi
AREA				
cm^2	square centimeters	0.16	square inches	in^2
m^2	square meters	1.2	square yards	yd^2
km^2	square kilometers	0.4	square miles	mi^2
ha	hectares (10,000 m^2)	2.5	acres	
MASS (weight)				
g	grams	0.035	ounces	oz
kg	kilograms	2.2	pounds	lb
t	metric ton (1,000 kg)	1.1	short tons	
VOLUME				
mL	milliliters	0.03	fluid ounces	fl oz
mL	milliliters	0.06	cubic inches	in^3
L	liters	2.1	pints	pt
L	liters	1.06	quarts	qt
L	liters	0.26	gallons	gal
m^3	cubic meters	35	cubic feet	ft^3
m^3	cubic meters	1.3	cubic yards	yd^3
TEMPERATURE (exact)				
°C	degrees Celsius	multiply by 9/5, add 32	degrees Fahrenheit	°F

Temperature scale:

°C	-40	-20	0	20	37	60	80	100
°F	-40	0	32	80	98.6	160	212
			water freezes		body temperature			water boils

Inches / cm ruler

iv.

TABLE OF CONTENTS

1. INTRODUCTION

1.1 Background

Ship structures are still designed deterministically according to working stress formats. Structural safety is quantified by the margin between the applied load and the capacity of the structure, which is measured by the safety factor. Since these formats use only one safety factor, they lack the flexibility to adjust the prescribed safety margin to account for some of the factors which are critical in design. These factors include such items as variability in the strength, loads, modeling uncertainties, and the likelihood of various load combinations.

Reliability methods have been used in the development of reliability-based design formats for civil engineering and offshore structures, and they have matured enough to be used to design ships more rationally. Reliability methods take into account more information than their deterministic counterparts in the analysis and design of structural systems. Such information includes uncertainties in the strength of various structural elements, uncertainties in loads, and modeling errors in analysis procedures. Probability-based design formats are more flexible and consistent than working stress formats because they provide uniform safety levels over various types of structures. Designers can use these formats, which are called load and resistance factor design (LRFD) formats, to account for uncertainties that are not considered properly by deterministic formats, without explicitly performing probabilistic analysis.

A commonly used LRFD format consists of the requirement that a factored (reduced) strength of a structural component is larger than a linear combination of factored (magnified) load effects. In this format, load effects are increased, and strength is reduced, by multiplying the corresponding characteristic (nominal) values with factors, which are called strength (resistance) factors and load factors, respectively. The characteristic value of some quantity is the value that is used in current design practice, and it is usually equal to a certain percentile of the probability distribution of that quantity. The load and strength factors are different for each type of load and strength. The higher the uncertainty associated with a load, the higher the corresponding load factor. These factors are determined probabilistically so that they correspond to a prescribed safety level. It is also common to consider two types of performance function, that correspond to collapse and unserviceability requirements. The difference between working stress and LRFD formats is that the latter use different safety factors for each type of load and strength. This makes it possible to take into account uncertainties in load and strength, and to scale their characteristic values accordingly in the design equation. Working stress formats cannot do that because they use only one safety factor.

1.2 Objective

This project is a part of a long term effort to develop a reliability based method for the structural design of ship structures. The main task in the development of a reliability-

1

based design method is the determination of the load factors and the strength (or resistance) factors. In order to achieve this task it is necessary to have a quantitative measure of the various uncertainties that are inherent in both the loads and the strength models. Earlier SSC projects have examined the uncertainties related to loads. The objective of this project is to develop and demonstrate a method for quantifying the bias and uncertainty in structural strength algorithms (or computational models) in order to further the overall goal.

2. TASKS

In order to achieve the project's objective the following tasks were proposed and have now been accomplished.

1) Develop a methodology for the modeling and analysis of uncertainties in strength parameters. The methodology should be suitable for the development of a reliability-based design method for ship structures. Strength parameters include both basic strength variables and strength predictors. The uncertainties include bias and randomness for the basic strength variables (e.g., yield stress, dimensions, sizes, etc.), and model uncertainties in strength predictors (e.g., buckling strength, plastic capacity, etc.).

2) Identify the failure modes of the principal structural members of ships.

3) For the failure modes that involve modeling uncertainty, review the availability of sufficient test data to demonstrate the method.

4) On the basis of this review, determine which failure mode is most suitable for this demonstration.

5) For the selected failure mode (panel compressive collapse) collect data about strength parameters and apply the method to assess the uncertainties in the strength parameters.

6) Determine further research needs for uncertainty modeling and analysis of strength parameters.

3

3. METHODOLOGY TO ASSESS UNCERTAINTY IN STRENGTH PARAMETERS

The development of reliability-based design criteria for marine structures requires the assessment of uncertainties in their predicted strength. The assessed uncertainties in strength can be used for direct reliability-based design of marine structures. Also, it is essential that the assessed uncertainties are suitable for the development of reliability-based design formats of marine structures.

The main task in the development of a reliability-based design code is the determination of the load factors and strength (or resistance) factors in the process of code calibration (Ellingwood, et al. 1980). In code development, it is common to normalize the mean values of strength or load parameters with respect to their corresponding characteristic (nominal) values for the purpose of convenience and of increasing the range of applicability of the collected statistical data to many design situations. Therefore, for a given design situation the mean values of the load effects and strength can be computed by using these ratios as multipliers. This approach is commonly performed as a part of uncertainty analysis of strength and load effects (Ang and Cornell 1974, and Ellingwood et al. 1980).

White and Ayyub (1987a, 1987b) demonstrated the development of reliability-based design formats of ship structures for ultimate hull strength and fatigue failure modes. Guedes Soares and Moan (1985) demonstrated how to develop checking equations (design equations) for the midship section under longitudinal bending. They took into account uncertainties in stillwater and wave bending moments in calibrating the load and strength factors. Committee V2 of ISSC (1985) also presented an example of calibrating load and strength factors for structural design of ship hulls.

The suggested methodology for the assessment of strength uncertainties of marine structures consists of the following steps:

1. Determination of nominal (characteristic) strength values.
2. Evaluation of corresponding experimental values (or improved analytical values).
3. Computation of stochastic characteristics, which can include mean value, coefficient of variation and distribution type, of the ratios of nominal to experimental values. The results of this step are an assessment of bias and uncertainties in strength parameters. Both objective and subjective knowledge have to be used in this analysis.
4. Performance of a parametric analysis of the stochastic characteristics of the strength ratios due to variations in the strength parameters and load proportions.
5. Development of a summary of results in dimensionless spaces.

4

The remainder of this section provides the needed background information for performing these steps.

3.1 Uncertainty Types

Uncertainties in structural engineering systems can be mainly attributed to ambiguity and vagueness in defining the parameters of the systems and their relations. The ambiguity component is generally due to non-cognitive sources. These sources include (1) physical randomness; (2) statistical uncertainty due to the use of limited information to estimate the characteristics of these parameters; and (3) modeling (or prediction) uncertainties which are due to simplifying assumptions in analytical and prediction models, simplified methods, and idealized representations of real performances. The vagueness related uncertainty is due to cognitive sources that include (1) the definition of certain parameters, e.g., structural performance (failure or survival), quality and deterioration of materials, skill and experience of construction workers and engineers, and conditions of existing structures; (2) other human factors; and (3) defining the inter-relationships among the parameters of interest, especially for complex systems.

Structural engineers and researchers deal with the ambiguity types of uncertainty in predicting the structural behavior and designing structural systems using the theories of probability and statistics. Probability distributions are used to model system parameters that are uncertain. Probabilistic structural methods that include structural reliability methods, probabilistic engineering mechanics, stochastic finite element methods, reliability-based design formats, random vibration, and other methods have been developed and used for this purpose. In this treatment, however, a realization was established of the presence of a cognitive type of uncertainty. Subjective probabilities have been used to deal with this uncertainty type, that are based on mathematics used for the frequency-type of probability. Uniform and triangular probability distributions have been used to model this type of uncertainty for some parameters. Bayesian techniques have also been used to gain information about these parameters, thereby updating the underlying distributions and probabilities. Regardless of the nature of the gained information, whether it is cognitive or non-cognitive, the same mathematical assumption and tools were used.

The cognitive types of uncertainty arise from mind-based abstractions of reality. These abstractions are, therefore, subjective, and lack crispness. This vagueness is distinct from ambiguity in source and natural properties. The axioms of probability and statistics are limiting for the proper modeling and analysis of this type and are not completely relevant nor completely applicable. The modeling and analysis of vagueness type of uncertainty in civil engineering systems is discussed along with applications of fuzzy set theory to such systems by Ayyub (1991) and Ayyub and Lai (1992). These types of uncertainty were not considered in this study.

5

The sources of uncertainty in the strength of a structure can also be conveniently categorized as either "subjective" or "objective" (e.g., Ang 1971). The subjective uncertainties are those that result from the engineer's lack of knowledge or information regarding the physical phenomena associated with structural failure. These are usually manifested in the form of imperfect analytical models which necessarily contain assumptions in order to make for a tractable solution. A more descriptive title for these types of uncertainty would be "modeling" uncertainties.

Some examples of the sort of uncertainties which might be considered "modeling uncertainties" are:

- Uncertainties associated with simple beam theory in ship primary bending; i.e., do plane sections really remain plane?
- Uncertainties in the effects of initial deformations on buckling strength.
- Uncertainties in the amount of plating to consider as acting as an effective flange due to shear lag effects.
- Uncertainties associated with using small-deflection plate theory.

The sources of this uncertainty include our imperfect knowledge of the failure mechanisms, the assumptions made in modeling the failure mechanism, and possible numerical errors in the analysis of the strength. Each of these sources of uncertainty needs to be considered when performing an analysis of the strength of a structure.

The objective uncertainties are those associated with quantities that can be measured and examined. Examples of such quantities are yield strength, fracture toughness, thickness, residual stress, and initial distortion. If enough data could be collected on these quantities, the uncertainties could be quantified by the statistical parameters determined from an analysis of the data. In some cases, while there is a great deal of data available, it is not always in a useful form (yield strength - Mansour 1984, Galambos 1978). In others, the expense of collecting data makes it unlikely that there will ever be enough good quality data to perform a high quality statistical analysis (residual stresses - Alpsten 1972). While the description of these sources of uncertainties as "objective" is widely accepted, we believe that there is a certain amount of vagueness contained in that identification, particularly to engineers not versed in reliability methods. Identifying this type of uncertainty as uncertainties in the "basic parameters" more clearly defines this genre.

It should be noted that classifying types of uncertainties in this manner is done merely for convenience. It is quite possible that as our knowledge regarding some of the failure mechanisms improves, things which have been identified as modeling uncertainties could become uncertainties in the basic parameters.

The fatigue failure mode is of great interest, but for the most part it is dealt with in detail design, *after* the principal structural members have been sized. Several procedures have been used for assessment of fatigue damage (Wirsching 1984, Wirsching and Chen 1987), such as Deterministic method, Spectral method, Weibull model, and Nolte-Hasford

model. In general, the spectral method is the most suitable for marine structures. As was demonstrated by Chen and Mavrakis (1988), the spectral method is more accurate than the Weibull model for the case of offshore platforms because its results are less sensitive with respect to the variability in the shape of the wave spectra compared to the results of the Weibull model. However, the spectral method is also the most computationally intensive. Moreover, this method requires the use of the weighted sea method for extreme value analysis. It is likely that the above conclusions also apply to ships. In the development of probability-based design guidelines for ships, we need to calculate fatigue reliability. Fatigue reliability can be evaluated by using Munse's model (Munse et al. 1982), Wirsching's model (Wirsching 1984), or advanced second moment methods (Madsen, Skjong and Moghtaderi-Zadeh 1986). A reliability-based design format for fatigue was demonstrated by White and Ayyub (1987b).

3.1.1. Inherent Uncertainty in Basic Strength Parameters

Almost all strength parameters have some levels of inherent uncertainty due to physical randomness. Therefore, the exact realization of the characteristics of these strength parameters is not possible. For practical purposes, these parameters can be characterized with moments and probability distributions. In developing reliability-based design codes, it is necessary to obtain the central tendency value (i.e., the first moment), a measure of dispersion, such as the variance (the second central moment), and the probability distribution type. Information on the probabilistic characteristics of the basic strength variables of structural systems, such as yield stress, endurance limit, modulus of elasticity, scantlings, slenderness, and initial imperfection, can be obtained by reviewing the literature. Several reviewed studies provide information about the inherent uncertainty in basic strength parameters, such as Galambos and Ravindra (1978), Mansour (1987), Stiansen et al. (1979), Daidola and Basar (1981), Guedes Soares and Soreide (1983), Ellingwood et al. (1980), and Ayyub et al. (1990).

The inherent variability of a parameter X can be expressed in the form of the mean value ratio, its coefficient of variation, and its probability distribution type. The mean value is expressed by the following notation:

$$\text{Mean basic strength ratio} = \frac{\overline{X}}{X_n} \tag{3-1a}$$

where $\overline{X}$ = sample mean value, and X_n = nominal or design value. The coefficient of variation (COV) of the ratio is expressed using the following notation:

$$\text{Coefficient of variation of basic strength ratio} = \text{COV}(\frac{X}{X_n}) \tag{3-1b}$$

The probability distribution of the ratio can also be of interest, and needs to be determined. Frequency analysis or statistical goodness-of-fit tests can be used for this

purpose. The normal or lognormal distributions are commonly used to model strength parameters. Other distributions were also used such as the Rayleigh distribution.

Equations 3-1a and 3-1b provide expressions for the mean and coefficient of variation of a strength parameter ratio. The benefit of expressing the results in the form of ratios is in providing the results in dimensionless multipliers that can be used for wide range of nominal values. Also, these expressions lend themselves for comparative analysis for assessing the level of inherent uncertainties in different strength parameters.

3.1.2. Prediction Uncertainty

As was discussed in previous sections, the prediction uncertainty is due to bias and variability in the predictions of analytical models due to their limitations, assumptions and model simplifications. This uncertainty can be quantified by determining the nominal (or characteristic) strength values of some strength measures of interest. Then the corresponding experimental values (or improved analytical values) need to be evaluated. Computations of stochastic characteristics, which include mean value, coefficient of variation and distribution type, of the ratios of experimental to nominal values are then performed. The results are assessments of bias and random uncertainties in strength parameters. Both objective and subjective knowledge have to be used in this analysis. The performance of a parametric analysis of the stochastic characteristics of the strength ratios due to variations in the strength parameters and load proportions can provide an assessment of the stability of the results and their ranges. Then, the results in dimensionless spaces need to be summarized.

According to measurement theory (Ang and Tang 1984), the error in an estimated quantity can be considered to consist of two types, the systematic (bias) component and the random (variability) component.

The bias component (B) can be expressed as

$$B = \frac{X_A}{X_D} \qquad (3-2)$$

where X_A = the actual strength, and X_D = the design value of the strength parameter. Sometimes, for convenience, the bias (B) is broken down into three components, the actual to experimental bias (B_1), experimental to predicted bias (B_2), and the predicted to design bias (B_2). The actual to experimental bias (B_1) is

$$B_1 = \frac{X_A}{X_E} \qquad (3-3)$$

The experimental to predicted bias (B_2) is given by

8

$$B_2 = \frac{X_E}{X_P} \tag{3-4}$$

where X_E = the experimental value of the strength parameter, and X_P = the predicted value of the strength parameter. The predicted to design bias (B_3) is given by

$$B_3 = \frac{X_P}{X_D} \tag{3-5}$$

Therefore, the total bias (B) given by Eq. 3-2 is the product of B_1 to B_3 as follows:

$$B = B_1 B_2 B_3 \tag{3-6}$$

The coefficient of variation of the bias, COV(B), can be considered to be a measure of the random component of uncertainty. Therefore it is of interest and needs to be assessed. In cases where the prediction bias includes several sources, the total variability (COV_T) can be computed using a first order approximation:

$$COV_T = \sqrt{COV_1^2 + COV_2^2 + ... + COV_n^2} \tag{3-7a}$$

where COV_i = the ith variability source. For example the coefficient of variation of the total bias COV(B) can be computed as:

$$COV(B) = \sqrt{COV^2(B_1) + COV^2(B_2) + COV^2(B_3)} \tag{3-7b}$$

The above equations are true if the COV's are small.

The probability distribution type of the corrected strength measure by the bias factor is also of interest and needs to be determined.

The statistics of predicted strength can be calculated using approximate methods (second moment) or exact methods (Monte Carlo simulation) (Ang and Tang 1975). Monte Carlo simulation methods are used to assess the random bias in cases where the predicted strength (X_P) is given in terms of a function, such as

$$X_P = g(X_1, X_2, ..., X_n) \tag{3-8}$$

where X_i (i = 1,2, ... n) = basic random variable. The function can be explicit as given by Eq. 3-8, or implicit in the form of an elaborate computational procedure that is possibly evaluated by computers. The mean predicted strength value can be obtained using Monte Carlo simulation as follows:

$$\overline{X}_P = \frac{1}{N}\sum_{i=1}^{N} X_{P_i} \tag{3-9}$$

9

where X_{P_i} = the predicted strength in the ith simulation cycle, and N = the total number of simulation cycles. The coefficient of variation of X_P can be computed as

$$COV(X_P) = \frac{\sqrt{\frac{1}{N-1}\sum_{i=1}^{N}\left(X_{P_i} - \overline{X}_P\right)^2}}{\overline{X}_P} \qquad (3\text{-}10)$$

The statistical error in the estimated mean values (Eq. 3-9) is given by

$$COV(\overline{X}_P) = \frac{\sqrt{\frac{1}{N(N-1)}\sum_{i=1}^{N}\left(X_{P_i} - \overline{X}_P\right)^2}}{\overline{X}_P} \qquad (3\text{-}11)$$

The distribution type can be determined using frequency analysis, or statistical goodness-0f-fit tests.

The mean value and coefficient of variation of X_P can be approximately evaluated using a first-order Taylor-series expansion as follows:

$$\mu_P \approx g(\mu_1, \mu_2, ..., \mu_n) \qquad (3\text{-}12a)$$

and

$$COV(X_P) \approx \sqrt{\frac{\sum_{i=1}^{n}\sum_{j=1}^{n}\rho_{ij}\frac{\partial g}{\partial X_i}\frac{\partial g}{\partial X_j}\sigma_{X_i}\sigma_{X_j}}{\left(g(\overline{X}_1, \overline{X}_2, ..., \overline{X}_n)\right)^2}} \qquad (3\text{-}12b)$$

where μ_i = mean value of X_i, r_{ij} = the correlation coefficient between X_i and X_j, and s = standard deviation. The partial derivetives are evaluated at the mean value.

3.1.3. Statistical Uncertainty

The selection of a method for quantifying uncertainty depends on the available information and its nature. These methods are generally based on statistical concepts, probability and Bayesian approaches.

In cases where small sample sizes are used to assess a parameter, the statistical uncertainty in the parameter needs to be quantified. For example, the sample mean and standard deviation can be computed for a sample of size n, such as, $x_1, x_2, ..., x_n$, as follows:

$$\text{sample mean, } \overline{X} = \frac{1}{n}\sum_{i=1}^{n} x_i \tag{3-13}$$

and

$$\text{Sample standard deviation, } s_X = \sqrt{\frac{1}{n-1}\sum_{i=1}^{n}(x_i - \overline{X})^2} \tag{3-14}$$

The estimated mean $(\overline{X})$ is uncertain due to the limited sample size and its dependence on the sample. This statistical uncertainty in the assessed mean can be determined as

$$COV(\overline{X}) = \frac{1}{\sqrt{n}}\frac{\sigma_X}{\overline{X}} \tag{3-15}$$

In equation (3-15) we can use the sample standard deviation instead of the population standard deviation if the latter is not available. This coefficient of variation of the sample mean accounts only for the statistical uncertainty. It does not account for other types of uncertainty that are inherent, for example, in the sampling or testing programs. In this study statistical uncertainty was not considered.

3.1.4. Subjective Assessment of Statistical Parameters

For some parameters, limited information about them might require an analyst to use judgment to quantify uncertainty. For example, if only a range on the parameter is assessed (L = lower limit of X , U = upper limit of X), then the mean value and coefficient of variation of X can be determined as

$$\text{Mean value, } \mu = \frac{1}{2}(L+U) \tag{3-16}$$

$\mapsto$

$$\text{Coefficient of variation, } COV(X) = \frac{1}{\sqrt{3}}\left(\frac{U-L}{U+L}\right) \tag{3-17}$$

If a triangular distribution is assumed over the range (L,U) with a mode at M, then the mean and standard deviation are given by

$$\text{Mean value, } \mu = \frac{L+M+U}{3} \tag{3-18}$$

$$\text{Standard deviation, } \sigma_X = \sqrt{\frac{L^2 + M^2 + U^2 - LU - LM - MU}{18}} \tag{3-19}$$

11

For example, if ± two standard deviations of a normal probability distribution are assumed to be represented by the range (L,U), then the mean and coefficient of variation for the normal probability distribution are given by

$$\text{Mean value, } \mu = \frac{L+U}{2} \tag{3-20}$$

$$\text{Coefficient of variation, COV(X)} = \frac{1}{2}\frac{U-L}{U+L} \tag{3-21}$$

3.2. Bayesian Techniques

Engineers commonly need to solve a problem, and they must make decisions based on limited information about one or more of the parameters of the problem. The types of information available to them can be

1. objective information based on experimental results, or observations;
2. subjective information based on experience, intuition, other previous problems that are similar to the one under consideration, or the physics of the problem.

The first type of information can be dealt with using the theories of probability and statistics as was described in the previous sections. In this type, probability is interpreted as the frequency of occurrence assuming sufficient repetitions of the problem, its outcomes, and parameters, as a basis of the information. The second type of information is subjective and can depend on the engineer or analyst studying the problem. In this type, uncertainty exists, and needs to be dealt with using probabilities. However, the definition of probability is not the same as the first type, it is viewed herein as a subjective probability that reflects the state of knowledge of the engineer or the analyst.

It is common in engineering to encounter problems with both objective and subjective types of information. In these cases, it is desirable to utilize both types of information to obtain solutions or make decisions. The subjective probabilities are assumed to constitute a prior knowledge about a parameter, with gained objective information (or probabilities). Combining the two types produces posterior knowledge. The combination is performed based on Bayes' theorem.

If A_1, A_2, ..., A_n represent the prior (subjective) information, or a partition of a sample space S, and $E \subset S$ represents the objective information (or arbitrary event) as shown in Figure 3.1, the theorem of total probability states that

$$P(E) = P(A_1) P(E|A_1) + P(A_2) P(E|A_2) + ... + P(A_n) P(E|A_n) \qquad (3\text{-}22)$$

This theorem is very important in computing the probability of the event E, especially in practical cases where the probability cannot be computed directly, but, the probabilities of the partitioning events and the conditional probabilities can be computed.

Bayes' theorem is based on the same conditions of partitioning and events as the theorem of total probability and is very useful in computing the posterior (or reverse) probability of the type $P(A_i|E)$, for i = 1, 2, ..., n. The posterior probability can be computed as follows:

$$P(A_i|E) = \frac{P(A_i)P(E|A_i)}{P(A_1)P(E|A_1)+P(A_2)P(E|A_2)+...+P(A_n)P(E|A_n)} \qquad (3\text{-}23)$$

The denominator of this equation is P(E), which is based on the theorem of total probability. According to Eq. 3-23, the prior knowledge, $P(A_i)$, is updated using the objective information, P(E), to obtain the posterior knowledge, $P(A_i|E)$. Additional information on Bayesian techniques is provided by Ang and Tang (1975).

3.2.1. Discrete Case

For an unknown parameter Θ, a prior distribution for the parameters can be subjectively determined, and expressed using a probability mass function as

$$P_\Theta(\theta_i) = P(\Theta=\theta_i) \qquad \text{for i = 1, 2, ..., n} \qquad (3\text{-}24a)$$

or, in an abbreviated form, as

$$P_\Theta(\theta_i) = P(\theta_i) \qquad \text{for i = 1, 2, ..., n} \qquad (3\text{-}24b)$$

Therefore, the parameter Θ is assumed to take n discrete values with probabilities given by Eqs. 3-24. The distribution of Θ reflects the uncertainty in this parameter including its randomness. It is possible to have a parameter that is not random, but uncertain, therefore requiring its description through a distribution as given by Eqs. 3-24.

13

Now assume that new (objective) information ε was obtained. Using Eq. 3-23, the posterior distribution of the parameter can be obtained as

$$P(\theta_i|e) = \frac{P(\theta_i)\,P(\varepsilon|\theta_i)}{P(\theta_1)\,P(\varepsilon|\theta_1)+P(\theta_2)\,P(\varepsilon|\theta_2)+\,...+P(\theta_n)\,P(\varepsilon|\theta_n)} \qquad (3\text{-}25a)$$

where $P(\theta_i|e)$ = the conditional probability of θ_i given e, or the posterior probability for θ_i; $P(\theta_i)$ = prior probability as given by Eqs. 3-24; and $P(e|\theta_i)$ = the probability of obtaining the new information (e) given a certain value (θ_i) for the parameter. The following notation for the posterior distribution is also common:

$$P'(\theta_i) = \frac{P(\theta_i)\,P(\varepsilon|\theta_i)}{P(\theta_1)\,P(\varepsilon|\theta_1)+P(\theta_2)\,P(\varepsilon|\theta_2)+\,...+P(\theta_n)\,P(\varepsilon|\theta_n)} \qquad (3\text{-}25b)$$

where $P'(\theta_i)$ = the conditional probability of θ_i given e, or the posterior probability for q_i.

Using the prior distribution of the parameter Θ given by Eqs. 3-24, the expected value of the parameter can be computed as

$$E(\Theta) = \sum_{i=1}^{n} \theta_i P(\theta_i) \qquad (3\text{-}26)$$

Based on the posterior distribution, the expected value of Θ can be computed as

$$E(\Theta|e) = \sum_{i=1}^{n} \theta_i P'(\theta_i) \qquad (3\text{-}27)$$

In many engineering problems, the parameter Θ can be used to define a probability distribution of a random variable X. The probability distribution of X can be either for a discrete random variable in the form of a probability mass function, $P_X(x)$, or for a continuous random variable in the form of a density function, $f_X(x)$. The Bayesian estimation of the parameter can be used to compute Bayesian probabilities that are obtained using the gained information about the parameters. For example, the probability that X is less than some value x_0 can be computed using the prior distribution as

$$P(X<x_0) = \sum_{i=1}^{n} P(X<x_0|\theta_i)P(\theta_i) \qquad (3\text{-}28)$$

or

14

$$F_X(x_0) \quad = \sum_{i=1}^{n} F_X(x_0|\theta_i) P(\theta_i) \tag{3-29}$$

where $F_X(x)$ = the cumulative distribution function of X evaluated at x_0. Using the posterior distribution results in the following expressions:

$$P(X<x_0) \quad = \sum_{i=1}^{n} P(X < x_0|\theta_i) P'(\theta_i) \tag{3-30}$$

or

$$F_X(x_0) \quad = \sum_{i=1}^{n} F_X(x_0|\theta_i) P'(\theta_i) \tag{3-31}$$

3.2.2. Continuous Case

For an unknown parameter Θ, a prior distribution for the parameters can be subjectively determined, and expressed using a probability density function $f_\Theta(\theta)$. The parameter Θ is assumed to be continuous with probabilities that can be computed based on its density function. Again, the distribution of Θ reflects the uncertainty in this parameter including its randomness.

Now assume that new (objective) information ε was obtained. Using Eq. 3-23, the posterior distribution for the parameter can be obtained as

$$f_\Theta(\theta|\varepsilon) = \frac{f_\Theta(\theta) \, P(\varepsilon|\theta)}{\displaystyle\int_{-\infty}^{\infty} P(\varepsilon|\theta) f_\Theta(\theta) \, d\theta} \tag{3-32}$$

where $f_\Theta(\theta)$ = the prior density function of Θ; $f_\Theta(\theta|e)$ = the posterior density function of Θ; and $P(e|\theta)$ = the probability of obtaining the new information (e) given a certain value for the parameter (θ). The probability $P(e|\theta)$ is called the likelihood function $L(\theta)$. The following notations for the posterior distribution is also common:

$$f'_\Theta(\theta) = \frac{f_\Theta(\theta)\, L(\theta)}{\displaystyle\int_{-\infty}^{\infty} L(\theta) f_\Theta(\theta)\, d\theta} \tag{3-33}$$

where $f'_\Theta(\theta)$ = the conditional density function of θ given e, or the posterior density function of Θ.

Using the prior density function of the parameter Θ, the expected value of the parameter can be computed as

$$E(\Theta) = \int_{-\infty}^{\infty} \theta f_\Theta(\theta)\, d\theta \tag{3-34}$$

Based on the posterior distribution, the expected value of Θ can be computed as

$$E(\Theta|\varepsilon) = \int_{-\infty}^{\infty} \theta f'_\Theta(\theta)\, d\theta \tag{3-35}$$

In many engineering problems, the parameter Θ can be used to define a probability distribution of a random variable X. The probability distribution of X can be either for a discrete random variable in the form of a probability mass function, $P_X(x)$, or for a continuous random variable in the form of a density function, $f_X(x)$. The Bayesian estimation of the parameter can be used to compute Bayesian probabilities that are obtained with the gained information about the parameters. For example, the probability that X is less than some value x_0 can be computed using the prior distribution as

$$P(X < x_0) = \int_{-\infty}^{\infty} P(X < x_0 | \theta) f_\Theta(\theta)\, d\theta \tag{3-36}$$

or

$$F_X(x_0) = \int_{-\infty}^{\infty} F_X(x_0 | \theta) f_\Theta(\theta)\, d\theta \tag{3-37}$$

16

where $F_X(x_0)$ = the cumulative distribution function of X evaluated at x_0. Using the posterior distribution results in the following expression:

$$P(X < x_0) = \int_{-\infty}^{\infty} P(X < x_0 | \theta) f'_{\Theta}(\theta) d\theta \qquad (3\text{-}38)$$

or

$$F_X(x_0) = \int_{-\infty}^{\infty} F_X(x_0 | \theta) f'_{\Theta}(\theta) d\theta \qquad (3\text{-}39)$$

3.2.3 Bayesian Statistics - Mean Value with Known Variance

The Bayesian methods that were developed in the previous sections can be used in the statistical analysis of data. In this section, two cases are considered to illustrate their use in statistical analysis. The first case deals with a random variable X that is normally distributed with a known standard deviation. The mean value of the random variable is of interest, and is estimated using Bayesian methods. In the second case, the random variable X is also normally distributed, but its standard deviation is unknown. In this case, both the mean value and the variance of the random variable are of interest, and are estimated using Bayesian methods.

A random variable X is considered to be normally distributed with a known variance σ^2. The mean value of the random variable is of interest, and is unknown. The prior distribution of the unknown mean (μ) is normal with a mean value and variance μ_0, and σ_0^2, respectively. New (objective) information was obtained by a sample of size n. The mean value based on the sample is $\overline{X}$. We are interested in determining the posterior distribution of the mean. Using Eq. 3-33, the following expression can be established:

$$f(\mu) = \frac{f(\mu) L(\mu)}{\int_{-\infty}^{\infty} L(\mu) f(\mu) d\mu} \qquad (3\text{-}40)$$

17

where $f(\mu)$ = the prior density function of μ, which is normal with mean and variance of μ_0, and σ_0^2, respectively, (i.e., $N(\mu_0, \sigma_0^2)$); $f'(\mu)$ = the posterior density function of the unknown mean μ; and $L(\mu)$ = the likelihood function for the sample of size n. The likelihood function can be computed as the product of n values of the density function of the normal distribution with a mean μ and standard deviation s, each evaluated at a sampled value x_i. The product can be expressed as

$$L(\mu) = \frac{1}{(2\pi)^{n/2}\sigma^n} \exp\left[-\frac{1}{2}\sum_{i=1}^{n}\left(\frac{x_i - \mu}{\sigma}\right)^2\right] \qquad (3\text{-}41)$$

It can be shown that by substituting Eq. 3-41 in Eq. 3-40, the resulting $f'(\mu)$ is normally distributed with the following mean value and variance, respectively:

$$\mu' = \frac{n\overline{X}\sigma_0^2 + \mu_0\sigma^2}{n\sigma_0^2 + \sigma^2} \qquad (3\text{-}42a)$$

$\mapsto$

$$\sigma'^2 = \frac{\sigma_0^2\sigma^2}{n\sigma_0^2 + \sigma^2} \qquad (3\text{-}42b)$$

The resulting μ', and s' are the posterior mean and standard deviation of the unknown mean value μ. Using the normal posterior distribution, any Bayesian probabilities of interest for the random variable X can be computed.

The prior and posterior mean values and variances can also be used in other aspects of statistical analysis such as confidence intervals, and hypothesis testing. For example, they can be used to establish the following prior confidence interval on the mean:

$$\mu_0 - z_{\alpha/2}\sigma_0 \leq \mu \leq \mu_0 + z_{\alpha/2}\sigma_0 \qquad (3\text{-}43a)$$

Also, they can be used to establish the following posterior confidence interval:

$$\mu' - z_{\alpha/2}\sigma' \leq \mu \leq \mu' + z_{\alpha/2}\sigma' \qquad (3\text{-}43b)$$

where (1-a) is the confidence level. In a similar approach prior hypothesis testing, and posterior hypothesis testing can be performed.

3.2.4. Bayesian Statistics - Mean Value with Unknown Variance

The random variable X in this case is considered to be normally distributed with a unknown mean value (μ), and unknown variance (σ^2). Both the mean value and variance of the random variable are of interest, and are unknown. The prior joint distribution of the unknown mean (μ), and unknown variance (σ^2) is assumed to be normal-Gamma which is defined as the product of a normal distribution for the mean (μ), and a Gamma distribution for the variance (σ^2). The prior information about the mean and variance is based on a sample of size N with sample mean and variance of $\overline{X}_0$ and S_0^2, respectively. New (objective) information was obtained by a sample of size n. The mean value and variance based on the sample are $\overline{X}$ and S^2, respectively. We are interested in determining the posterior distribution of the mean and variance. Using Eq. 3-33, it can be shown that the posterior distribution is also a normal-Gamma.

The posterior mean ($\overline{X}'$), and posterior variance (S'^2) can be shown to be

$$\overline{X}' = \frac{N\overline{X}_0 + n\overline{X}}{n'} \tag{3-44}$$

and

$$S'^2 = \frac{(N-1)S_0^2 + N\overline{X}_0^2 + (n-1)S^2 + n\overline{X}^2 - n'\overline{X}'^2}{n'-1} \tag{3-45}$$

where
$$n' = N + n \tag{3-46}$$

The resulting values from Eqs. 3-44 to 3-46 are the posterior mean and standard deviation of the unknown mean and variance.

3.3. Relative Importance of Strength Parameters

The relative importance of different strength parameters needs to be assessed for the purpose of allocating resources in quantifying unknown uncertainties, quality control, development of design changes, and reliability improvement. Parametric analysis, sensitivity factors, and weighted sensitivity factors can be used for that purpose. They offer some benefits in certain aspects towards this objective.

3.3.1. Parametric Analysis

Monte Carlo simulation methods can be used to assess the mean value, coefficient of variation and distribution type of the predicted strength (X_p) which is according to a function of the type

$$X_p = g(X_1, X_2, ..., X_n) \qquad (3\text{-}47)$$

where X_i ($i = 1,2, ... n$) = basic random variable. The function can be explicit as given by Eq. 3-47, or implicit in the form of an elaborate computational procedure that is possibly evaluated by computers. The mean predicted strength value can be obtained using Monte Carlo simulation according to Eq. 3-9. The coefficient of variation of X_p can be computed using Eq. 3-10. The statistical error in the estimated mean value is given by Eq. 3-11. The distribution type can be determined using frequency analysis, or statistical goodness-of-fit tests.

The objective of parametric analysis is to investigate the effect of perturbing the mean value, coefficient of variation, or changing the distribution type of only one of the basic random variables on the mean value, coefficient of variation, or distribution type of the predicted strength X_p. The analysis is typically repeated for every basic random variables. The effects of X_p can be normalized into some convenient dimensionless quantity, and then ranked according to their gravity.

In this study, two methods of parametric analysis were developed. The first method finds the uncertainty effect of each basic random variable when only the corresponding variable is random and the other variables are fixed at values equal to their respective means. For this purpose, Monte-Carlo simulation for each random variable, while keeping the other variables fixed at their mean values needs to be performed. Then the resulting mean and coefficient of variation of the predicted strength (X_p) can be calculated. The results can be expressed using the following parametric coefficients (P_{1i}):

$$P_{1i} = \frac{COV(X_P)_i}{\sqrt{\sum_{i=1}^{n} \left(COV(X_P)_i\right)^2}} \qquad (3\text{-}48)$$

where P_{1i} is the parametric coefficient of the $\underline{ith}$ random variable using method 1; and $COV(X_P)_i$ is the coefficient of variation of the predicted strength due to uncertainty in the $\underline{ith}$ random variable.

The second method calculates the derivatives of the coefficient of variation of the predicted strength with respect to the coefficients of variation of the basic random variables. The sensitivities are found in reference to a "base" strength calculated using the

statistics of the basic random variables. In this case, the parametric coefficient (P_{2i}) of the uncertainty in the $i\underline{th}$ basic random variable is calculated using the following equation:

$$P_{2i} = \frac{\Delta COV(X_P)_i}{\sqrt{\sum_{i=1}^{n}(\Delta COV(X_P)_i)^2}} \tag{3-49}$$

where P_{2i} is the parametric coefficient of the $i\underline{th}$ random variable using method 2; and DCOV(X_P)$_i$ is the change in the coefficient of variation of the predicted strength due to a change in the coefficient of variation of the $i\underline{th}$ basic random variable by some percent. The percent change needs to be the same for all the basic random variables.

3.3.2. Sensitivity Coefficients

The sensitivity coefficients are defined in this study as the normalized change in predicted strength due to a change in the moments of the basic random variables. In this method, all the random variables are generated in the simulation of the predicted strength. The following four cases were developed:

1. The sensitivity coefficient for the mean predicted strength due to a change in the mean value of a basic random variable ($C_{\mu\mu i}$) is computed as

$$C_{\mu\mu_i} = \frac{\dfrac{\Delta \overline{X}_{Pi} / \overline{X}_P}{\Delta \overline{X}_i / \overline{X}_i}}{\sqrt{\sum_{i=1}^{n}\left(\dfrac{\Delta \overline{X}_{Pi} / \overline{X}_P}{\Delta \overline{X}_i / \overline{X}_i}\right)^2}} \tag{3-50a}$$

where $\Delta\overline{X}_i$ = change in the mean value of the <u>ith</u> basic random variable; $\overline{X}_P$ = the mean value of the predicted strength; and $\Delta\overline{X}_{Pi}$ = change in the mean value of the predicted strength due to the change in the mean value of the <u>ith</u> basic random variable. The means of the basic random variables are perturbed one random variable at a time, while keeping the means of the remaining random variables at their non-perturbed means. Their means are also perturbed using the same percent of their respective means. The selection of the percent change should be based on realistic possible levels for the means. The percent change and $\overline{X}_P$ in Eq. 3-50a cancel out from it to produce the following equation:

$$C_{\mu\mu_i} = \frac{\Delta\overline{X}_{Pi}}{\sqrt{\sum_{i=1}^{n}\left(\Delta\overline{X}_{Pi}\right)^2}} \tag{3-50b}$$

2. The sensitivity coefficient for the coefficient of variation of predicted strength due to a change in the mean value of a basic random variable ($C\sigma\mu_i$) is computed as

$$C_{\sigma\mu_i} = \frac{\dfrac{\Delta COV(X_P)_i / COV(X_P)}{\Delta\overline{X}_i / \overline{X}_i}}{\sqrt{\sum_{i=1}^{n}\left(\dfrac{\Delta COV(X_P)_i / COV(X_P)}{\Delta\overline{X}_i / \overline{X}_i}\right)^2}} \tag{3-51a}$$

where $COV(X_P)$ = the coefficient of variation of the predicted strength; and $\Delta COV(X_P)_i$ = change in the coefficient of variation of the predicted strength due to the change in the mean value of the <u>ith</u> basic random variable. The means of the basic random variables are perturbed one random variable at a time, while keeping the means of the remaining random variables at their non-perturbed means. The means are also perturbed using the same percent of their respective means. The percent change and $COV(X_P)$ in Eq. 3-51a cancel out from it to produce the following equation:

22

$$C_{\sigma\mu_i} = \frac{\Delta COV(X_P)_i}{\sqrt{\sum_{i=1}^{n}(\Delta COV(X_P)_i)^2}}$$ (3-51b)

3. The sensitivity coefficient for the mean predicted strength due to a change in the coefficient of variation of a basic random variable ($C\mu\sigma_i$) is computed as

$$C_{\mu\sigma_i} = \frac{\dfrac{\Delta\overline{X}_{Pi}/\overline{X}_P}{\Delta COV(X_i)/COV(X_i)}}{\sqrt{\sum_{i=1}^{n}\left(\dfrac{\Delta\overline{X}_{Pi}/\overline{X}_P}{\Delta COV(X_i)/COV(X_i)}\right)^2}}$$ (3-52a)

where $\Delta COV(X_i)$ = change in the coefficient of variation of the i<u>th</u> basic random variable; $\overline{X}_P$ = the mean value of the predicted strength; and $\Delta\overline{X}_{Pi}$ = change in the mean value of the predicted strength due to the change in the coefficient of variation of the i<u>th</u> basic random variable. The coefficients of variation of the basic random variables are perturbed one random variable at a time, while keeping the COV's of the remaining random variables at their non-perturbed coefficients. The COV's are also perturbed using the same percent of their respective non-perturbed values. The coefficients of variation can be perturbed by perturbing the corresponding standard deviations of the basic random variables. The percent change and $\overline{X}_P$ in Eq. 3-52a cancel out from it to produce the following equation:

$$C_{\mu\sigma_i} = \frac{\Delta\overline{X}_{Pi}}{\sqrt{\sum_{i=1}^{n}(\Delta\overline{X}_{Pi})^2}}$$ (3-52b)

4. The sensitivity coefficient for the coefficient of variation of the predicted strength due to a change in the coefficient of variation of a basic random variable ($C_{\sigma\sigma i}$) is computed as

23

$$C_{\sigma\sigma_i} = \cfrac{\dfrac{\Delta COV(X_P)_i / COV(X_P)}{\Delta COV(X_i) / COV(X_i)}}{\sqrt{\displaystyle\sum_{i=1}^{n}\left(\dfrac{\Delta COV(X_P)_i / COV(X_P)}{\Delta COV(X_i) / COV(X_i)}\right)^2}} \qquad\qquad (3\text{-}53a)$$

$COV(X_P)$ = the coefficient of variation of the predicted strength; and

$\Delta COV(X_P)_i$ = change in the coefficient of variation of the predicted strength due to the change in the coefficient of variation of the $i\underline{th}$ basic random variable. The coefficients of variation of the basic random variables are perturbed one random variable at a time, while keeping the remaining random variables at their non-perturbed coefficients. They are also perturbed using the same percent of their respective non-perturbed values. The coefficients of variation can be perturbed by perturbing the corresponding standard deviations of the basic random variables. The percent change and $COV(X_P)$ in Eq. 3-53a cancel out from it to produce the following equation:

$$C_{\sigma\sigma_i} = \cfrac{\Delta COV(X_P)_i}{\sqrt{\displaystyle\sum_{i=1}^{n}\left(\Delta COV(X_P)_i\right)^2}} \qquad\qquad (3\text{-}53b)$$

3.3.3. Weighted Sensitivity Coefficients

In the previous section, the sensitivity coefficients are defined as the normalized changes in the moments of the predicted strength due to changes in the moments of the basic random variables. The first two cases deal with the sensitivity coefficients for the predicted strength due to changes in the mean values of the basic random variables using a constant percent change. The latter two cases deal with the sensitivity coefficients for the predicted strength due to changes in the coefficients of variation of the basic random variables using a constant percent change. It needs to be noted that in the first two cases, a constant percent change in the mean values can result in different percentiles (or cumulative probabilities) for the different random variables according to their respective probabilistic characteristics. In order to impose a constant cumulative probability, the definition of the first two cases needs to be revised by basing the changes in the means on a constant percent change of their respective standard deviations, instead of a constant percent change of their respective means. The results are the weighted sensitivity

coefficients for the first two cases. The latter cases do not require any revision. The revised first two cases are as follows:

1. The sensitivity coefficient for the mean predicted strength due to a change in the mean value of a basic random variable ($W\mu\mu_i$) is computed as

$$W_{\mu\mu_i} = \frac{\dfrac{\Delta \overline{X}_{Pi} / \overline{X}_P}{\Delta \overline{X}_i / \overline{X}_i}}{\sqrt{\displaystyle\sum_{i=1}^{n} \left(\frac{\Delta \overline{X}_{Pi} / \overline{X}_P}{\Delta \overline{X}_i / \overline{X}_i} \right)^2}} \tag{3-54a}$$

where $\Delta \overline{X}_i$ = change in the mean value of the $\underline{i\text{th}}$ basic random variable; $\overline{X}_P$ = the mean value of the predicted strength; and $\Delta \overline{X}_{Pi}$ = change in the mean value of the predicted strength due to the change in the mean value of the $\underline{i\text{th}}$ basic random variable. The means of the basic random variables are perturbed one random variable at a time, while keeping the remaining random variables at their non-perturbed means. They are perturbed using the same percent of their respective standard deviations. The percent change and $\overline{X}_P$ in Eq. 3-54a cancel out from it to produce the following equation:

$$W_{\mu\mu_i} = \frac{\dfrac{\Delta \overline{X}_{Pi}}{COV(X_i)}}{\sqrt{\displaystyle\sum_{i=1}^{n} \left(\frac{\Delta \overline{X}_{Pi}}{COV(X_i)} \right)^2}} \tag{3-54b}$$

2. The sensitivity coefficient for the coefficient of variation of predicted strength due to a change in the mean value of a basic random variable ($W\sigma\mu_i$) is computed as

$$W_{\sigma\mu_i} = \frac{\dfrac{\Delta COV(X_P)_i \, / \, COV(X_P)}{\Delta \overline{X}_i \, / \, \overline{X}_i}}{\sqrt{\displaystyle\sum_{i=1}^{n} \left(\dfrac{\Delta COV(X_P)_i \, / \, COV(X_P)}{\Delta \overline{X}_i \, / \, \overline{X}_i} \right)^2}}$$ (3-55a)

where $COV(X_P)$ = the coefficient of variation of the predicted strength; and

$\Delta COV(X_P)_i$ = change in the coefficient of variation of the predicted strength due to the change in the mean value of the ith basic random variable. The means of the basic random variables are perturbed one random variable at a time, while keeping the remaining random variables at their non-perturbed means. They are perturbed using the same percent of their respective standard deviations. The percent change and $COV(X_P)$ in Eq. 3-55a cancel out from it to produce the following equation:

$$W_{\sigma\mu_i} = \frac{\dfrac{\Delta COV(X_P)_i}{COV(X_i)}}{\sqrt{\displaystyle\sum_{i=1}^{n} \left(\dfrac{\Delta COV(X_P)_i}{COV(X_i)} \right)^2}}$$ (3-55b)

4. FAILURE MODES AND STRENGTH ASSESSMENT MODELS

4.1 Identification of Failure Modes

As pointed out by Pittaluga (1987), historically the principal obstacles to achieving reliability-based design have been (a) the lack of accurate and efficient algorithms for calculating the limit states, and (b) the lack of computer implementation of these algorithms. But since then both obstacles have been overcome. In 1988 SNAME published *Ship Structural Design* by Hughes (1988), which combines and builds on the work of many ship structures researchers, and presents the underlying theory and the solution algorithms for all of the relevant failure modes. Secondly, all of these algorithms have been implemented in the MAESTRO computer program (Hughes 1985), which requires only a PC and is now widely used by designers, shipyards, classification societies and many other organizations (e.g., nine navies and two coast guard agencies).

Table 4.1 lists the failure modes of the principal members of ship structures and gives the failure category and the computational algorithm source for each of them.

Failure Modes of Principal Members	Failure Category	Computational Algorithm Source	Status re Avail. Data
PANEL		(SSD denotes *Ship Structural Design*)	
Collapse			
Stiffener Flexure	Collapse	SSD Sec. 14.2	OK
Combined Buckling	Collapse	SSD Sec. 13.2 - 13.4	Insuff.
Membrane Yield	Collapse	SSD Sec. 12.5	N. A.
Stiffener Buckling	Collapse	SSD Sec. 13.1 & 15.5	Insuff.
Stiffener Unserviceability			
(Initial Yield)			
Tension, Flange	Yield	Beam Theory & SSD Sec. 8.6	N. A.
Tension, Plate	Yield	"	N. A.
Compression, Flange	Yield	"	N. A.
Compression, Plate	Yield	"	N. A.
Plate Unserviceability			
Yield, plate bending	Yield	SSD Sec. 9.1 & 9.2	N. A.
Local buckling	Unserv.	SSD Sec. 12.6	OK
Allowable Permanent Set	Yield	SSD Sec. 9.3 - 9.5 & (H&C 91)	OK
BEAM			
Collapse			
Tripping	Collapse	SSD Sec. 13.1	Insuff.
Flexural-Torsional Buckling	Collapse	SSD Sec. 15.4 & 15.5	Insuff.
Plastic Hinge	Collapse	SSD Sec. 16.1 & 16.2	OK
Unserviceability (Initial Yield)			
Bending	Yield	Beam Theory	N. A.
Web shear	Yield	" "	N. A.
GRILLAGE			
Collapse			
Overall Buckling	Collapse	SSD Sec. 10.2 & 13.5,6	Insuff.
Plastic Hinge	Collapse	SSD Sec. 16.1 - 16.4	Insuff.

Table 4.1 Identification of Failure Modes for Principal Structural Members

27

4.2 Selection of Failure Modes for this Project

4.2.1 Necessity of Experimental Data

In general, the only way to assess the accuracy of a failure theory and its associated computational algorithm is from physical data, either model or full scale. That is, in structural engineering, apart from a few exceptions, it is inadvisable to try to assess the accuracy of a theory by means of another theory. For ship structures this important principle raises a major difficulty because there are many possible failure modes, and for some of them there is not sufficient experimental data. For other types of structures the requisite experiments have been performed. For example, for box girder bridges the steel portion (the box), has a simple geometry and the number of different possible failure modes is small; therefore it has been easier to obtain the necessary measurements. Also this testing process received very large international support in the 70's because of a series of structural failures of new bridges.

For aircraft the large production numbers make it possible to conduct numerous full scale tests, including even the testing to destruction of a prototype. In offshore structures the enormous financial scale of the oil industry - in both costs and revenues - has motivated large expenditure by the industry and by some governments to pay for whatever structural tests were needed. For example, over a period of about ten years the American Petroleum Institute (an industry-wide funding agency) sponsored the development of a completely new and comprehensive family of failure algorithms for stiffened cylinders of all relevant proportions and stiffening arrangements. This included a very comprehensive series of 1/4 scale collapse tests - the largest such testing program ever conducted apart from submarine hulls (for which the results are less relevant because of the greater pressure, and are not available anyway).

4.2.2 Failure Modes That Do Not Qualify

For some failure modes the limit value is not a calculated quantity but rather a specific independent quantity such as yield stress, or a specified maximum allowable response value under a nominated "design" load. Two examples are maximum (elastic) deflection and maximum allowable permanent set. Since the limit value does not contain any *calculational* or *modeling* uncertainty, these failure modes are not relevant for this project. Yield stress does contain some bias and uncertainty, but it is obtained from material sampling, which is a separate aspect of rationally-based design. In Table 4.1 these failure modes have "N.A." (Not Applicable) in the column headed "Status re Available Data". This leaves ten failure modes that involve calculated failure values. Of these, four were found to have sufficient data for statistical analysis; these are labeled OK in the Table. The other six do not have sufficient data, and they are labeled "Insuff."

4.2.3 Selection Criteria and Final Choice

The final choice of failure mode was based on the degree of seriousness, as measured by the following criteria:

(1) size or importance of the members

(2) sudden failure (e.g., buckling) vs. progressive failure in proportion to overload

(3) consequence of failure: does member collapse or merely become unserviceable

(4) existence of alternative load paths (redundancy of member)

Once these criteria are stated the choice becomes obvious. Stiffened panel collapse due to flexural (beam-column) failure of the stiffeners, the first failure mode, is more serious than the other three modes in all of the above criteria. The two modes of plate unserviceability are much less serious, and the plastic hinge collapse of a beam is proportional to the load. Also, in a ship a beam is usually part of a 3D framework and so there are several alternative load paths.

5. ALGORITHMS AND DATA FOR COMPRESSIVE COLLAPSE OF STIFFENED PANELS

5.1 Available Algorithms

5.1.1 "Standard" Algorithm

The best (most thoroughly validated and widely accepted) computational model for this failure mode is that developed in the UK under the guidance and sponsorship of the Merrison Committee, which led to the UK LRFD Code for steel box girder bridges, BS5400 (British Standards Institute, 1982). This computational model is directly applicable to ship panels and is presented for that application in Section 14.2 of Ship Structural Design (SSD). It has also been adopted by Lloyds Register of Shipping and is implemented in the LR computer program for panel strength: LR Pass Program 20202. It is also implmented in the MAESTRO program. Because of its thorough validation and wide acceptance, we will herein refer to this as the "Standard" algorithm.

The Standard algorithm is presented and validated in Chapter 14 of SSD, and this chapter is included herein as Appendix B. In this model each stiffener is regarded as an isolated beam-column, with the plating acting as one of the two flanges. If the stiffener is a tee section, then the beam-column is monosymmetric. Because of the relatively large width of the plate flange, the neutral axis of the beam-column is close to the plating; and hence the largest flexural stress occurs in the stiffener flange. Because of the unsymmetry about the neutral axis, the two directions of primary bending (bending in the plane of the web) have quite different consequences. Figure 14.2 of Appendix B illustrates the two cases. When the bending deflection is toward the plating, the flexural stress in the stiffener flange is compressive, and it combines with the applied axial compressive stress, so that the stiffener flange is the most highly stressed location in the cross section. Eventually it reaches the yield stress and the beam-column collapses. In this case we speak of the collapse as being "stiffener-induced". In the terminology of SSD, this is called a "Mode I" collapse. In contrast, when the bending deflection is toward the stiffener, the compressive flexural stress now occurs in the plating and it combines with the applied axial compressive stress. Eventually this combined compressive stress causes the plate to buckle and the beam-column, having lost its major flange, simultaneously collapses. In this case we speak of the collapse as being "plate-induced". In the terminology of SSD, this is called a "Mode II" collapse.

The accuracy of the Standard algorithm over all combinations of lateral and in-plane loads is demonstrated in Section 14.4 of Appendix B. Figure 14.11 gives a good overall summary of the results.

5.1.2 Other Algorithms

Prior to the publication of the Standard algorithm, various researchers had developed five other methods: Faulkner (1975B), Murray (1975), Carlsen (1980), Dwight and Little (1976) and Horne and Narayanan (1977).. Faulkner's method (1975B) is based on a Johnson-Ostenfeld approximation together with an effective width approach for plate behavior. This method was also presented in Faulkner et al (1973). The methods of Murray (1975), Carlsen (1980), Dwight and Little (1976), and Horne and Narayanan (1977) are all based on a Perry-Robertson formulation, also with an effective width model for the plating. The main differences in these methods are the ways they account for the effects of residual stress, initial imperfections, and eccentricity due to loss of plate effectiveness.

5.1.3 Smith Algorithm

A quite different algorithm is presented in (Smith 1975), which makes use of an extremely detailed model and large amounts of iteration. For example, the web of each stiffener is divided vertically into ten or more "layers" or "zones", and a new solution is performed each time the stress distribution changes in any zone. The solution also involves incremental stepping along a series of idealized stress-strain curves for the plating. The total computation is much larger than in the Standard algorithm, and yet as shown on pages 484,5 of SSD, the Standard algorithm gives comparable results, provided that it is used in close association with a three-dimensional finite element analysis of the structure, so that the true boundary conditions for the panel are known. This is the way the Standard algorithm is used in the MAESTRO program, and the finite element analysis is not an extra computational burden because it must be performed in any case in order to determine what are the actual or working stresses in the panel, without which the panel could not be designed or even assessed as to its adequacy.

In view of the large computational burden of the Smith algorithm and the fact that the computer program for it is not publicly or commercially available, the Smith algorithm is not suitable for the purposes of this project.

5.2 Summary of Current Code-based Design Practices

Since the ultimate goal of the SSC research program is to develop a probability-based design procedure for ship structures, we thought it would be helpful to briefly summarize the current situation in regard to code-based (or rule-based) design, because some organizations have already adopted probabilistic-based design guidelines, and others are in a state of transition.

5.2.1 AISC Load and Resistance Factor Design Code

The AISC Load and Resistance Factor Design (LRFD) Specification was first introduced in 1986. The specification was developed under the leadership of Galambos

(e.g., Pinkham and Hansell 1978, Galambos 1972, Galambos and Ravindra 1978, Galambos 1981, and Ravindra and Galambos 1978). The general format for the LRFD specification is

$$\phi R \geq \sum_{i=1}^{n} \gamma_i L_i \qquad (5\text{-}1)$$

where ϕ = strength reduction factor, R = resistance or strength according to some failure mode, g = load amplification factor, L = load type, and n = number of combined loads. The development of the LRFD code was based on a probability-based model (Galambos and Ravindra 1978, Ravindra and Galambos 1978, Ellingwood, et al. 1980, and Galambos, et al. 1982), calibration with the 1978 ASIS Allowable Stress Design Specification, and expert judgment based on previous design experiences. In developing the specification, it was necessary to change the design practice from working stress to limit stress, and from allowable to ultimate which was also reliability-based.

In preparation for the development of the AISC LRFD specification, uncertainties in strength parameters of steel structures were investigated and summarized by Ellingwood (1980). Also, the study included other materials such as timber, and reinforced and prestressed concrete. The results of this study were used to quantify strength uncertainties in marine structures.

5.2.2 AASHTO Code

Currently, the AASHTO Specification is being revised to an LRFD format. The National Cooperative Highway Research Program (NCHRP) has published the third Draft of LRFD Specifications and Commentary in 1992 titled "Development of Comprehensive Bridge Specifications and Commentary." The document is marked not for distribution pending review and approval. It is widely expected that the AASHTO LRFD code will closely follow much of the AISC code. Many of the individuals instrumental in the development of the AISC LRFD code are involved with the AASHTO effort.

5.2.3 API RP 2A Recommended Practice

The eighteenth edition (September, 1989) of the API Recommended Practice for Planning, Designing and Constructing Fixed Offshore Platforms is not yet an LRFD code. The code is primarily concerned with the design of tubular members and joints. The code makes extensive reference both to the AISC Code and to recommended practices of the

American Welding Society (AWS), though it specifically warns against using the new AISC LRFD Code. This is because the load and resistance factors used in the AISC Code are based on a calibration with building design practices. There is research currently in progress to attempt to develop load and resistance factors which would be useful in an offshore design. In the area of fatigue design the code relies on extensive studies performed by Wirsching and others to take into account the probabilistic nature of the random loading. However, the RP 2A fatigue code still recommends using a design life of two times the expected life and requires that the cumulative damage ratio remains below 1 for the design life of the structure.

5.2.4 U.S. Navy Design Data Sheets

In naval ship structural design the current design methods do not address failure modes or strength values explicitly. Instead the U. S. Navy uses a series of "design data sheets" which spell out a particular sequence of calculations, the result of which is either the (minimum) required member sizes or minimum values of size-related member properties, such as section modulus, from which the sizes may be determined. There are usually several such calculation procedures to be performed, and each procedure has been developed starting with the assumption (based on experience) that for that particular type of ship, one or two particular failure modes will govern the design.

In the U.S. Navy the two principal documents for the design of structural members are DDS 100-4 *Strength of Structural Members*, and DDS-100-6 *Longitudinal Strength Calculations*. Both of these documents have been in place for a long time, with the newer DDS 100-4 having an effective date of February 1979. The principal references for DDS 100-4 date back to the work of Dr. Friedrich Bleich in the 1950's (Bleich, 1952; Bleich and Ramsey, 1958). While the procedure in DDS 100-4 has its roots in sound analysis, simplistic modeling of the interaction of load components and arbitrary factors of safety render the actual level of safety present in the final design results an unknown quantity. There is an effort underway through the Naval Sea Systems Command to update and improve the Design Data Sheets. It is very likely that the update will be in the form of a reliability-based design code.

5.2.5 American Bureau of Shipping Rules

The American Bureau of Shipping published annually the latest revision to its Guidelines for the construction of steel merchant vessels. Though many of the procedures and formulae in the publication are empirically-based, there has been a steadily increasing effort to introduce a probabilistic basis into the selection of some of the coefficients used in the design equations. To help to make the rules more accessible and readable, ABS has begun to publish the rules in a computer CD ROM format. With the search and retrieval software available with the rules, it is significantly easier to find the needed topic and all relevant factors to the design of a particular component.

Their most recent effort to update and improve the classification procedure has been the introduction of the *ABS SafeHull System* (Grove and Coulter, 1993). Though available only for tankers at the time of this report, there is an effort underway to produce a similar system for bulk carriers. The system is a suite of computer programs aimed at assisting the structural designer in evaluating design alternatives and producing a safe design suitable for classification. The strength assessment in the programs covers the failure modes of yielding, buckling, and fatigue. The SafeHull System is a computerized implementation of the strength assessment procedures published in the "Guide for Dynamic Based Design and Evaluation of Tanker Structures" and the "Guide for the Fatigue Strength Assessment of Tankers" (ABS, 1993a and 1993b).

5.2.6 Lloyd's Register of Shipping Rules

The complete set of LR Rules for ship classification is now available on CD ROM. For this project the 1989 edition of the Lloyd's Rules was investigated. The ship structures related issues are contained in Parts 3 and 4. The general organization and type of rules are similar to those of ABS. There is no explicit assessment of strength in specific failure modes, rather the procedure leads one to design a safe structure by simple formulae aimed at defining specific scantlings. As a result, information about levels of safety included in the design are not apparent. However, Lloyd's does allow for direct calculations either through its *LR PASS* program or through the designer's own calculation procedure. In the latter case the designer would be required to provide details of the calculations and any programs used for the analysis.

5.2.7 Det Norske Veritas Rules

Det Norske Veritas's role is similar to that of ABS and Lloyd's. Though not widely used in the United States for ship design, DnV Rules are extensively used in the offshore field. Most of the calculations in the DnV rules are similar in nature to the other classification societies - that is they are aimed at assisting the designer in developing adequate scantlings without burdening him with the analysis of which failure mode or modes is the most critical. The basis for much of the calculations and equations in the DnV rules can be found in the *Ships' Load and Strength Manual* (Lersbryggen, 1978). This manual contains a comprehensive set of approximate formulae for the strength of stiffened panels. These formulae are, in general, developed from the underlying theory through the use of suitable engineering approximations. While very useful, the manual does not provide any new theory or approach to the strength assessment of stiffened panels.

5.3 Available Test Data

The main focus of this study is the uncertainty in the strength of longitudinally stiffened panels under axial compression. The data sets used in this study are the those which were readily obtainable and which had sufficient data for the purpose. Other sources of data were either found to be proprietary or of insufficient scope or lacking

some of the required data. There may well be other sources that we did not find due to limited publication. In the end, sufficient data was found to be available only for single bay panels under purely axial compression. Even here there were only three test series which fulfilled the requirements – the nominally identical and parametric series reported in Faulkner (1977) and the panels reported in Michelutti (1977).

The tests reported in Smith (1975) are for three-bay panels, and in general they were each different and they each involved a different mode of failure, including stiffener tripping and grillage buckling. The only exception was one pair of nominally identical panels. Unfortunately there are very few other three-bay panel tests, and none which are sufficiently similar in loading and geomery to be grouped with Smith's tests.

Faulkner (1977) reported on four test programs: the student series, the nominally identical series, the residual welding stress series, and the parametric series. The nominally identical and parametric series data are analyzed in this study. The student series was deemed inappropriate for use as a result of vagueness in the reporting. The residual stress series was conducted to investigate the effect of residual stress on the overall strength of a welded panel, and consists of two sets of panels. This series was not used herein because the first set was stress relieved by baking, and the second set is not fully documented. The second set was constructed similarly to the nominally identical series, but the welding methods were varied to create different amounts of residual stress. The dimensions and material properties are not reported for the panels, nor are their statistics aside from the mean values.

The nominally identical tests were conducted to quantify the strength uncertainties resulting from normal shipyard construction methods. The panels were all constructed from the same design with variation resulting purely from fabrication and material randomness. The panels consisted of plating reinforced with five stiffeners, oriented longitudinally approximating quarter scale deck panels of one bay length. Each panel was loaded axially to compressive failure. In order to make the panels are more sensitive to variations in dimensions and residual stress, they were designed such that the stiffener slenderness parameter, λ_s, was of the order of 0.9, and the plate slenderness parameter, β, was of the order of 2.1. Faulkner(1977) presented an analysis of the subjective and objective uncertainties associated with these tests. In Section 6.3.2 we compare our analysis with his and give reasons why we believe ours to be more accurate.

The parametric series tests were conducted to examine the effect on ultimate strength of varying slenderness ratios. The slenderness ranges were 1,2,3,4 for β and 0.375, 0.750, 1.125 for λ_s. They were of the same scale as the nominally identical series, constructed from plating with 5 longitudinal stiffeners, and of one bay length. The loading was purely axial and increased until ultimate failure. The construction methods were consistent for each panel. All but three of the panels had tee stiffeners.

The tests conducted by Michelutti (1977) consisted of single bay models with combined axial and lateral pressure loads. Of the 15 models reported, three were axially loaded and two of these were used in this study.

The details of all of the panels and test programs are discussed in the following chapter.

6. DEMONSTRATION OF UNCERTAINTY ASSESSMENT FOR COLLAPSE OF STIFFENED PANELS

In this chapter we demonstrate the estimation of random and modeling uncertainties in the strength of stiffened panels that fail under inelastic collapse, using data from two series of tests reported by Faulkner (1977) and one series reported by Michelutti and Murray (1977). Section 6.1 describes the tests and the panels used in these tests.

6.1 Description of Panels

6.1.1 Faulkner's nominally identical series

The nominally identical series of panel tests in Faulkner (1977) were conducted to examine strength uncertainties in longitudinally stiffened panels under axial compressive loading. The models were fabricated at a naval shipyard under normal conditions and tested to failure. Of the 13 models tested, 4 failed in stiffener-induced collapse (Mode I) and 9 failed in plate-induced collapse (Mode II). (For brevity we will use the "Mode" terminology; a description of the two modes was given in Section 5.1.1). The four panels that failed in Mode I initially had unusually large eccentricities, and they were straightened out after construction, and before testing, by means of an unspecified amount of heating. We did not include these four panels because of the artificial and completely unknown amount of bias that they contain.

Figure 6-1 depicts a panel in the nominally identical series. The panels were designed to represent a quarter scale deck panel and were stiffened by five stiffeners cut from 3"x1" Ministry of Defense (UK) Standard Tees. Simply supported boundary conditions were simulated by applying the load through knife edges at the elastic neutral axis. End caps were used to shed the load from the knife edge into the cross section. The stiffness added to the panels by these end caps shorten the simply supported length for analysis purposes to the reported effective length. The effective length formulation is treated in Faulkner (1977).

As the panels were nominally identical, any differences in the panels were due to randomness in the variables. The statistics of the measured material properties and the dimensions of the panels are reported in Table 6-1, along with the nominal (design) values. The actual scantlings of each panel were not reported in Faulkner (1977). All random variables in Table 6-1 were assumed to be normal. The effective length (a_e), stiffener spacing (b), and stiffener flange breadth (b_f) were all considered constant, as follows.

$$a_e = 790.0 \text{ mm},$$
$$b = 183.0 \text{ mm},$$
$$b_f = 25.4 \text{ mm}.$$

We used effective length in all calculations. For simplicity, in the rest of the section we will refer to effective length using the term "length" and denote it by "a".

The plate free edges had a width of b/3 to approximate the same buckling stress as the supported plate.

Random Variable	Nominal Value[1]	Mean	Standard Deviation	COV (%)
Plate Thickness (TPL)	3.0 mm	3.07 mm	0.027937 mm	0.91
Depth of stiffener (d)	32.5 mm	32.5 mm	0.26975 mm	0.83
Web thickness (TSW)	4.4 mm	4.90 mm	0.01519 mm	0.31
Flange thickness (TSF)	6.4 mm	5.84 mm	0.012848 mm	0.22
Plate yield stress (SigY(PL))	240 N/mm^2	238 N/mm^2	19.754 N/mm^2	8.3
Stiffener yield stress (SigY(STF))	240 N/mm^2	295 N/mm^2	16.52 N/mm^2	5.6
Eccentricity (e)	±0.5273[2]	±0.5273[2]	0.5273[3]	100.
Tension zone parameter, η, due to residual stresses[4]	2.772	2.7095	0.294	10.85
Young's modulus	208 kN/mm^2	201 kN/mm^2	3.015 kN/mm^2	1.5

Notes:
[1]Nominal dimensions from Ministry of Defense (UK) Standard Tee Bar catalog
[2]The mean and nominal values were estimated to be -a/1500 for Mode I and +a/1500 for Mode II.
[3]The standard deviation of the eccentricity was assumed to be equal to the length of the panel over 1500.
[4]Pages 393-394 of Hughes (1988) address this parameter. The nominal and mean values of η are based on the assumption that $\sigma_r/\sigma_Y = 0.10$, where σ_r is the compressive residual stress and σ_Y is the yield stress of the plating.

Table 6-1. Uncertainties in Geometry and Material Properties of Stiffened Panel

The compressive residual stress, which was measured after fabrication, corresponds to a tension zone parameter (η) of 4.2. The residual stress is not directly specified in the algorithm that we used to predict strength, where the residual stress is fixed at a value approximately equal to ten percent of yield stress of the plating. In this study we used a

mean tension zone parameter, $\eta = 2.710$, which corresponds to a residual stress equal to ten percent of the yield stress.

The statistics of the panel eccentricity were not given and so we had to use an assumed distribution, based on the following statement from Section 2.2 of Faulkner (1977): "the stiffener deformations were very small, usually much less than a/1000 and in no case greater than a/500...". We therefore assumed mean eccentricities of -a/1500 for Mode I and +a/1500 for Mode II, with a standard deviation of a/1500. To check if our assumption on the standard deviation of the panel eccentricity was reasonable, we estimated the standard deviation of the eccentricity of fourteen panels studied by Michelutti and Murray (1977). The standard deviation was found to be a/1376, which indicated that our assumption was reasonable.

Finally, it is observed from Table 6-1 that the eccentricity, the yield stresses of the plate and stiffener and the residual stress have the largest coefficients of variation.

6.1.2. Faulkner's parametric series

The second set of panels used in this study is the set referred to as the parametric series in Faulkner (1977). In this series 24 panels were tested to study the effect of varying slenderness ratios on the column strength. 19 of these panels failed in Mode II and were used in this study. Of the five not used, 2 experienced tripping failure and 3 had flat bar stiffeners instead of T-shaped stiffeners.

The panel dimensions and properties were reported for each panel and are given in Table 6-2. The panels had the same layout as the nominally identical series, with 5 stiffeners aligned longitudinally and b/3 free-edge plate width. The stiffeners were also cut from 3" x 1" Admiralty tees. Residual compressive stresses were measured and found to correspond to a range of η from 3 to 4.5. For the strength predictions η was defaulted to 2.710 as in the nominally identical series. The test procedure was identical with the exception of the load being applied at the midpoint of the distance between the initial (elastic) neutral axis and the predicted final neutral axis. The predicted final neutral axis location was based on an assumption of 40t of the plating being effective.

The panel mid span eccentricity was reported for each panel. For the nominal calculations the mean eccentricity was set to one standard deviation (a/1500), and it was negative for Mode I and positive for Mode II.

Model	a (mm)	b (mm)	TPL (mm)	d (mm)	TSW (mm)	b$_f$ (mm)	TSF (mm)	SigY (PL)	SigY (STF)
1	244.00	88.40	3.07	23.60	4.88	12.70	6.17	250.00	283.00
2	384.00	147.00	2.62	36.60	4.83	12.70	6.22	250.00	262.00
3	638.00	221.00	2.54	60.20	4.90	12.70	6.10	256.00	247.00
4	523.00	236.00	2.01	49.80	4.80	12.70	6.25	221.00	250.00
5	488.00	88.40	3.07	23.60	4.88	12.70	6.17	225.00	259.00
6	767.00	147.00	2.62	36.60	4.83	12.70	6.22	239.00	259.00
7	1275.00	221.00	2.54	60.20	4.90	12.70	6.10	270.00	246.00
8	1046.00	236.00	2.01	49.80	4.80	12.70	6.25	247.00	259.00
9	732.00	88.40	3.07	23.60	4.88	12.70	6.17	230.00	283.00
10	1151.00	147.00	2.62	36.60	4.83	12.70	6.22	239.00	258.00
11	1913.00	221.00	2.54	60.20	4.90	12.70	6.10	239.00	252.00
12	1570.00	236.00	2.01	49.80	4.80	12.70	6.25	249.00	266.00
13	262.00	88.40	3.10	26.40	3.10	0.00	0.00	253.00	261.00
14	244.00	177.00	3.05	23.60	4.85	12.70	6.15	242.00	269.00
15	422.00	265.00	3.07	40.10	4.95	12.70	6.20	227.00	267.00
16	384.00	295.00	2.57	36.60	4.90	12.70	6.12	244.00	273.00
17	523.00	88.40	3.10	26.40	3.10	0.00	0.00	229.00	256.00
18	488.00	177.00	3.05	23.60	4.85	12.70	6.15	229.00	246.00
19	843.00	265.00	3.07	40.10	4.95	12.70	6.20	253.00	266.00
20	767.00	295.00	2.57	36.60	4.90	12.70	6.12	261.00	247.00
21	785.00	88.40	3.10	26.40	3.10	0.00	0.00	258.00	262.00
22	732.00	177.00	3.05	23.60	4.85	12.70	6.15	242.00	262.00
23	1265.00	265.00	3.07	40.10	4.95	12.70	6.20	244.00	262.00
24	1151.00	295.00	2.57	36.60	4.90	12.70	6.12	239.00	267.00

Note: Yield stresses of stiffener and plate are expressed in N/mm^2

Table 6-2: Properties of Panels in Parametric Series

6.1.3 Panels A6 and H: Michelutti (1977)

Fifteen panels were tested in a variety of loading conditions. Three of these panels were loaded in purely axial compression. Of these three, a panel called "panel J" failed in Mode I and the remaining two panels called "Panels A6 and H" failed in mode II. Panel J was predisposed to fail in Mode I by moving the point of load application closer to the free edge of the stiffeners from the centroid. The two other panels, A6 and H, were not arranged to favor either failure mode.

Panels A6 and H share similar dimensions and properties with the most significant difference being overall length. The panels are stiffened by five bulb stiffeners and are loaded at the elastic neutral axis. The panel properties are listed in Table 6-3.

40

Panel	a (mm)	b (mm)	t_p (mm)	d (mm)	t_w (mm)	b_f (mm)	t_f (mm)	SigY (PL)	SigY (Stf)
A6	4930	530	9.60	152.0	7.31	28.6	15.9	368	383
H	3450	530	9.47	152.0	7.08	28.6	15.9	378	389

Note: Yield stresses are expressed in N/mm^2

Table 6-3. Properties of Panels from Michelutti (1977)

6.2 Results for random uncertainty

We estimated the uncertainty in the compressive strength of the stiffened panels described in Section 6.1 due to random uncertainties in geometry and material properties for two failure modes: stiffener initiated inelastic buckling (Mode I) and plate initiated inelastic buckling (Mode II). Section 6.2.1 presents the results. We also estimated the effect of each random uncertainty in geometry and material properties on the strength, and ranked these uncertainties in terms of importance. Those results are presented in Section 6.2.2.

6.2.1. Effect of random uncertainties on strength

Several combinations of axial and transverse in-plane loads and lateral pressure were studied to cover the range of realistic combinations of these loads. Specifically, the lateral pressure, p, ranged from -0.07 MPa to 0.07 MPa (positive pressure is from the plate to the stiffener). We considered four cases where transverse stress was 0, 1/16, 1/8 and 1/4 of the applied axial stress.

The statistics of the strength were estimated using Monte-Carlo simulation. In each replication, we predicted the axial strength of a panel corresponding to a set of samples of the random variables using the Standard algorithm described in Section 5.1.1 and presented in full in Appendix B.

The Standard algorithm assumes a fixed design value for residual stress, equal to ten percent of the yield stress. In contrast, Faulkner's algorithm (1973) explicitly allows for residual stress. Therefore, in order to account for the uncertainty in residual stress, we used two separate Monte-Carlo simulations. In the first simulation we used Faulkner's algorithm (1973) to predict strength, and we estimated the COV of the strength due to residual stress only, $COV_{residual}$, by fixing all other variables at their mean values. In the second simulation, we used the Standard algorithm to estimate the COV of the strength due to all of the other factors, COV_{other}. Then we obtained the total uncertainty in the strength, COV_T, using the following equation, which is derived from eq.(3.7):

$$COV_T = (COV_{residual}^2 + COV_{other}^2)^{1/2} \qquad (6-1)$$

41

In this equation, COV_T is the COV of the strength due to all uncertainties. For Mode I, the residual stress does not significantly affect the strength. Therefore, we assumed that $COV_T = COV_{other}$ for Mode I.

A panel fails under Mode I or Mode II depending on the direction of the eccentricity and lateral pressure. As a result, some of the samples generated in one simulation failed under Mode I and the others under Mode II. We separated the samples depending on the mode under which they failed and estimated the mean and COV of each mode separately.

The mean value of the strength for Mode I was found to be 247.5 MPa and the COV 10.20%. The corresponding values for Mode II were 156.5 MPa and 6.33%. The mean strength, the nominal strength and the mean strength plus and minus one and two standard deviations are plotted in Figures 6-2 to 6-9 as a function of the lateral pressure. The nominal strength was defined as the smallest of the strengths of Modes I and II that correspond to the nominal values of the variables in Table 6-1. Figures 6-2 to 6-5 are for applied transverse stress equal to 0 (case A), 1/16 (case B), 1/8 (case C) and 1/4 (case D) of the axial stress, respectively. The corresponding results for Mode II are shown in Figures 6-6 to 6-9.

The curves for the mean strength and the mean plus and minus one and two standard deviations extend to the range of positive pressures from 0 to 0.035 MPa for Mode I (Figure 6-2) because, although positive pressures favor Mode II, the panel may still fail under Mode I in this range because the eccentricity is random. Let us consider a panel that has failed. For each value of the lateral pressure in the range from 0 to 0.035 MPa each collapse mode has a conditional probability of occurrence (conditioned on the event that the panel has failed), which depends on the pressure and the probability distribution of the eccentricity. The summation of the conditional probabilities of occurrence of the two modes is one for a given value of the pressure. For positive pressures the conditional probability of occurrence of mode I decreases as the pressure increases because positive pressure favors plate induced collapse. The interaction curves for Mode II extend to the range of negative pressures for the same reason.

We observe the following from the Figures.

1. The standard deviation of the strength for Mode I changes considerably with pressure. For example, when there is no applied transverse stress, the standard deviation changes from about 11 MPa to 27 MPa when the pressure changes from -0.07 MPa to +0.35 MPa (Figure 6-2).

2. The range of variation of the standard deviation of the strength for Mode I is smaller for larger values of the applied transverse stress than for smaller values (Figures 6-2 to 6-5).

3. The variability in the strength due to random uncertainty is almost independent of the applied lateral pressure for Modes II. (Figures 6-6 to 6-9).

4. The nominal strength is considerably smaller than the mean strength for pressures from -0.07 to -0.0175 MPa, which means that if we predict the strength using the nominal values of the random variables we will be on the conservative side (see Figures 6-2 to 6-5). We believe that the main reason is that the nominal yield stress of the stiffener is significantly lower than the measured value (Table 6-1).

5. The nominal strength is almost identical to the mean for pressures from -0.0175 to 0.07 MPa (Figures 6-6 to 6-9). This is because some of the nominal values used to predict the strength were conservative (e.g., plate and web thickness), and others were non conservative (e.g., plate yield stress)(Table 6-1), and yet close to the measured values.

6.2.2. Ranking of random uncertainties

We ranked uncertainties in terms of importance using the three methods described in Section 3.3: Parametric Analysis and the two methods using Sensitivity Coefficients (unweighted and weighted). The coefficients measure the effect of random uncertainties in strength parameters on strength. They can be used to allocate resources in design and in collecting data for the statistical properties of the random variables. In the following we present the results:

Parametric Analysis

This method finds the effect of each uncertainty on strength when the corresponding variable is random and the remaining variables are fixed at their means. Uncertainties are ranked using the corresponding parametric coefficients, P_{1i}, that are calculated from equation 3-48.

$$P_{1i} = \frac{COV(X_P)_i}{\sqrt{\sum_{i=1}^{n}(COV(X_P)_i)^2}} \qquad i=1,...,n \qquad (3-48)$$

where $COV(X_p)_i$ is the COV of the predicted strength due to the uncertainty in the ith random variable and n is the number of random variables. Table 6-4 presents the COV's of the predicted strength due to each uncertainty and the parametric coefficient of each random variable for Modes I and II. Figure 6-10 shows the contribution of each uncertainty to the sum in equation 3-48, for Modes I. Figure 6-11 shows the corresponding results for Mode II.

43

Random Variable	Mode I: $COV(X_p)_i$ (%)	Mode I: Parametric coefficient	Mode II: $COV(X_p)_i$ (%)	Mode II: Parametric coefficient
Plate Thickness	0.10	0	0.58	0.09
Depth of stiffener	0.33	0.03	0.08	0
Web thickness	0.01	0	0.01	0
Flange thickness	0.04	0	0.01	0
Plate yield stress	0.01	0	5.39	0.87
Stiffener yield stress	4.82	0.48	0.01	0
Young's modulus, plate	0.19	0.01	0.47	0.08
Young's modulus, stiffener	0.39	0.03	0.04	0
Eccentricity	8.90	0.88	2.86	0.46
Residual stress	--	--	0.76	0.12

Table 6-4. Ranking of uncertainties using Parametric Analysis for Modes I and II

The following are observed:

- Mode I:

1. The uncertainty in eccentricity is the most important uncertainty for Mode I.
2. The uncertainty in the yield stress of the stiffener is the second most important uncertainty.
3. All other uncertainties are unimportant

- Mode II

1. The uncertainty in the yield stress of the plate is the most important.
2. The uncertainty in the residual stress, eccentricity, Young's modulus, and plate thickness are also important.
3. All other uncertainties are unimportant.

Nikolaidis et al. (1992) also found that the uncertainty in the yield stress of the plating was the most important among the uncertainties in geometry and material properties, in the case of a stiffened panel failing in Mode II, for which b/t=324, and a/b=1.35.

Sensitivity coefficients

We calculated the sensitivity coefficients using equations 3-51 to 3-53.

Tables 6-5 and 6-6 show the sensitivity coefficients $C_{\mu\mu_i}$, and $C_{\sigma\mu_i}$ for Mode I and Mode II, respectively. Tables 6-7 and 6-8 show the sensitivity coefficients $C_{\mu\sigma_i}$, and $C_{\sigma\sigma_i}$ for Mode I and Mode II, respectively. Tables 6-9 and 6-10 show the sensitivity coefficients $W_{\mu\mu_i}$, and $W_{\sigma\mu_i}$ for Mode I and Mode II, respectively.

r.v.	$C_{\mu\mu}$
SigY (Stf)	0.860
HSW	0.333
E (Stf)	0.264
TPL	0.175
TSF	0.165
E (PL)	0.130
Eccentricity	0.067
TSW	0.005
SigY (PL)	0.001

r.v.	$C_{\sigma\mu}$
HSW	0.621
E (Stf)	0.487
TPL	0.403
TSF	0.353
E (PL)	0.292
Eccentricity	0.063
SigY (Stf)	0.027
TSW	0.008
SigY (PL)	0

Table 6-5. Mode I: ranking based on sensitivity of predicted strength to perturbations of the means of the random variables.

r.v.	$C_{\mu\mu}$
TPL	0.791
SigY (PL)	0.543
E (PL)	0.261
HSW	0.075
Residual Stress	0.062
E (Stf)	0.027
Eccentricity	0.019
TSF	0.014
TSW	0.003
SigY (Stf)	0

r.v.	$C_{\sigma\mu}$
SigY (PL)	0.864
TPL	0.445
HSW	0.218
TSW	0.063
Residual Stress	0.040
TSF	0.037
Eccentricity	0.032
E (Stf)	0.015
E (PL)	0.015
SigY (Stf)	0

Table 6-6. Mode II: ranking based on sensitivity of predicted strength to perturbations of the means of the random variables.

46

r.v.	$C_{\mu\sigma}$
Eccentricity	0.999
SigY (Stf)	0.021
E (Stf)	0.003
HSW	0.002
TPL	0
SigY (PL)	0
E (PL)	0
TSF	0
TSW	0

r.v.	$C_{\sigma\sigma}$
Eccentricity	0.871
SigY (Stf)	0.491
E (Stf)	0.004
HSW	0.002
E (PL)	0.001
TPL	0
TSF	0
SigY (PL)	0
TSW	0

Table 6-7. Mode I : ranking based on sensitivity of predicted strength to perturbations of the standard deviations of the random variables.

r.v.	$C_{\mu\sigma}$
Eccentricity	0.993
SigY (PL)	0.116
Residual Stress	0.006
TPL	0.004
E (PL)	0.003
HSW	0.001
E (Stf)	0.001
TSW	0
TSF	0
SigY (Stf)	0

r.v.	$C_{\sigma\sigma}$
SigY (PL)	0.968
Eccentricity	0.197
Residual Stress	0.153
TPL	0.011
E (PL)	0.008
HSW	0
E (Stf)	0
SigY (Stf)	0
TSF	0
TSW	0

Table 6-8. Mode II: ranking based on sensitivity of predicted strength to perturbations of the standard deviations of the random variables.

Coefficients $C_{\sigma\sigma_i}$ show the effect of changing the standard deviations of the random variables to the COV of the strength. It is observed that the most important uncertainties for Mode I, ranked in terms of importance, are in the eccentricity and yield stress of the stiffener. These results are consistent with the results from parametric analysis. For Mode II, the yield stress of the plate is the most important random variable while the eccentricity and residual stress are less important, although they are not negligible. All other uncertainties are negligible.

47

r.v.	$W_{\mu\mu}$
SigY (Stf)	0.851
HSW	0.392
E (Stf)	0.253
TSF	0.161
E (PL)	0.129
TPL	0.106
Eccentricity	0.066
TSW	0.006
SigY (PL)	0.001

r.v.	$W_{\sigma\mu}$
HSW	0.729
E (Stf)	0.465
TSF	0.335
E (PL)	0.281
TPL	0.238
Eccentricity	0.060
SigY (Stf)	0.031
TSW	0.008
SigY (PL)	0

Table 6-9. Mode I: ranking based on sensitivity of predicted strength to weighted perturbations of the means of the random variables.

r.v.	$W_{\mu\mu}$
TPL	0.800
SigY (PL)	0.412
E (PL)	0.399
HSW	0.138
Residual Stress	0.093
E (Stf)	0.040
Eccentricity	0.029
TSF	0.022
TSW	0.004
SigY (Stf)	0

r.v.	$W_{\sigma\mu}$
SigY (PL)	0.840
HSW	0.510
TSW	0.132
Residual Stress	0.085
TSF	0.072
Eccentricity	0.063
E (PL)	0.030
E (Stf)	0.024
TPL	0.008
SigY (Stf)	0

Table 6-10. Mode II: ranking based on sensitivity of predicted strength to weighted perturbations of the means of the random variables.

A summary of the most important variables in each case is given in Table 6-11 for Mode I and Table 6-12 for Mode II. The three most important variables are listed in the order of impact on the predicted strength mean and coefficient of variation. If different values of the flange and web dimensions were used, the rankings could be different.

48

Sensitivity Coefficient	Most important random variable	2nd most important random variable	3rd most important random variable
$C_{\mu\mu}$	Stiffener Yield Stress	Stiffener Web Height	Stiffener Young's Modulus
$C_{\sigma\mu}$	Stiffener Web Height	Stiffener Young's Modulus	Plate Thickness
$C_{\mu\sigma}$	Eccentricity	Stiffener Yield Stress	Stiffener Young's Modulus
$C_{\sigma\sigma}$	Eccentricity	Stiffener Yield Stress	Stiffener Young's Modulus
$W_{\mu\mu}$	Stiffener Yield Stress	Stiffener Web Height	Stiffener Young's Modulus
$W_{\sigma\mu}$	Stiffener Web Height	Stiffener Young's Modulus	Stiffener Flange Thickness

Table 6-11. Mode I summary of results for sensitivity coefficient rankings.

Sensitivity Coefficient	Most important random variable	2nd most important random variable	3rd most important random variable
$C_{\mu\mu}$	Plate Thickness	Plate Yield Stress	Plate Young's Modulus
$C_{\sigma\mu}$	Plate Yield Stress	Plate Thickness	Stiffener Web Height
$C_{\mu\sigma}$	Eccentricity	Plate Yield Stress	Residual Stress
$C_{\sigma\sigma}$	Plate Yield Stress	Eccentricity	Residual Stress
$W_{\mu\mu}$	Plate Thickness	Plate Yield Stress	Plate Young's Modulus
$W_{\sigma\mu}$	Plate Yield Stress	Stiffener Web Height	Stiffener Web Thickness

Table 6-12. Mode II summary of results for sensitivity coefficient rankings.

6.3 Results for modeling uncertainty

Here the objective was to estimate the uncertainty in predicting strength due to idealizations and approximations in theory. We quantified modeling uncertainty by evaluating the mean and standard deviation of modeling bias (equation 3-3). We considered stiffened panels that are subjected to purely axial load because this is the only case for which sufficient experimental data is available. We again used the three data sets described in Section 6.1: those of Faulkner (1977) and of Michelutti and Murray (1977). The results are presented in this section. Then, in Section 6.3.2, we compare our results with those of Faulkner's own analysis of the data, and with the results of another study by Bonello. Finally, in Section 6.3.3, we demonstrate a Bayesian method for estimating modeling bias using both subjective information (estimates of experts) and objective information (measurements).

<u>Uncertainty in panel end rotational restraint</u>

To attempt to account for uncertainty in panel end rotational restraint would introduce enormous complexity into the modeling of panel strength. We believe that this would be counter productive because:

- There is not sufficient experimental data available. To obtain such data would require extensive testing of a large number of multi-bay stiffened panels under several loading conditions.

- In typical ship structures the cross frames are of open section and have relatively little torsional stiffness. Therefore they provide only a small amount of rotational restraint, and so ship panels usually have little more than simple support. With sufficient lateral pressure panels can behave as if they were clamped, but obviously such pressure may not always be present. Therefore the usual design practice for ship panels is to assume simple support, because this idealization is the closest to reality and it lies on the conservative side.

- In multibay panels the individual panels are approximately identical and are therefore all approaching collapse at about the same time. Therefore support of one panel by another cannot be assumed.

6.3.1 Estimation of modeling uncertainty

There are only two sets of data that are sufficiently complete to obtain predictions of modeling uncertainty - the parametric series and the nominally identical series of Faulkner (1977). We first estimated the total bias and then derived the modeling bias using equations 3-5 and 3-6, together with the estimates of random bias from Section 6.2. We did not estimate the modeling bias directly from equation 3-3 because this equation

requires prediction of the strength analytically for each panel, and Faulkner did not provide sufficient information on the location of the applied load to do so.

Parametric series

Table 6-2 presents the geometry and material properties of the panels. Two of the panels tripped and the others all failed in Mode II. Three of the latter panels had significantly different geometry than the rest; their stiffeners had no flange. Therefore, we only considered the remaining nineteen panels.

Table 6-13 presents the nominal and measured strength, and the total bias of each of the nineteen panels. The theoretical strengths are not presented. The theory expects the loading to be centered on the elastic neutral axis. As the loading was applied midway between the elastic neutral axis and the neutral axis at failure, consistent predictions with measurements were not forthcoming. Attempts were made to include loading alignment in the panel eccentricity with mixed success. Thus, to preclude adding to the modeling uncertainty through further approximations, we decided to use only total bias results for the parametric series data. Figure 6-12 shows the correlation between experiments and nominal values of the ultimate stress divided by the yield stress. Table 6-14 presents the nominal values of the parameters of each panel that we used to predict nominal strength.

Nominal strength Mode II (MPa)	Experimental Strength Mode II. (MPa)	Total bias
203.71	255.71	1.26
168.31	186.92	1.11
134.81	Tripped	
121.33	131.54	1.08
199.50	196.11	0.98
164.72	185.25	1.12
131.93	Tripped	
118.90	129.78	1.09
188.51	179.00	0.95
155.42	162.36	1.04
124.89	120.54	0.97
113.60	114.24	1.01
No flange		
165.83	190.24	1.15
130.84	134.28	1.03
116.88	126.50	1.08
No flange		
162.64	152.85	0.94
128.25	145.25	1.13
114.72	117.39	1.02
No flange		
151.92	128.24	0.84
119.99	122.26	1.02
108.82	94.46	0.87

Table 6-13. Estimation of total bias from parametric series

Model	a (mm)	b(mm)	TPL(mm)	HSW(mm)	TSW(mm)	BSF(mm)	TSF(mm)
1	244.00	88.40	3.00	17.43	4.40	12.70	6.40
2	384.00	147.00	2.50	30.38	4.40	12.70	6.40
3	638.00	221.00	2.50	54.10	4.40	12.70	6.40
4	523.00	236.00	2.00	43.55	4.40	12.70	6.40
5	488.00	88.40	3.00	17.43	4.40	12.70	6.40
6	767.00	147.00	2.50	30.38	4.40	12.70	6.40
7	1275.00	221.00	2.50	54.10	4.40	12.70	6.40
8	1046.00	236.00	2.00	43.55	4.40	12.70	6.40
9	732.00	88.40	3.00	17.43	4.40	12.70	6.40
10	1151.00	147.00	2.50	30.38	4.40	12.70	6.40
11	1913.00	221.00	2.50	54.10	4.40	12.70	6.40
12	1570.00	236.00	2.00	43.55	4.40	12.70	6.40
13	262.00	88.40	3.00	26.40	4.40	0.00	0.00
14	244.00	177.00	3.00	17.45	4.40	12.70	6.40
15	422.00	265.00	3.00	33.90	4.40	12.70	6.40
16	384.00	295.00	2.50	30.48	4.40	12.70	6.40
17	523.00	88.40	3.00	26.40	4.40	0.00	0.00
18	488.00	177.00	3.00	17.45	4.40	12.70	6.40
19	843.00	265.00	3.00	33.90	4.40	12.70	6.40
20	767.00	295.00	2.50	30.48	4.40	12.70	6.40
21	785.00	88.40	3.00	26.40	4.40	0.00	0.00
22	732.00	177.00	3.00	17.45	4.40	12.70	6.40
23	1265.00	265.00	3.00	33.90	4.40	12.70	6.40
24	1151.00	295.00	2.50	30.48	4.40	12.70	6.40

Notes:

1. The following assumptions were made regarding nominal values:
   a. Yield stress of stiffener and plate = 240 N/mm^2
   b. Tension zone parameter due to residual stress = 2.772.
   c. The nominal eccentricity=a/1500

2. Stiffeners of panels 13, 17 and 21 have no flange

Table 6-14: Nominal values of parameters corresponding to material properties and
geometry of Panels in Parametric Series

The mean value of the samples of total bias in Table 6-13 is 1.0367, the standard deviation 0.10 and the COV 0.097. The standard deviation of mean total bias is 0.023 which is only about 2% of the mean. This means that the sample size was large enough for estimating the mean bias accurately. From equations 3-5 and 3-7, we found that the mean value of modeling bias is 1.05 and its COV 0.074. Therefore, the analytical method that we used to predict strength was conservative, and, on the average, underestimates strength by approximately 5%.

Nominally identical series

This set consisted of 13 nominally identical panels. Nine of these panels failed in Mode II and four of them (panels 8-11) failed in Mode I. Table 6-15 presents the stress at failure and total bias of the first group of panels. The nominal failure stress was found to be equal to 158.47 N/mm². Using the results in Table 6-15 we found that the mean total bias was 1.1562 and its COV 0.06555. From equations (3-5) and (3-7), we found that the mean modeling bias is 1.17 and its COV 0.0195. We believe that the COV of modeling bias is unrealistically low because the panels were nominally identical, which means that the scatter of the ratio of experimental results vs. predictions was too low.

Panel	Measured Collapse Load (KN)	Measured Stress at Failure (MPa)	Total Bias
1	717	178.5012	1.126368
2	717	178.5012	1.126368
3	786	195.6791	1.234764
4	751	186.9657	1.179781
5	725	180.4928	1.138936
6	646	160.8253	1.104831
7	705	175.5137	1.107517
12	804	200.1603	1.263041
13	773	192.4427	1.214341

Table 6-15. Experimental results and total bias from nominally identical series

The COV of the measurements of strength of the four panels that failed in Mode II was very low. This is probably because, as explained in Section 6.1.1, these panels were initially very eccentric and they were artificially straightened by heating them. These unusual statistics seem to confirm our decision not to include these panels.

54

<u>Michelutti's results</u>

Michelutti and Murray (1977) tested fifteen panels, thirteen of which were nominally identical. Three panels were axially loaded, and the rest were subjected to combined bending and axial loading. Of the three panels that were axially loaded, two failed in Mode II, while the other panel was designed to fail in Mode I. We analyzed only the results of the two panels that failed in Mode II. The eccentricity of one panel, called A6 by Michelutti and Murray, was equal to a/530. The eccentricity of the other panel, called H, was not reported. We assumed that the eccentricity of panel H was a/1500. Table 6-16 compares predicted and measured failure stresses for panels A6 and H. It is observed that theory underestimated the strength of both panels. Modeling bias was about 1.05 for both panels.

Since there were only two samples, we did not try to estimate the statistics of bias from this table. However, we used that data to demonstrate the Bayesian method for estimating bias, which will be described in the Section 6.3.3.

Panel	Predicted Stress at Failure/Yield Stress	Measured Stress at Failure/Yield Stress	Modeling Bias
A6	0.39	0.41	1.05
H	0.62	0.66	1.06

Table 6-16. Predicted and Measured Strength of Panels Studied by Michelutti

6.3.2 Comparison of estimates of bias with results from other studies

<u>Faulkner (1976)</u>

Faulkner (1976) evaluated the total and modeling bias on the basis of the results of the nominally identical series. He analyzed the results of all the thirteen panels together, regardless of the mode in which they failed, and regardless of the artificial straghtening of four of them, all of which failed in Mode I. Also he neglected any uncertainty in eccentricity. He found the COV of the total bias to be 0.109, and the COV of the random bias to be 0.057. Then using equation (3-7) he found the COV of the modeling bias to be 0.093.

Our results, which were based on nine of these panels, all of which failed in Mode II, are considerably different. We found that the COV of the total bias is 0.0655, the COV of the random bias is 0.0626, and the COV of the modeling bias is 0.0195.

We believe that Faulkner overestimated total bias because he considered panels that failed in Mode I and II together, and that he underestimated random bias because he neglected eccentricity. Using these in equation (3-7) necessarily gives an overestimate of

the modeling bias. Also it is important to note that, strictly speaking, nominally identical panels are inappropriate for estimating modeling bias and total bias, because their similarity will cause an underestimate of the COV of total and nominal bias. Therefore, the estimates of bias from the parametric series, presented in Section 6.3.1., are more realistic.

The results discussed in the remaining of this subsection are for failure Mode II and for the case where panels are subjected to axial loads only.

Bonello et al (1992)

Bonello et al (1992) developed a computer program for predicting the strength of stiffened, multi-span panels using an inelastic beam-column formulation. They compared predictions using this program with a database of measurements from 85 tests on single and multi-span stiffened panels. The panels were subjected to axial compression only. Bonello et al. (1992) found that the mean modeling bias was 1.02 and the COV of modeling bias 0.08. They also compared the computer predictions with some data that they called "numerical data" (63 cases), and found a mean bias of 1.05 and a COV of 0.05. They attributed the difference in the COV's to the fact that the COV corresponding to the experiments included the effect of scatter due to experimental errors.

Bonello et al also calculated the mean and COV of modeling bias for the strength algorithms used by various authorities, based on 23 tests. (They did not indicate whether these tests were a subset of the 85 tests in the database). Table 6-17 presents the results. The estimates from the present study are also included in this Table.

Reference where method for strength prediction is described	Mean Modeling Bias	COV of Modeling Bias
Bonello (1992)	1.10	0.08
BS5400 (1982)	1.10	0.13
DnV (1987)	1.10	0.16
ECCS (1990) (Column approach)	1.08	0.14
ECCS (1990) (Orthotropic plate approach)	1.14	0.15
API RP2V (1987)	1.34	0.34
Present study	1.05	0.074

Note: All of the above values are based on the 23 tests except for those of the Present study, which are based on 19 tests from Faulkner's parametric series.

Table 6-17. Comparison of modeling uncertainties of prediction methods used by various authorities and results from present study.

Guedes Soares and Soreide (1983)

Guedes Soares and Soreide (1983) estimated the statistics of modeling bias for four different prediction methods: Carlsen (1980), Dwight and Little (1976), Faulkner (1975B), and Horne and Narayanan (1977). They obtained the experimental values from three test series: Horne and Narayanan (1976), Horne, Montague and Narayanan (1977) and Faulkner (1977) (of the latter they only used the results of the parametric series). They also compared predictions from Carlsen's and Faulkner's methods with data they called "numerical data", which were reported by Carlsen (1980).

Faulkner's method (1975B) is based on a Johnson-Ostenfeld approximation together with the effective width approach for plate behavior. This method was also presented in Faulkner et al (1973). Moreover, Faukner (1977) compared predictions of this method with results from parametric series tests. The methods of Carlsen (1980), Dwight and Little (1976), and Horne and Narayanan (1977) are based on a Perry-Robertson formulation.

As it happens, Guedes Soares and Soreide (1983) chose to deal with the inverse of modeling bias; that is, they used the ratio of experimental/predicted values. Therefore we repeated their analysis in order to obtain the statistics of modeling bias. Table 6.18 presents these statistics for Faulkner's and Carlsen's methods, which were derived using Faulkner's parametric series (Faulkner 1977). The bias of the Standard algorithm estimated in Section 6.3.1. is also presented in Table 6.18. In order to obtain results that can be compared with the estimates of bias of the Standard algorithm we used only 19 panels to derive the results in Table 6.18. Specifically, we discarded two panels that failed in tripping in tests and three panels whose stiffeners had no flange (see Table 6-13). Table 6.19 presents the modeling bias of the methods of Carlsen (1980), Dwight and Little (1976), Faulkner (1975B), and Horne and Narayanan (1977) for each of the stiffener and plate induced collapse modes. It also presents the statistics of bias of these methods obtained by analyzing data on both failure modes together. The estimates in Table 6.19 were based on results in Horne and Narayanan (1976) and Horne Montague and Narayanan (1977).

Method	Mean bias	bias COV
Carlsen (1980)	1.18	0.10
Faulkner (1977)	1.01	0.07
Standard	1.05	0.07

Table 6-18: Modeling Bias of Carlsen's, Faulkner's and the Standard methods for the test series of Faulkner.

Method	Stiffener Induced Collapse (Mode I)		Plate Induced Collapse (Mode II)		Modes I and II	
	Mean bias	bias COV	Mean bias	bias COV	Mean bias	bias COV
Carlsen (1980)	1.04	0.05	1.09	0.08	1.08	0.07
Dwight and Little (1976)	0.98	0.08	1.04	0.07	1.03	0.07
Faulkner (1975B)	0.95	0.07	1.00	0.06	0.099	0.07
Horne and Narayanan (1977)	1.06	0.06	1.06	0.10	1.06	0.09

Table 6-19: Modeling Bias of Carlsen's, Dwight and Little, Faulkner and Horne and Narayanan's methods for the test series of Horne et al.

It is observed that the mean bias of Faulkner's method is closer to one than that of the other methods and its COV is small, ranging from 0.06 to 0.07. The results of this method correlated particularly well with the parametric series tests (Table 6.18). On the other hand this method is not conservative; its average bias is less than one for some tests, which means that it overestimates strength in these tests. Carlsen's method is the most conservative. The average bias of this method for parametric series is 1.18. The results of this method have larger scatter than those of Faulkner's method and those of the Standard method. Dwight's and Little's method and Horne's method are also conservative, and the latter is slightly more conservative than the former. Both methods have small scatter -- their COV's are smaller than 0.10.

Guedes Soares and Soreide (1983) also compared predictions of Faulkner's and Carlsen's methods with numerical data by Carlsen (1980). They found that Carlsen's method correlated better than Faulkner's method with the numerical data.

6.3.3 Demonstration of the use of Bayesian estimation

In Chapter 3 we described two methods for using both objective and subjective information to estimate modeling bias . One method estimates the mean bias assuming that the standard deviation of bias is known. The other method estimates both the mean and standard deviation of bias. In this section we provide a qualitative demonstration of both methods. Bayesian estimation requires subjective estimates of statistical properties, which are normally obtained from a formal survey of expert opinion. Since this was merely a demonstration we specified the values ourselves, and we varied them systematically over a wide range in order to better assess the effect of subjective estimates on the statistics of bias.

6.3.3.1 Estimation of mean bias

We used equations (3-42 a and b) to estimate the posterior mean of bias and standard deviation of mean bias, respectively. We assumed that the bias was normal and that the standard deviation was known. To demonstrate the method, we used experimental data from the Parametric tests and from Michelutti's tests, together with values of subjective estimates of mean bias, which were chosen so as to adequately cover the range of such estimates.

Parametric series

We estimated the mean of total bias using subjective estimates and data from the parametric series. We varied the subjective estimate of mean bias (prior estimate of mean bias) from 0.9 to 1.3 and its standard deviation from 0.025 to 0.3. The standard deviation of total bias was fixed at 0.1 (this value is equal to the standard deviation of total bias obtained from parametric series).

Figure 6-13 presents the posterior mean bias as a function of the prior estimate of mean bias. Two curves corresponding to the mean + and - one standard deviation of mean bias are also presented. The probability that the actual value of mean bias is within the range defined by these curves is 68%. The standard deviation of the prior estimate of mean bias was assumed to be 0.1 in this figure. The mean bias obtained from the parametric series only is shown by the dotted line. We observe the following from Figure 6-13:

- The posterior estimate of mean bias and the width of the ± one standard deviation range are insensitive to prior knowledge.

- The standard deviation of the estimate of mean bias from the sample, which as mentioned in Section 6.3.1 is 0.023, is equal to the standard deviation of the posterior mean bias.

The reason that the posterior mean and standard deviation are insensitive to prior knowledge is that the confidence in the estimate of mean bias obtained from the samples is high because the sample size is large. Therefore, the posterior estimate of mean bias is not affected by prior knowledge.

Figure 6-14 shows the posterior mean as a function of the standard deviation of the prior mean. It is observed that prior knowledge affects the mean only for very small standard deviations in the range from 0.025 to 0.125. In real life it is very difficult to guess the mean bias with such high accuracy. Therefore, since the sample size of parametric series data is large, and the accuracy of the mean bias estimated from that sample is high, we do not need subjective estimates to estimate the mean bias. In cases like this, where the sample size is large, there is no point in using Bayesian estimation.

Finally, it is observed that the standard deviation of the posterior estimate is lower than both the standard deviation of the sample mean and the prior estimate of mean bias. This can be explained by examining equation (3-42b) in which the standard deviation of the posterior estimate of mean, σ'^2, is less than both the standard deviation of the prior estimate of mean, σ_0, and the standard deviation of bias, σ.

Michelutti's data

In this case we only have two samples of modeling bias. The sample mean is 1.058. We assumed that the standard deviation of modeling bias was 0.078 (this value was obtained from the parametric series)

Figure 6-15 shows the posterior mean bias as a function of the prior estimate of this value. The standard deviation of the prior estimate of mean bias is 0.1 for the results in this figure. In this case the posterior estimate of the mean bias is affected significantly by prior information. This happens because we have only two samples and therefore there is high uncertainty in the mean bias.

Figure 6-16 shows the posterior mean as a function of the standard deviation of the prior estimate of the mean. For small standard deviations, the posterior estimate of the mean is significantly different than the prior mean, which means that prior knowledge affects significantly the posterior estimate. On the other hand, for high values of the standard deviation of prior mean, the posterior mean is almost equal to the sample mean. This happens because when the standard deviation of the prior estimate is large, there is little confidence in this estimate and so the posterior mean is almost the same as the sample mean.

In conclusion, in cases where the sample size is small (say less than five), and there is a reliable subjective estimate of mean bias, the Bayesian approach is useful because it estimates the mean bias considering both subjective and objective information. The

estimate obtained from the Bayesian method can be more reliable than the sample mean bias.

6.3.3.2. Estimation of both mean and standard deviation of bias

This method uses equations (3-44) to (3-46). We used these equations to demonstrate how to update prior knowledge of the mean and standard deviation of bias, which was obtained from a sample of size N, using a new sample set. The above equations do not require the samples used to derive the prior estimates of mean and standard deviation but only the mean, standard deviation and sample size. This method is useful in cases where the original sample set, from which prior knowledge of the mean and standard deviation was obtained, is not available. This is typical in real life because in many cases only the statistics of bias and the number of samples are published.

The prior estimates of the mean and standard deviation of bias were assumed to be 1.1 and 0.1, respectively. We also assumed the following five sample values of bias: 1.0, 0.98, 0.95, 1.05 and 1.02. The mean of this sample is 1.0 and the standard deviation is 0.034. The standard deviation of the mean is 0.015. We calculated the posterior mean and standard deviation for different values of the sample size, N, on which the prior estimates were based in the range from 2 to 100.

Figures 6-17 and 6-18 show the posterior mean and standard deviation of bias, respectively, as a function of N. Two curves corresponding to the mean + and - one standard deviation of the mean are also shown. It is observed that the mean and standard deviation of bias are sensitive to N for small values of n but for large values they become insensitive and converge to the prior estimates as N becomes large (say greater than 50). Moreover, Figure 6-17 shows that, as we expected, the confidence in the mean bias increases as N increases.

7. CONCLUSIONS AND RECOMMENDATIONS FOR FUTURE RESEARCH

7.1 Conclusions

This project has developed and demonstrated a methodology for estimating the statistics of random and modeling uncertainties in structural strength algorithms. It has also presented a method for determining the relative impact of the basic strength parameters on the random uncertainty. Three different ranking methods were presented with a total of seven variations.

The methods of determining the random and modeling uncertainties were demonstrated for the axial compressive failure of longitudinally stiffened panels, for both Mode I (plate-induced) and Mode II (stiffener-induced) failure. The random uncertainty was estimated for Faulkner's nominally identical series. For pure axial loading, the COV of the strength was found to be 10.2% for Mode I and 6.33% for Mode II Plots were presented of the interaction between the axial strength of the panels and the lateral pressure for Modes I and II, for four different applied, transverse in-plane loadings. For these load combinations the random bias ranged from 1.1 to 1.5 for Mode I and from 1.0 to 1.1 for Mode II. The COV's ranged from 3 % to 15 % for Mode I and from 2 % to 9 % for Mode II.

The following ranking was obtained for Faulkner's nominally identical series of panels. For stiffener induced collapse (Mode I) the most important basic strength parameters are the stiffener yield strength, the eccentricity of the panel, and the height of the stiffener. For plate induced collapse (Mode II) the most important variables are the yield strength of the plate, the thickness of the plate, and the eccentricity of the panel.

The modeling uncertainties were evaluated for Mode II failure of axially loaded, longitudinally stiffened panels. The standard algorithm predictions for Faulkner's parametric series gave a modeling bias mean of 1.05 and a COV of 7.4 %. The standard algorithm predictions for the Michelutti panels also gave a modeling bias of 1.05.

A comparison with other studies was undertaken. The results from Bonello (1992) gave a mean modeling bias of 1.02 and a COV of 8 %. In a comparison with other prediction algorithms for a different experimental sample set, Bonello reported mean modeling biases ranging from 1.05 to 1.34. Guedes Soares and Soreide (1992) gave results for Faulkner's parametric series. The mean modeling bias for several strength prediction methods ranged from 1.01 to 1.18 and the COV's ranged from 7 to 10 %. A variety of algorithm predictions for other experimental data are reported. For Mode I and Mode II, the mean modeling bias ranges from 0.99 to 1.08 and the COV's ranged from 6 to 10 %.

A Bayesian method for estimation of the mean and COV of modeling bias was developed and demonstrated. This method uses both subjective information and results from comparison of predictions with tests. The method is useful in cases where limited experimental data is available.

The above results help gain insights into levels of uncertainty possible in structural strength design and analysis, whether for use deterministically or in a reliability-based format. However, the accuracy of the estimates of random and modeling uncertainty is limited by the availability of appropriate experimental data. Moreover, the findings discussed above are limited to the specific algorithms and data sets used in the analysis.

7.2 Recommendations for future research

7.2.1 Estimation of modeling bias for other failure modes

The assessment of uncertainty in strength models can only be done when sufficient experimental data is available. As shown in Table 4.1 and as discussed in Section 4.2, of the ten failure modes that involve modeling uncertainty, only four have sufficient data available. Of these, the two plate failure modes are merely unserviceability rather than collapse, and they are also very local. In contrast, of the six failure modes for which data is lacking, all are of the collapse type. Moreover, they all involve large portions of structure, which makes them doubly important. Therefore the obvious need is for sufficient structural testing to be done for these six other failure modes.

Of these six, the second, third and fourth are the most common for ship structures:

- Panel collapse due to stiffener buckling, which can be either:
  - local buckling of the web or flange (easily avoided by using standard sections)
  - "tripping" (torsional buckling due to axial compression)
  - flexural-torsional buckling (torsional buckling due to bending of the stiffener, caused usually by lateral loads on the panel)

- Beam collapse due to tripping

- Beam collapse due to flexural-torsional buckling

These three have some features in common: they all involve buckling, and the two types of torsional buckling can occur for both stiffeners and beams. Therefore we believe that the biggest need in regard to structural uncertainty is a carefully planned and coordinated series of tests involving these three failure modes. Using the results of these tests and the methodology for estimating modeling uncertainties that was presented in this report we can estimate the statistics of modeling bias of selected strength analysis algorithms.

63

Because tripping is one of the failure modes that we regard as most in need of attention, we devoted some extra time and effort in this project to review the current approaches to tripping. This review is presented in Appendix A, and we hope that it will encourage and facilitate the experimental research that is required in this area.

7.2.2 Analysis of random uncertainties

The procedure presented in Section 6.1 needs to be applied to a series of panels that have different dimensions. These panels should be selected in a way that their dimensions cover entire range of values encountered in practical applications. Then the results should be carefully analyzed using the methodology presented in this report to identify the most important uncertainties and estimate their effect on strength. It is hoped that this will allow general conclusions to be drawn that are applicable to the majority of panels used in ship structures.

The above procedure should be also applied to other components failing under the most important modes in Table 4.1, and also to the entire ship hull failing under global bending to study random uncertainties in these modes.

Finally, the statistical properties of statistical parameters and the type of distribution of random and modeling bias should be presented. This information is important in both reliability analysis and in developing a reliability based design code for ships.

8. BIBLIOGRAPHY

Adamchak, J.C., 1982, "ULTSTR: A Program for Estimating the Collapse Moment of a Ship's Hull Under Longitudinal Bending," David Taylor Research Center, Structures Department, Report 82/076.

Alpsten, G.A., 1972 "Variations in Mechanical Properties and Cross-Sectional Properties of Steel," Tall Building Criteria and Loading, Vol. Ib, Proceedings, Int. Conf. on Planning and Design of Tall Buildings, Lehigh University, Bethlehem, PA, Aug. 1972.

American Bureau of Shipping, "Guide for the Dynamic Based Design and Evaluation of Tanker Structures," September 1993.

American Bureau of Shipping, "Guide for Fatigue Strength Assessment of Tankers," September 1993.

American Institute of Steel Construction, 1990, Specifications for the Design, Fabrication and Erection of Structural Steel for Buildings, AISC, 1990.

American Institute of Steel Construction, 1986, Manual of Steel Construction, Load and Resistance Factor Design, AISC.

American Petroleum Institute, 1987, Bulletin on Stability Design of Cylindrical Shells, API Bulletin 2U.

American Petroleum Institute, 1987, Bulletin on Design of Flat Plate Structures, API Bulletin 2V.

Ang, A.H., and Cornell, C.A., 1974 "Reliability Bases of Structural Safety and Design," Journal of Structural Engineering, ASCE, Vol. 100, No. 9, pp. 1755-1769.

Ang, A. H.-S., and Ellingwood, B.R., 1971 "Critical Analysis of Reliability Principles Relative to Design," prepared for the conference on applications of statistics and probability to soil and structural engineering, Hong Kong, Sept. 1971.

Ang, A. H.-S., and Tang, W., Probability Concepts in Engineering Planning and Design, Volumes I (1975) and II (1984), John Wiley and Sons, NY.

Ayyub, B.M., 1991. Systems framework for fuzzy sets in civil engineering, international journal of Fuzzy Sets and Systems, North-Holland, Amsterdam, 40(3), 491-508.

Ayyub, B.M. and Haldar, H., 1984, "Practical Structural Reliability Techniques," Journal of Structural Engineering, ASCE, Vol. 110, No. 8, pp. 1707-1724.

Ayyub, B.M. and White, G.J., 1987, "Reliability-Conditioned Partial Safety Factors," Journal of Structural Engineering, ASCE, Vol. 113, No. 2, pp. 279-294.

Ayyub, B.M., White, G.J., and Purcell, E.S., 1989, "Estimation of the Structural Service Life of Boats," Naval Engineers Journal, American Society of Naval Engineers, Vol. 101, No. 3, pp. 156-166.

Ayyub, B. M., and White, G. J., 1990, "Structural Life Expectancy of Marine Vessels," international journal of Marine Structures: Design, Construction and Safety, published by Elsevier Applied Science and International Ship & Offshore Structures Congress, Vol. 3, No. 4, pp. 301-317.

Ayyub, B. M., White, G. J., Bell-Wright, T. F., and Purcell, E. S., 1990, "Comparative Structural Life Assessment of Patrol Boat Bottom Plating," Naval Engineers Journal, American Society of Naval Engineers, Vol. 102, No. 3, pp. 253-262.

Ayyub, B.M., and Lai, K.-L., 1991, "Selective Sampling in Simulation-Based Reliability Assessment," International Journal of Pressure Vessel and Piping, Vol. 46, No. 2, pp. 229-249.

Ayyub, B.M., and Chia, C.-Y., 1992, "Generalized Conditional Expectation for Structural Reliability Assessment," international journal on Structural Safety, Vol. 11, No. 2, pp. 131-146.

Ayyub, B.M., and Lai, K.-L., 1992, "Structural Reliability Assessment with Ambiguity and Vagueness in Failure," Naval Engineers Journal, American Society of Naval Engineers, Vol. 104, No. 3, pp. 21-35.

Bea, R.G., 1989, "Reliability Based Evaluations of Hydrodynamic Loadings on Coastal and Ocean Structures," Institution of Engineers, Australia, Civil College Overseas Speaker Program.

Bleich, F., 1952, *Buckling Strength of Metal Structures*, McGraw-Hill Book Co, New York, NY.

Bleich, F. and Ramsey, L.B., 1958 "A Design Manual for the Buckling Strength of Metal Structures," Society of Naval Architects and Marine Engineers, Technical and Research Bulletin No. 2-2.

Bonello, M. A., Chryssanthopoulos, M. K., And Dowling, P. J., "Ultimate Strength Design of Stiffened Plates under Axial Compression and Bending," Charles Smith Memorial Conference: Recent Developments in Structural Research, DRA, Dunfermline, Scotland, July 1992, Paper No. 7.

British Standards Institution, BS5400: Steel, Concrete and Composite Bridges; Part 3: Code of Practice for Design of Steel Bridges, 1982.

Caldwell, J.B., and Rutherford, S., 1990, "Ultimate Longitudinal Strength of Ships: A Case Study," Trans. SNAME, Vol. 98.

Carlsen, C. A., "A Parametric Study of Collapse of Stiffened Plates in Compression," The Structural Engineer, Vol. 56B, pp. 33-40.

CEB(Comite European du Beton), 1976, "Common Unified Rules for Different Types of Construction and Material," Joint Committee on Structural Safety CEB-CECM-FIP-IABSE-IASS-RILEM, CEB Bulletin No. 116E.

Chen, H. H., et al., 1983, "Correlation of Theoretical and Measured Hydrodynamic Pressures for the SL-7 Containership and the Great Lakes Bulk Carrier S.J. CORT," Ship Structure Committee, Report SSC-325.

Chen, Y. N., and Mavrakis, S. A., 1988, "Closed-Form Spectral Fatigue Analysis for Compliant Offshore Structures," Journal of Ship Research, Vol. 32, No. 4, December, pp. 297-304.

Chen, H. H., et al., 1983, "Correlation of Theoretical and Measured Hydrodynamic Pressures for the SL-7 Containership and the Great Lakes Bulk Carrier S.J. CORT," Ship Structure Committee, Report SSC-325.

Cornell, C.A., 1969,"A Probability-B Structural Code," Journal of the American Concrete Institute, 66(12), December.

Daidola, J.C. and Basar, N.S., 1981, "Probabilistic Structural Analysis of Ship Hull Longitudinal Strength," Ship Structure Committee," Report No. SSC-301.

Das, P.K., and Garside, J.F., 1991, "Structural Redundancy for Continuous and Discrete Systems," Ship Structures Committee Report, SSC-354.

Design Data Sheet, DDS1100-4, 1955, "Structural Design of Flat Platting and Stiffeners Subjected to Water Pressure," The U.S. Navy, Bureau of Ships, Washington, D.C.

Design Data Sheet, DDS1100-3, 1956, "Strength of Structural Members," The U.S. Navy, Bureau of Ships, Washington, D.C.

Design Data Sheet, DDS100-4, 1979, "Strength of Structural Members," The U.S. Navy, Bureau of Ships, Washington, D.C.

Dow, R.S., Hugill, R.C., Clark, J.D., and Smith, C.S., 1981, "Evaluation of Ultimate Ship Hull Strength," Extreme Loads and Response Symposium, SNAME, pp. 133-147.

Dowling, P.J., Chatterjee, S., Frieze, P.A., and Moolani, F.M., 1973, "The Experimental and Predicted Collapse Behavior of Rectangular Stiffened Steel Box Girders," Int'l. Conference on Steel Box Girder Bridges, Institute of Civil Engineers, London.

Det norske Veritas, Buckling Strength Analysis of Mobile Offshore Units, Classification Note 30.1, October 1987.

Dwight J. B. and Little, G. H., "Stiffened Steel Compression Flanges -- a Simpler Approach," The Structural Engineer, Vol. 54A, pp. 501-509.

Ellingwood, B., Galambos, T.V., MacGregor, J.C., and Cornell, C.A., 1980, "Development of a Probability Based Load Criterion for American National Standard A58," National Bureau of Standards Publication 577, Washington D.C.

ISSC Report of Committee V.2, 9th International Ship Structures Congress, 1985.

European Convention for Constructing Steelwork, European Recommendations for the Design of Longitudinally Stiffened Webs and Stiffened Compression Flanges, ECCS Technical Working Group 8.3, First Edition, 1990.

Faulkner, D., et. al. 1973, "Synthesis of Welded Grillages to With stand Compression and Normal Loads," Computers and Structures, 3, 1973, pp. 221-246.

Faulkner, A., 1975(A), "A Review of Effective Plating for Use in the Analysis of Stiffened Plating in Bending and Compression," J. of Ship Research, 19(1).

Faulkner, D., 1975(B), "Compression strength of Welded Grillages," Ship Structure Design Concepts, J. M. Evans (Editor), Cornell maritime Press, 1975, pp. 633-712.

Faulkner, D., 1977, "Compression Tests on Welded Eccentrically Stiffened Plate Panels", Proceedings of International Symposium on Steel Plated Structures, P. J. Dowling et al. (editors), Crosby Lockwood Staples, London, pp. 130-139.

Ferro, G, 1982, "Advances in the Calculation of the Maxima of Ship Responses," Euromech Colloquim 155, Reliability Theory of Structural Engineering Systems, Engineering Academy of Denmark, DIALOG 5-82, June.

Ferro, G. and Mansour, A.E., 1985, "Probabilistic Analysis of the Combined Slamming and Wave Induced Responses," Journal of Ship Research, Vol. 29, No. 3, pp. 170-185.

Franklin, P and Hughes,O.F. "An Approach to Conducting Timely Structural Fatigue Analysis of Large Tankers", Aerospace and Ocean Engineering Department, Virginia Polytechnic Institute and State University Report VPI-AOE-192, Blacksburg, Va. September 1992.

Fujino, M., Kawada, J., Yoon, B. S., 1985, "A Study on Wave Loads Acting on a Ship in Large Amplitude Wave," Society of Naval Architects of Japan, Vol's. 156, and 158.

Fujino, M., Yoon, B. S., 1986, "A Practical Method of Estimating Ship Motion and Wave Loads in Large Amplitude Wave," International Shipbuilding Progress, Vol. 33, pp. 159-172.

Fukuda, J.,1967, "Theoretical Determination of Design Wave Bending Moments," Japan Shipbuilding and Marine Engineering, Vol. 2, No. 3, pp. 13-22.

Galambos, T.V., 1972, "Load Factor Design of Steel Buildings," Engineering Journal, AISC, 9(3), 108-113.

Galambos, T.V., 1981, "Load and Resistance Factor Design," Engineering Journal, AISC, 18(3), 78-84.

Galambos, T. V. and Ravindra, M. K., 1978, "Properties of Steel for Use in LRFD," Journal of Structural Engineering, ASCE, Vol. 104(9), 1459-1468.

Galambos, T.V., Ellingwood, B., MacGregor, J.G., and Cornell, C.A., 1982, "Probability Based Load Criteria: Assessment of Current Design Practice," Journal of Structural Engineering, ASCE, 108(5), 959-977.

Galambos, T. V. and Ravindra, M. K., 1978, "Load and Resistance Factor Design," Journal of Structural Engineering, ASCE, pp. 1335-1356.

Gerard, G., 19xx, Introduction to Structural Stability Theory.

Grove, Todd W. and William G. Coulter, 1993, "Practical Application of a New Advanced Dynamic Based Hull Structural Strength Design and Evaluation Criteria," Proceedings of the Ship Structures Symposium '93, Arlington, VA, Nov 16-17, 1993, pp. K-1.

Guedes Soares, C. and Moan, T., 1982, "Statistical Analysis of Stillwater Bending Moments and Shear Forces Tankers, Ore and Bulk Carriers," Norwegian Maritime Research, Vol. 10, No. 3, pp. 33-47.

Guedes Soares, C. and Soreide, T.H., 1983, "Behavior and Design of Stiffened Plates Under Predominantly Compressive Loads," International Shipbuilding Progress," Vol. 30, No. 341, pp. 13-27.

Guedes Soares, C. and Moan, T., 1985, "Uncertainty Analysis and Code Calibration of the Primary Load Effects in Ship Structures," Proceedings, 4th International Conference on Structural Safety and Reliability (ICOSSAR '85), Kobe, Japan, Vol. 3, pp. 501-512.

Guedes Soares, C, 1984, "Probabilistic Models for Load Effects in Ship Structures," Department of Marine Technology, Norwegian Institute of Technology, Trondheim, Norway, Report No. UR-84-38.

Guedes Soares, C. and Moan, T., 1988, "Statistical Analysis of Still-water Load Effects in Ship Structures," SNAME Transactions, Vol. 96, pp. 129-156.

Guedes Soares, C., 1990, "Effect of Heavy Weather Maneuvering on the Wave-Induced Vertical Bending Moments in Structures," Journal of Ship Research, Vol. 34, No. 1., March 1990, pp. 60-68.

Hasofer, A. M., and Lind, N.C., 1974, "An Exact and Invariant First Order Reliability Format," Journal of Engineering Mechanics, ASCE, pp. 111-121.

Horne, M.R., and Narayanan, R., 1976, "Ultimate Capacity of Stiffened Plates Used in Grillages," Proc. of Inst. of Civil Engrs., Vol. 61, pp. 253-280.

Horne. M. R., Montague, P. and Narayanan, R., 1977, "Influence on Strength of Compression Panels of Stiffener Section, Spacing, and Weld Connection", Proc. of Inst. of Civil Engrs., Vol. 63, Part 2, pp. 1-20.

Horne, M.R., and Narayanan, R., 1977, "Design of Axially Loaded Stiffened Plates," J. of Structural Engineering, ASCE, 113(ST11), pp. 2243-2257.

Hughes, O.F., 1985, "A General Method for Computer-Aided Optimum Structural Design of Large, Complex Thin-Wall Structures," ICCAS 85 Proceedings, Trieste.

Hughes, O. F.,1988, *Ship Structural Design*, SNAME, Jersey City, N.J., second edition (first edition published by Wiley, 1983).

Hughes, O.F. and Caldwell, J.B., 1991 *Marine Structures; Selected Topics, Examples and Problems*, SNAME, Jersey City, NJ.

Jensen, J. J., and Pedersen, P. T.,1981, "Bending Moments and Shear Forces in Ships Sailing in Irregular Seas," Journal of Ship Research, Vol. 25, No. 4, December, pp. 243-251.

Kaneko, Y., Takahashi, T., 1986, "Comparison Between Non-linear Strip Theory and Model Experiment on Wave Bending Moment Acting on a Semi-displacement Type High-speed Craft," Tr. West-Japan Society of Naval Architects, Vol. 71, March.

Kaplan, P. and Sargent, T.P., 1972, "Further Studies of Computer Simulation of Slamming and Other Wave-Induced Vibratory Structural Loadings on Ships in Waves," Ship Structure Committee, Report No. SSC-231.

Kaplan, P., 1984, "Analysis and Assessment of Major Uncertainties Associated with Ship Hull Ultimate Failure," Ship Structure Committee, Report No. SSC-332.

Kaplan, P., 1986, "Analysis and Predictions of Flat Bottom Slamming Impact of Advanced Marine Vehicles in Waves," International Shipbuilding Progress, March.

Kim, C. M.,1982, "Hydrodynamic Loads on the Hull Surface of the Seagoing Vessel," SNAME Spring Meeting/STAR Symposium, Honolulu.

Kutt, L.M., Piaszczyk, C.M., Chen, Y.K., and Liu, D., 1985, "Evaluation of the Longitudinal Ultimate Strength of Various Ship Hull Configurations," SNAME Transactions, Vol. 93, pp. 33-53.

Lai, K.-L. and Ayyub, B.M., 1989, "Structural Reliability Assessment Using Latin Hypercube Sampling," Proceedings, 5th International Conference on Structural Safety and Reliability(ICOSSAR '89), San Francisco.

Larabee, R. D., and Cornell, C. A.,1981, "Combination of Various Load Processes," Journal of the Structural Division, ASCE, Vol. 107, pp. 223-239.

Lersbryggen, P., Ed., 1978, *Ship's Load and Strength Manual*, Det norske Veritas, Hovik, Norway,.

Lewis, E.V., 1967, "Predicting Long Term Distribution of Wave Induced Bending Moments in Ship Hull," SNAME Spring Meeting.

Lewis, E. V. et al., 1978, "Great Lakes Carriers Hull Stress Monitoring System," MarAd Report No. MA-RAD-940-79048, Dec. 1978.

Lindemann, K, and Robertson, S., 1981, "S03 Project-Final Report," U.S. Coast Guard Report No. CG-M-9-81, U.S. Coast Guard Headquarters, Washington, D.C.

Liu, P. L., and Kiureghian, A. D.,1986, "Optimization Algorithms for Structural Reliability Analysis," Dept. of Civil Engineering, University of California at Berkeley, Report No. UCB/SESM-86/09.

Madsen, H. O., Krenk, S., and Lind, N. C., 1986, Methods of Structural Safety, Prentice-Hall, Edglewood Cliffs, NJ.

Madsen, H. O., Skjong, R., and Moghtaderi-Zadeh, M., 1986, "Experience on Probabilistic Fatigue Analysis of Offshore Structures," Proceedings, 5th International Symposium on Offshore Mechanics and Arctic Engineering, ASME, New York.

Mansour, A.E., 1977, "Gross Panel Strength Under Combined Loading," Ship Structures Committee Report SSC-270.

Mansour, A.E. and Lozow, J., 1982, "Stochastic Theory of the Slamming Response of Marine Vehicles in Random Seas," Journal of Ship Research, Vol. 26, No. 4, pp. 276-285.

Mansour, A.E., et al, 1984, "Implementation of Reliability Methods to Marine Structures," Trans. SNAME.

Mansour, A.E., 1987, "Extreme Value Distributions of Wave Loads and Their Application to Marine Structures," Marine Structural Reliability Symposium, Arlington, Virginia, 1987.

Mansour, A.E., Yang, J.M., and Thayamballi, A., 1990, "An Experimental Investigation of Ship Hull Ultimate Strength," Trans. SNAME, Vol. 98.

Mansour, A.E., 1987, Tutorial Summary on Structural Reliability Theory Directed at the Marine Industry, Ship Structures Committee Report, U.S. Coast Guard.

Mattu, R. K.,1980, "Methodology for Combining Dynamic Responses," NUREG-0484, Rev. 1, Office NRR, V.S. NRC, May, 1980.

Melchers, R.E., 1987, Structural Reliability Analysis and Prediction, Ellis Horwood Limited, UK.

Michelutti, W. M., Murray, N. W., 1977, "The Collapse Behavior of Stiffened Plates under Combined Axial and Bending Loads," 6th Australian Conference on the Mechanics of Structures and Materials, Univ. of Canterbury, Christchurch, New Zealand.

Moses, F., 1985, "Implementation of a Reliability-Based APIRP2A Format," Final Report, APIPRAC 83-22, American Petroleum Institute.

Moses, F., 1986, "Development of Preliminary Load and Resistance Design Document for Fixed Offshore Platforms," Final Report, APIPRAC 85-22, American Petroleum Institute.

Munse, W. H., Wilbur, T. W., Tellalian, M. L., Nicoll, K., and Wilson, K.,1982, "Fatigue Characterization of Fabricated Ship Details for Design," Ship Structure Committee, Report No. S.S.C.-318.

Murray, N.W., 1975, "Analysis and Design of Stiffened Plates for Collapse Loads," The Structural Engineer, London, England, Vol. 53, pp. 153-158.

Naess, A.,1982, "Extreme Value Estimates Based on Envelope Concept," Applied Ocean Research, No. 3, Vol. 4.

National Cooperative Highway Research Program (NCHRP), 1992, "Development of Comprehensive Bridge Specifications and Commentary," Third Draft of LRFD Specifications and Commentary, National Research Board.

NBCC(National Building Code of Canada), 1975, 1977, 1980, National Research Council of Canada, Ottawa, Ontario.

Nikolaidis, E., Perakis, A. N., and Parsons, M. G.,1989, "Probabilistic Torsional Vibration Analysis of a Marine Diesel Engine Shatting System: The Level Crossing Problem," Journal of Applied Mechanics, pp. 953-959, Vol. 56, No. 4.

Nikolaidis, E., Ayyub, B.M., Hughes, O., and White, G.J., 1992, "Assessment of Reliability of Ship Structures," Small Business Innovation Research Program, SBIR-Phase I, Topic Number N91-100.

Nikolaidis, E. and Kapania, R.K., 1990, "System Reliability and Redundancy of Marine Structures: A Review of the State of the Art," Journal of Ship Research, Vol. 34, No. 1, pp. 48-59.

Nikolaidis, E. and Kaplan, P., 1991, "Uncertainties in Stress Analysis of Marine Structures," Ship Structure Committee, Report S.S.C.-363, 1991. Also accepted for publication in International Shipbuilding Progress.

NKB (The Nordic Committee on Building Regulations), 1978, "Recommendations for Loading and Safety Regulations for Structural Design," NKB Report, No. 36, Copenhagen.

Nordenstrom, N.,1973, "Wave Loads, Statistical Approach," Report of Committee 3, 5th International Ship Structures Congress, Hamburg.

Ochi, M.K. and Motter, L.E., 1973, "Prediction of Slamming Characteristics and Hull Responses for Ship Design," SNAME Transactions, Vol. 81, pp. 144-176.

Ochi, M.K., 1978, "Wave Statistics for the Design of Ships and Ocean Structures," SNAME Transactions, Vol. 86, pp. 47-69.

Ochi, M.K., 1979(a), "Principles of Extreme Value Statistics and Their Application," Proceedings of Extreme Loads Response Symposium SNAME, pp. 15-30.

Ochi, M.K., 1979(b), "Extreme Values of Waves and Ship Responses Subject to the Markov Chain Condition," Journal of Ship Research, Vol. 23, No. 3, pp. 188-197.

Ochi, M.K., 1981, "Principles of Extreme Value Statistics and Their Application," Extreme Loads Response Symposium, SNAME, Arlington, VA.

Ochi, M. K.,1990, Applied Probability and Stochastic Processes, John Wiley and Sons, New York.

Olufsen, A. and Bea, R.G., 1990 "Uncertainties in Extreme Wave Loading on Fixed Offshore Platforms," OMAE Proceedings.

Petrie, G.L., Maclean, W.M., Cojeen, H.P., and Schudel, L.G., 1986, "The Usefulness of Response Monitoring for Estimation of Bow Structural Loadings," Marine Technology, Vol. 23, No. 3.

Pinkham, C.W., and Hansell, W.C., 1978, "An Introduction to Load and Resistance Factor Design for Steel Buildings," Engineering Journal, AISC, 15(1), 2-7.

Pittaluga, A., 1987, "Reliability Based Ship Design in the 90's: Realistic Scenario or a Dream? Registro Italiano Navale, Technical Bulletin N. 100, Genova.

Raff, A. I.,1972, "Program SCORES - Ship Structural Response in Waves," Ship Structure Committee, Report No. SSC-230, Washington, D.C..

Rask, I.,1986, "Slamming Pressure in Short-Crested and Oblique Seas," Report No. 105, Dept. of Marine Structural Engineering, Chalmers University of Technology, Goteborg.

Ravindra, M. K. and Galambos, T. V., 1978, "Load and Resistance Factor Design for Steel," Journal of Structural Engineering, ASCE, 104(9), 1337-1353.

Salvesen, N., Tuck, E. O., and Faltinsen, O.,1970, "Ship Motions and Sea Loads," SNAME Transactions, Vol. 28, pp. 250-287.

Smith, C.S., 1975 "Compressive Strength of Welded Steel Ship Grillages," *Trans. RINA*, 117, pp. 325-359.

Soding, H., 1974, "Calculation of Long-Term Extreme Loads and Fatigue Loads of Marine Structures," The Dynamics of Marine Vehicles and Structures in Waves, Bishop, R.E.D. and Price, W.G.(Eds.), Institution of Mechanical Engineers, London, pp. 373-387.

Takemoto, M.,1984, "Wave Impact Test of a Wedge with Rectangular Plates and Analysis," Journal of Society of Naval Architects of Japan, December, 1984.

Takemoto, M., Hashizume, Y., and Oka, S., 1985, "Full-scale Measurement of Wave Impact Loads and Hull Response of a Ship in Waves," Journal of the Society of Naval Architects of Japan, Vol. 158.

Thoft-Christensen, P. and Murotsu, Y., 1986, Applications of Structural Systems Reliability Theory, Springer Verlag, Berlin.

Timoshenko, S.and Woinowsky-Krieger, S., 1959, "Theory of Plates and Shells",McGraw-Hill.

Troesch, A.W., 1984, "Wave-Induced Hull Vibrations: An Experimental and Theoretical Study," J. Ship Research, Vol. 28, No. 2, 141-150.

Turkstra, C.J., 1970, Theory of Structural Safety, SM Study No. 2, Solid Mechanics Division, University of Waterloo, Waterloo, Ontario.

Vantorre, M.,1986, "Third-Order Theory for Determining the Hydrodynamic Forces on Axisymmetric Floating or Submerged Bodies in Oscillatory Heaving Motion," Ocean Eng., Vol. 13, No. 4, 339-371.

Vulovich, R., Hirayama, T., Toki, N., and Mizuno, M., 1989, "Characteristics of Hull Stresses Measured on a Large Containership in Rough Seas," SNAME Transactions, Vol. 97, pp. 397-428.

Wen, Y. K.,1977, "Statistical Combination of Extreme Loads," Journal of Structural Division, ASCE, Vol. 103, No. ST5, May 1977, pp. 1079-1093.

Wen, Y.K. and Pearce, H.T., 1982, "Combined Dynamic Effects of Correlated Load Processes," Nuclear Engineering and Design, Vol. 75, pp. 179-189.

White, G.J. and Ayyub, B.M., 1985, "Reliability Methods for Ship Structures," Naval Engineers Journal, ASNE, Vol. 97, No. 4, pp. 86-96.

White, G.J. and Ayyub, B.M., 1987a, "Probability-Based Design Formats for Marine Structures," Journal of Ship Research, SNAME, Vol. 31, No. 1, pp. 60-69.

White, G.J. and Ayyub, B.M., 1987b, "Reliability-Based Fatigue Design for Ship Structures," Naval Engineers Journal, ASNE, Vol. 99, No. 3, pp. 135-149.

Williams, D.G., and Chapman, J.C., 1974, "Tests on a One Eighth Scale Model of the Double-Bottom Structure," *Trans. RINA*, pp. 329-345.

Winterstein, S.R. and Cornell, C.A., 1984, "Load Combinations and Clustering Effects," Journal of Structural Engineering, Vol. 110, No. 11, pp. 2690-2708.

Wirsching, P. M.,1984, "Fatigue Reliability for Offshore Structures," Journal of Structural Engineering, Vol. 110, No. 10, pp. 2340-2356.

Wirsching, P. H., and Chen, Y. N.,1987, "Considerations of Probability-Based Fatigue Design for Marine Structures," Proceedings of the Marine Structural Reliability Symposium, pp. 31-43.

Wu, Y.-T. and Wirsching, P.H., 1987, "New Algorithm for Structural Reliability Estimation," Journal of Engineering Mechanics, Vol. 113, No. 9.

Yang, J.-S., Nikolaidis, E., and Haftka, R.T., 1990, "Design of Aircraft Wings Subjected to Gust Loads: A System Reliability Approach," Computers and Structures, Vol. 36, No. 6, pp. 1057-1066.

Yang, J.-S. and Nikolaidis, E., 1991, "Design of Aircraft Wings Subjected to Gust Loads: A Safety Index Based Approach," AIAA Journal, Vol. 29, No. 5, pp. 804-812.
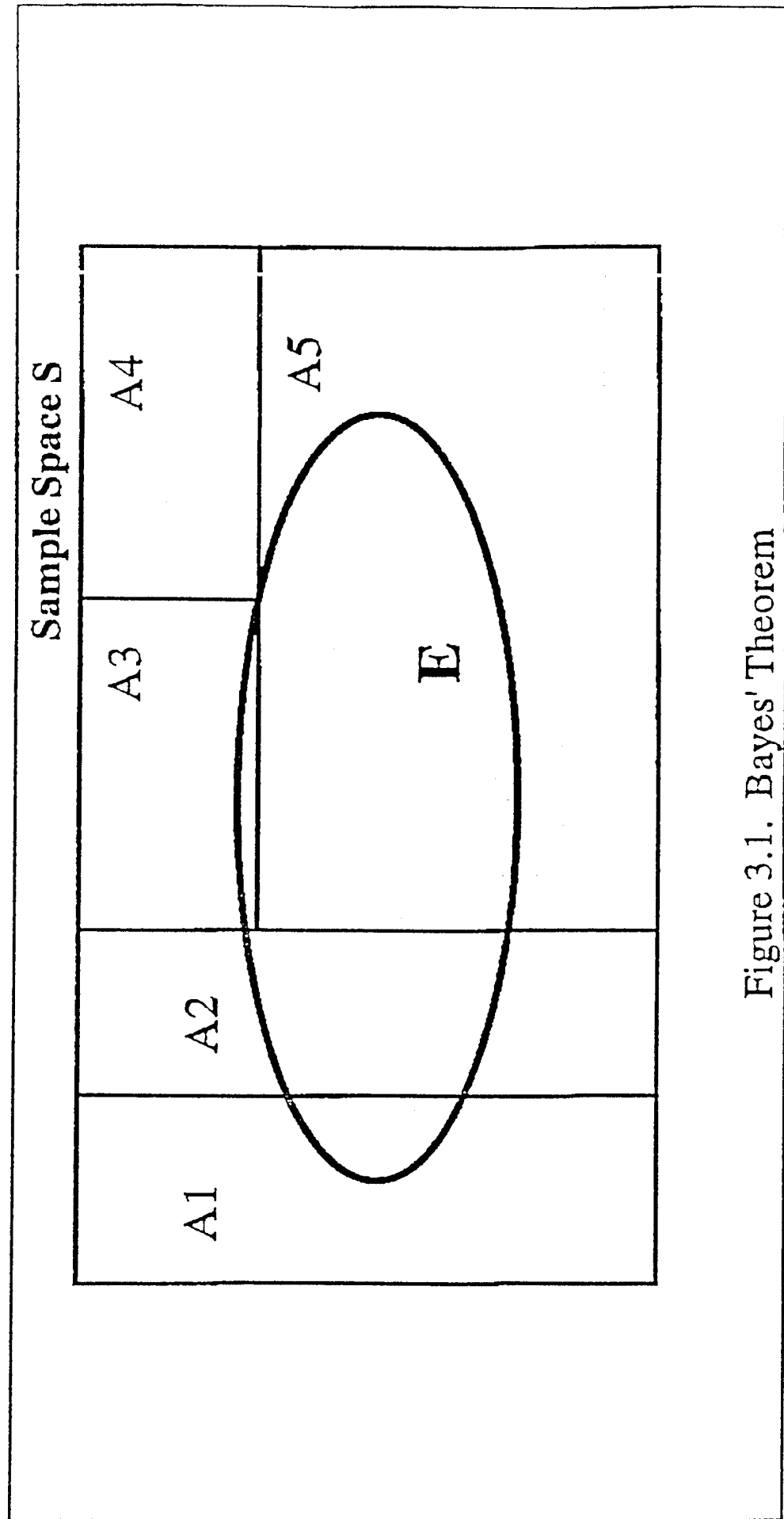
FIGURES

Sample Space S

A1 A2 A3 A4 A5

E

Figure 3.1. Bayes' Theorem

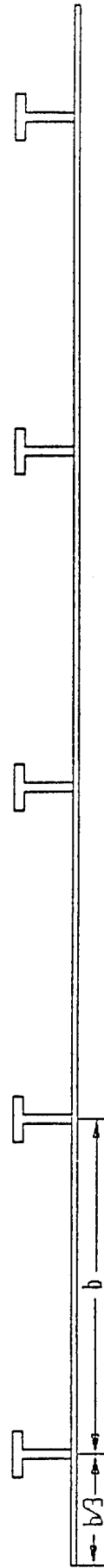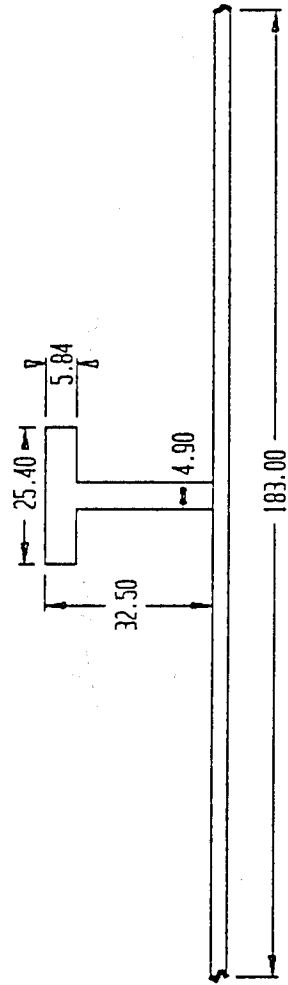Length=790 mm

5.84

25.40

4.90

183.00

32.50

dimensions are in millimeters

b

b/3

Figure 6-1. Cross-sectional View of a Panel in Nominally Identical Series
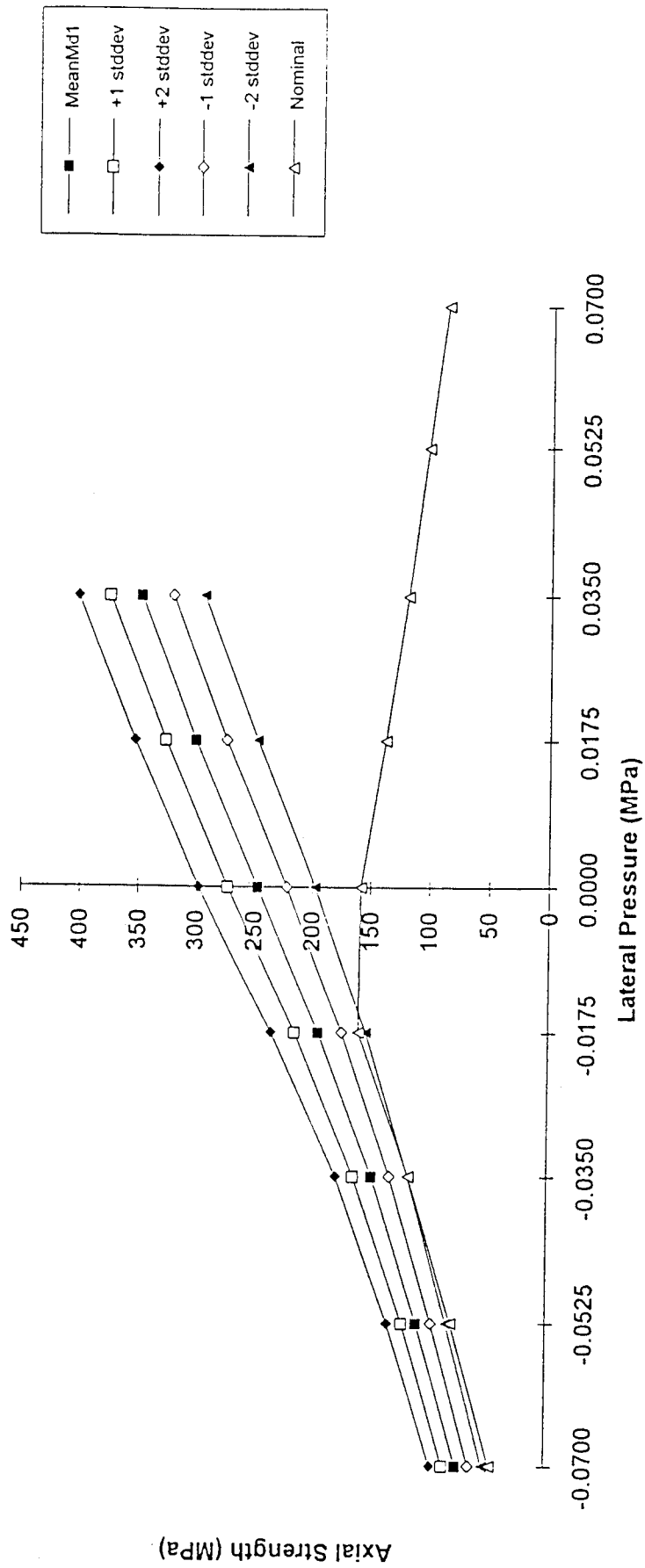
79

Figure 6-2. Case A, Mode I Failure (Panel with Negative Eccentricity): Effect of Random Uncertainties on Strength.

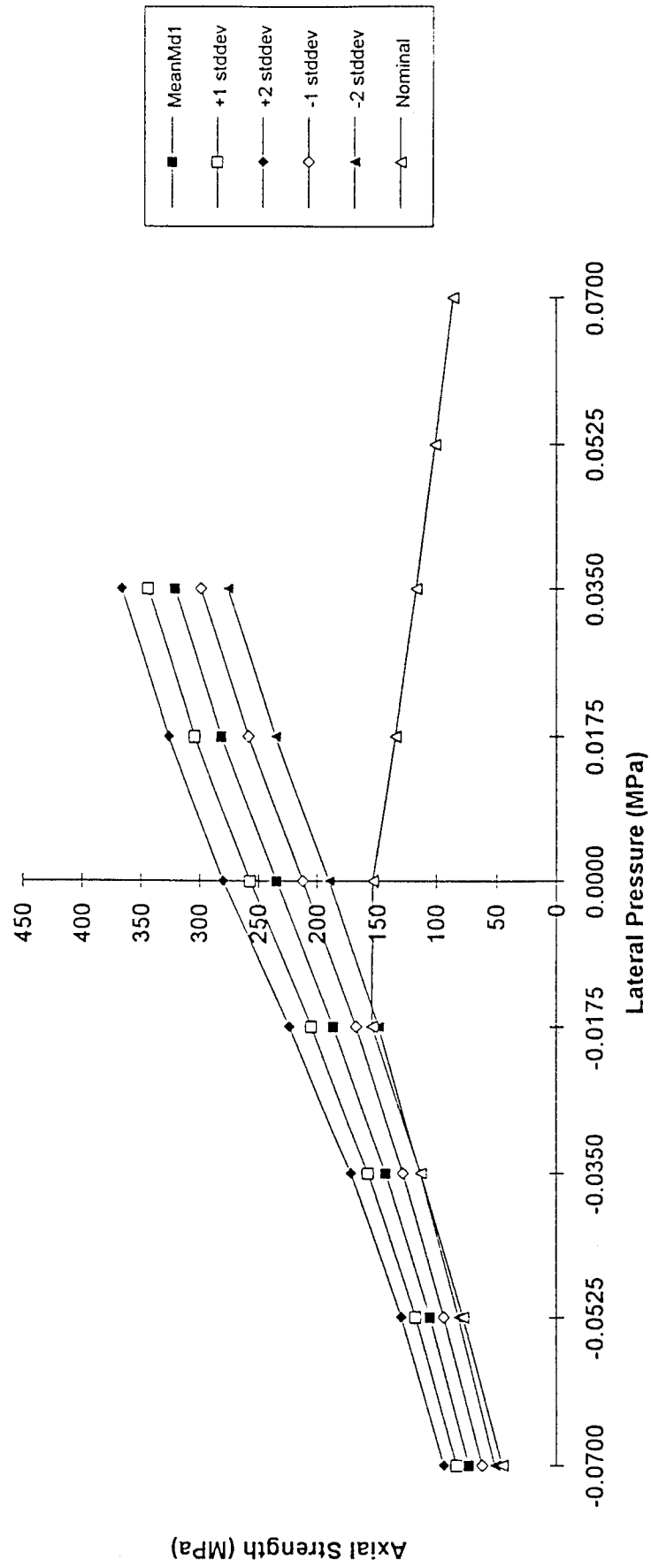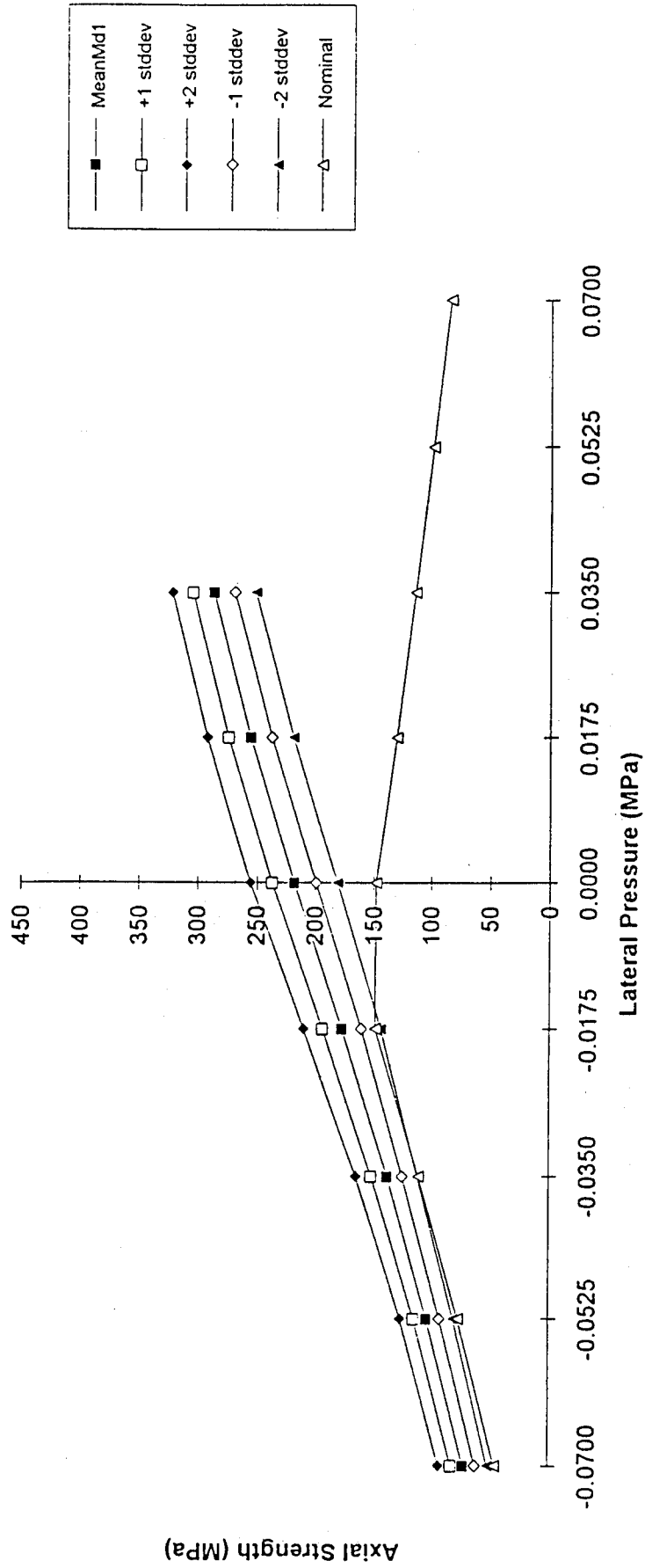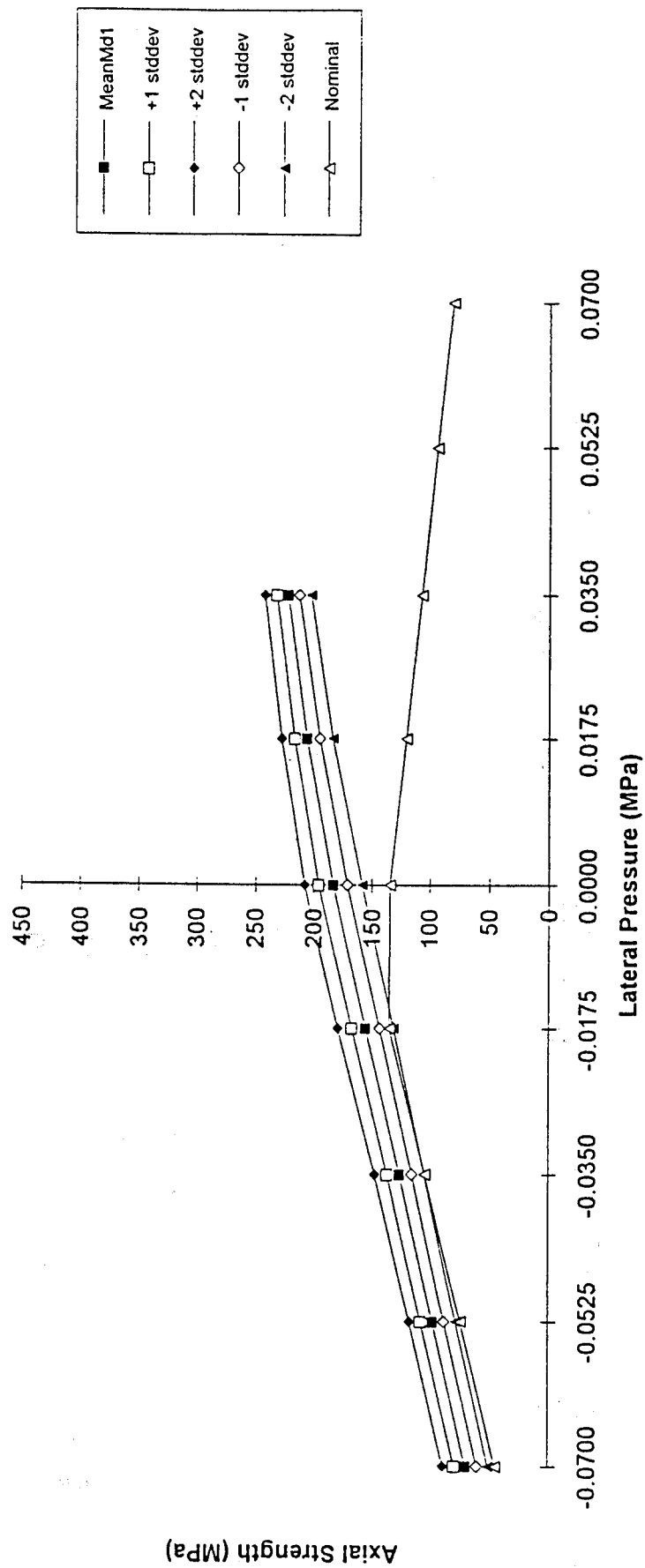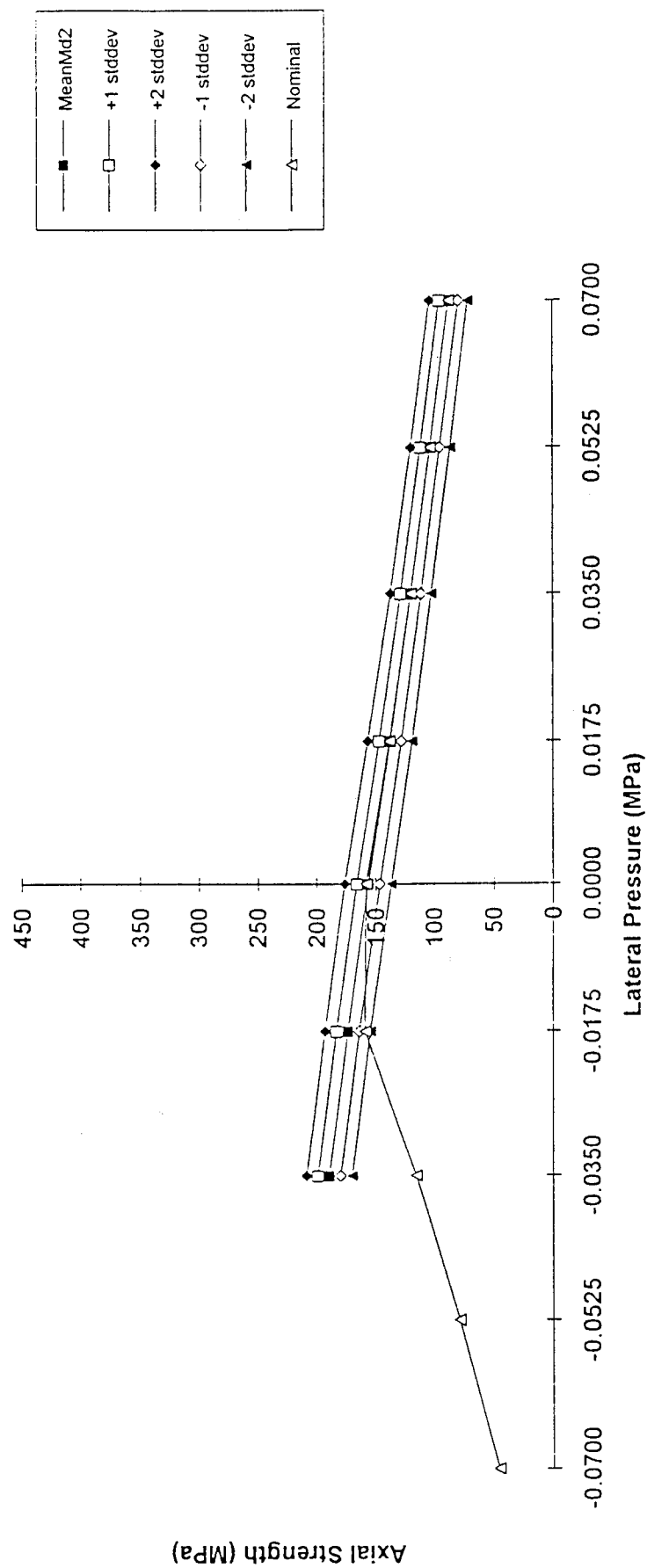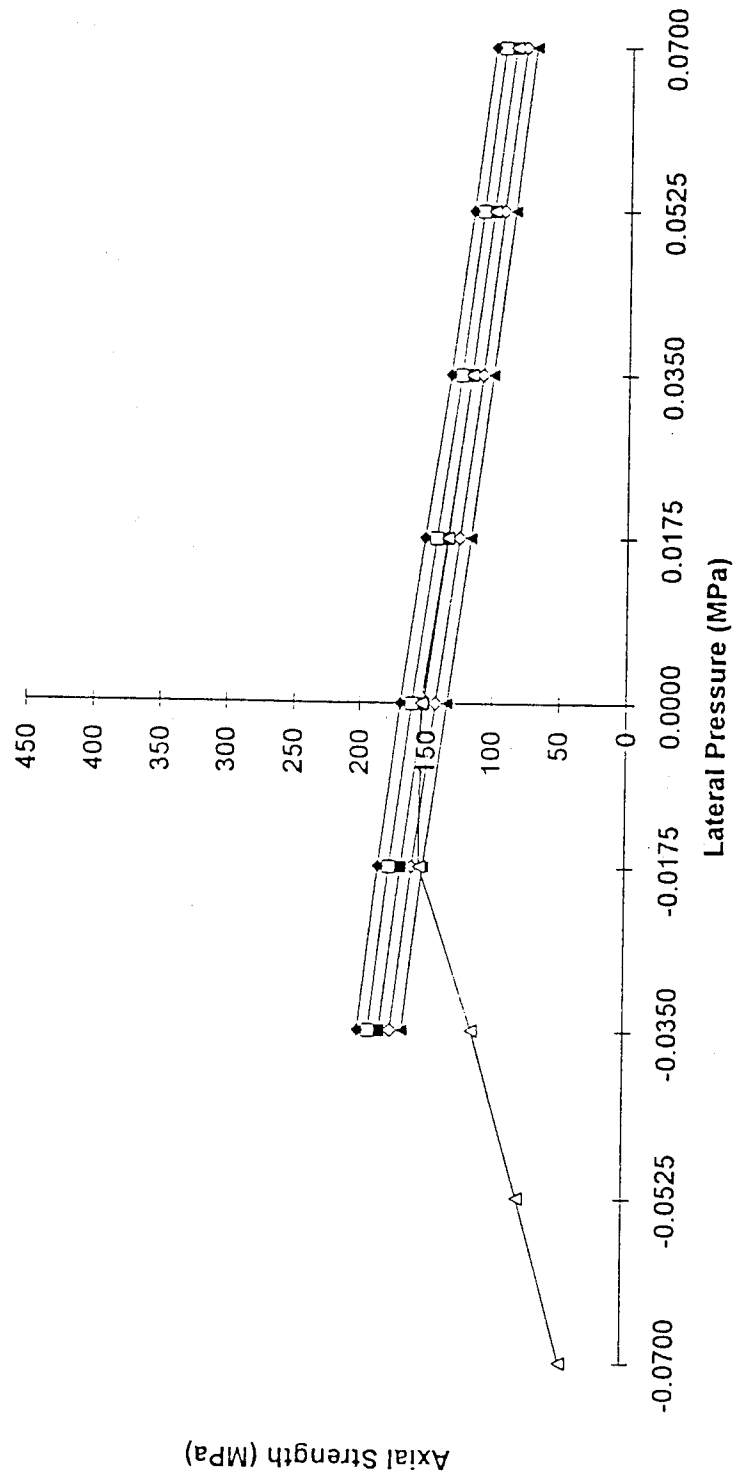Figure 6-3. Case B, Mode I Failure (Panel with Negative Eccentricity): Effect of Random Uncertainties on Strength.

81

Figure 6-4. Case C, Mode I Failure (Panel with Negative Eccentricity): Effect of Random Uncertainties on Strength.

82

Figure 6-5. Case D, Mode I Failure (Panel with Negative Eccentricity): Effect of Random Uncertainties on Strength.

83

Figure 6-6. Case A, Mode II Failure (Panel with Positive Eccentricity): Effect of Random Uncertainties on Strength.
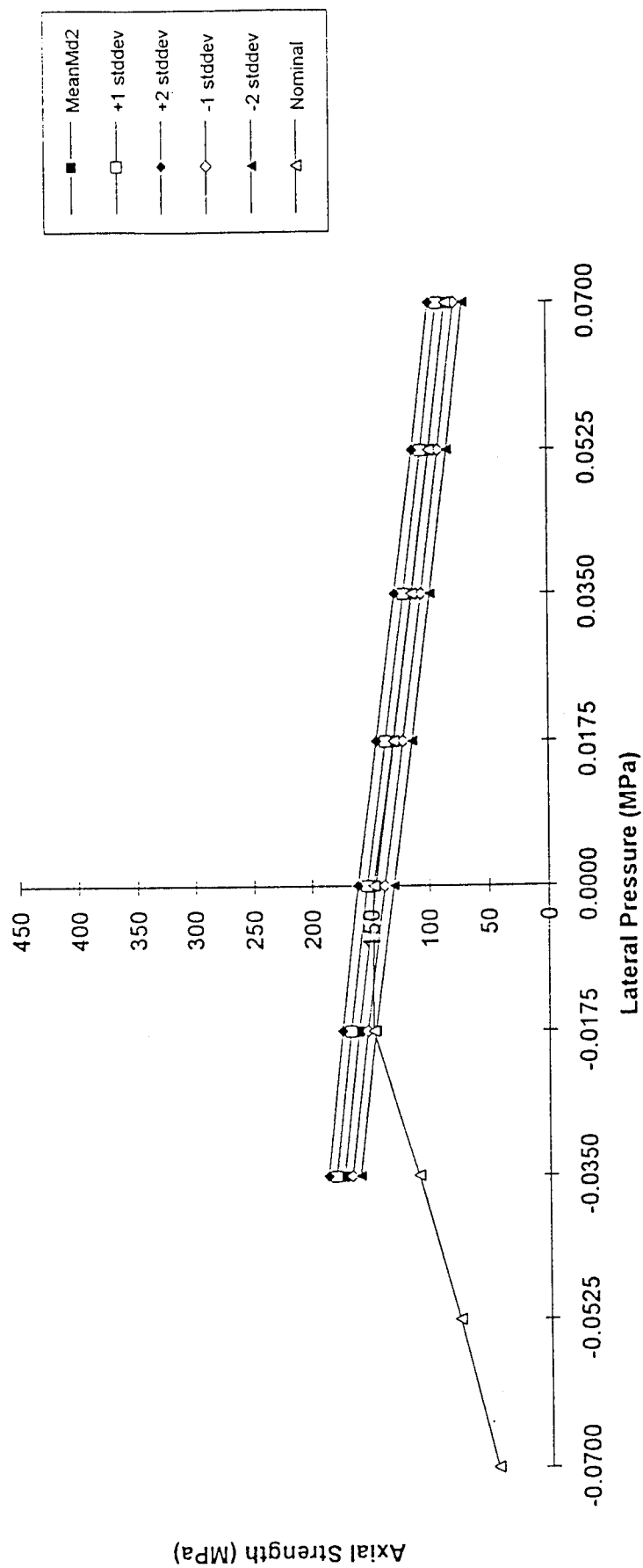
84

Figure 6-7. Case B, Mode II Failure (Panel with Positive Eccentricity):
Effect of Random Uncertainties on Strength.

85

Figure 6-8. Case C, Mode II Failure (Panel with Positive Eccentricity): Effect of Random Uncertainties on Strength.

Figure 6-9. Case D, Mode II Failure (Panel with Positive Eccentricity): Effect of Random Uncertainties on Strength.
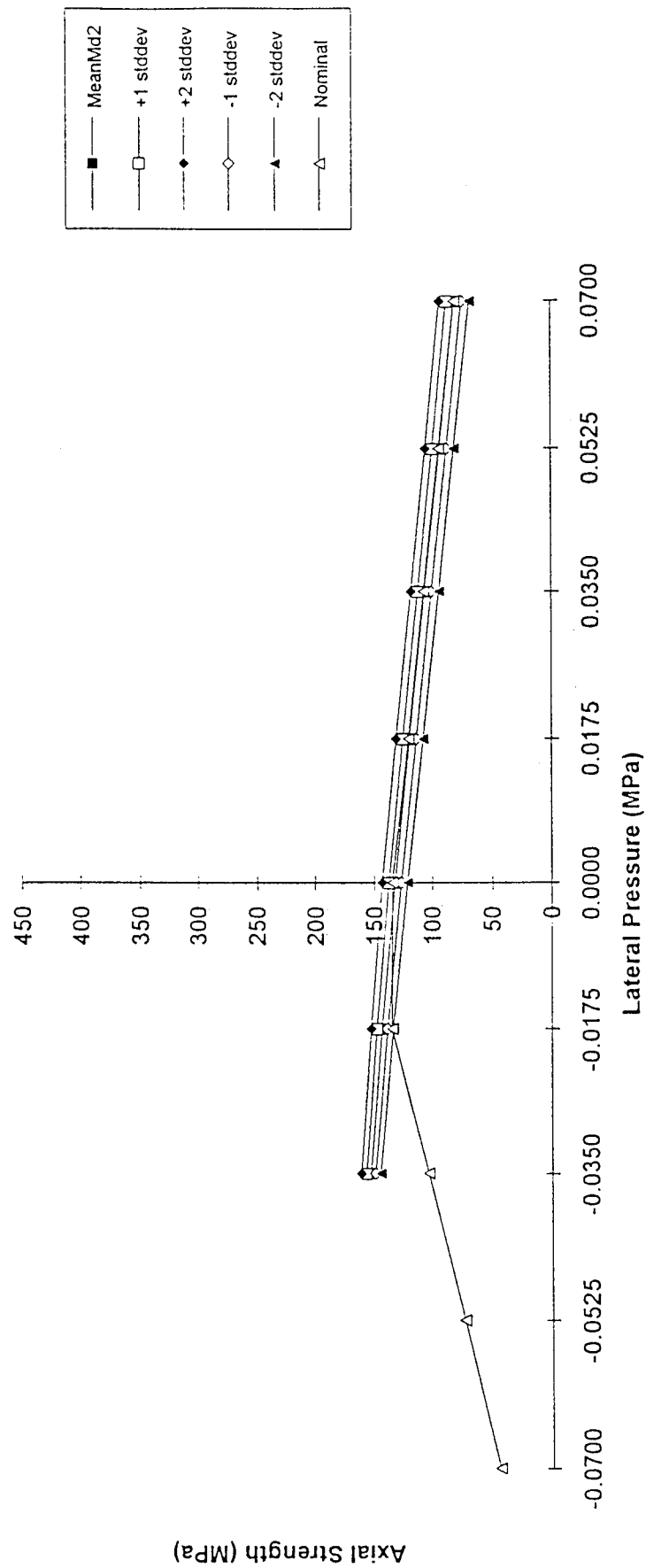
Figure 6-10. Mode I, Parametric Analysis: Contributions of Random Uncertainties to Uncertainty in Strength
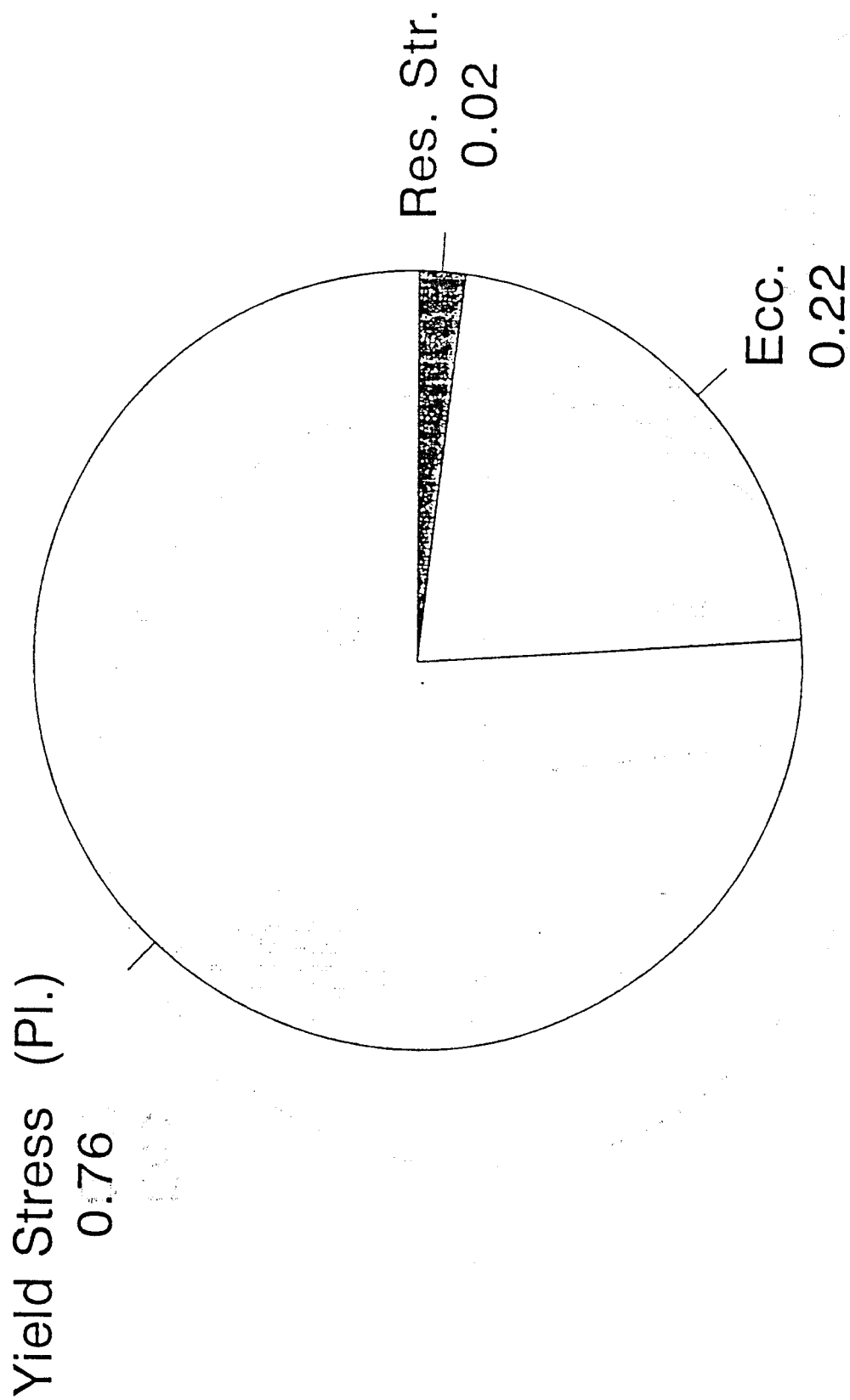
Figure 6-11. Mode II, Parametric Analysis: Contributions of Random Uncertainties to Uncertainty in Strength
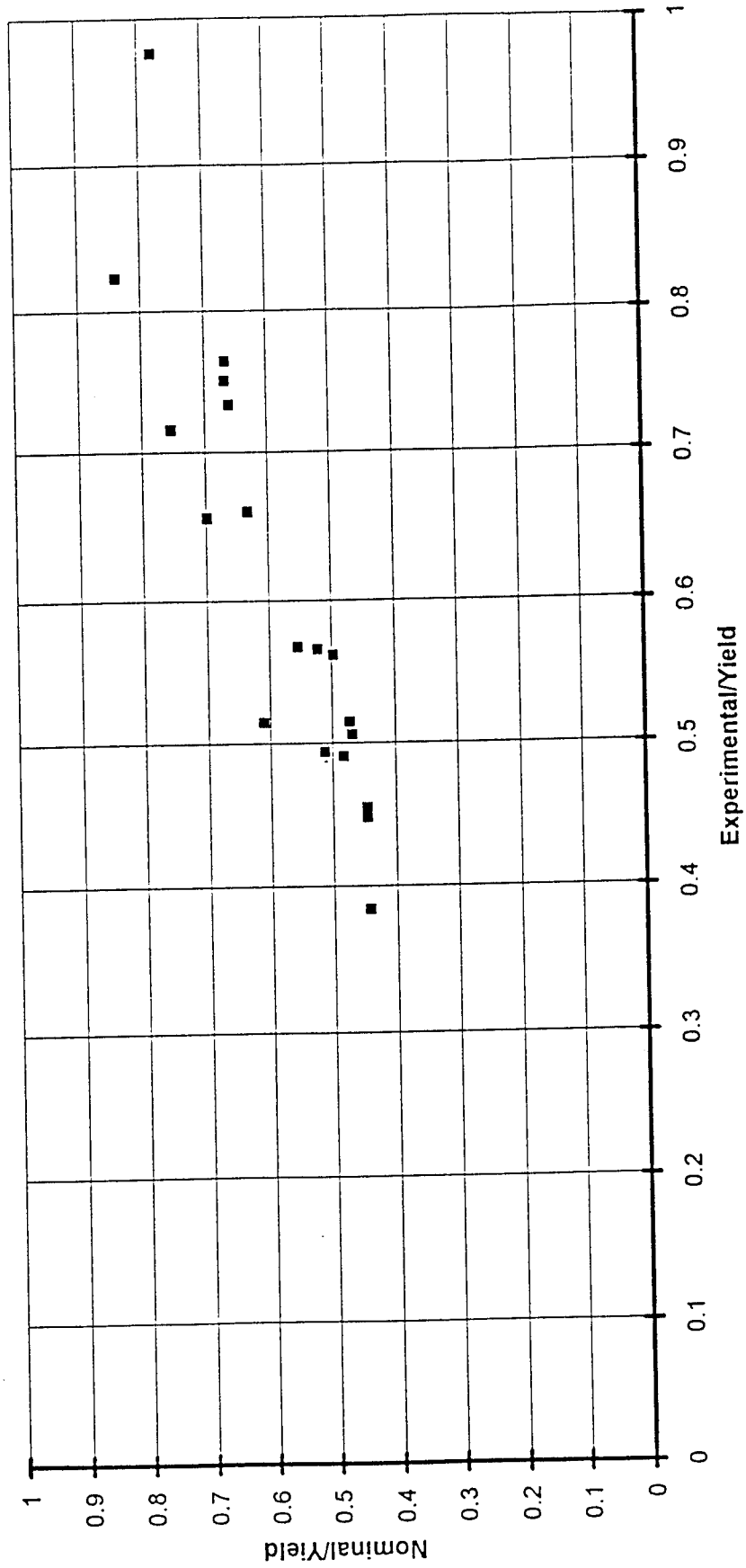
Figure 6-12. Correlation Between Experimental and Nominal Values of Strength for Parametric Series

Posterior Mean
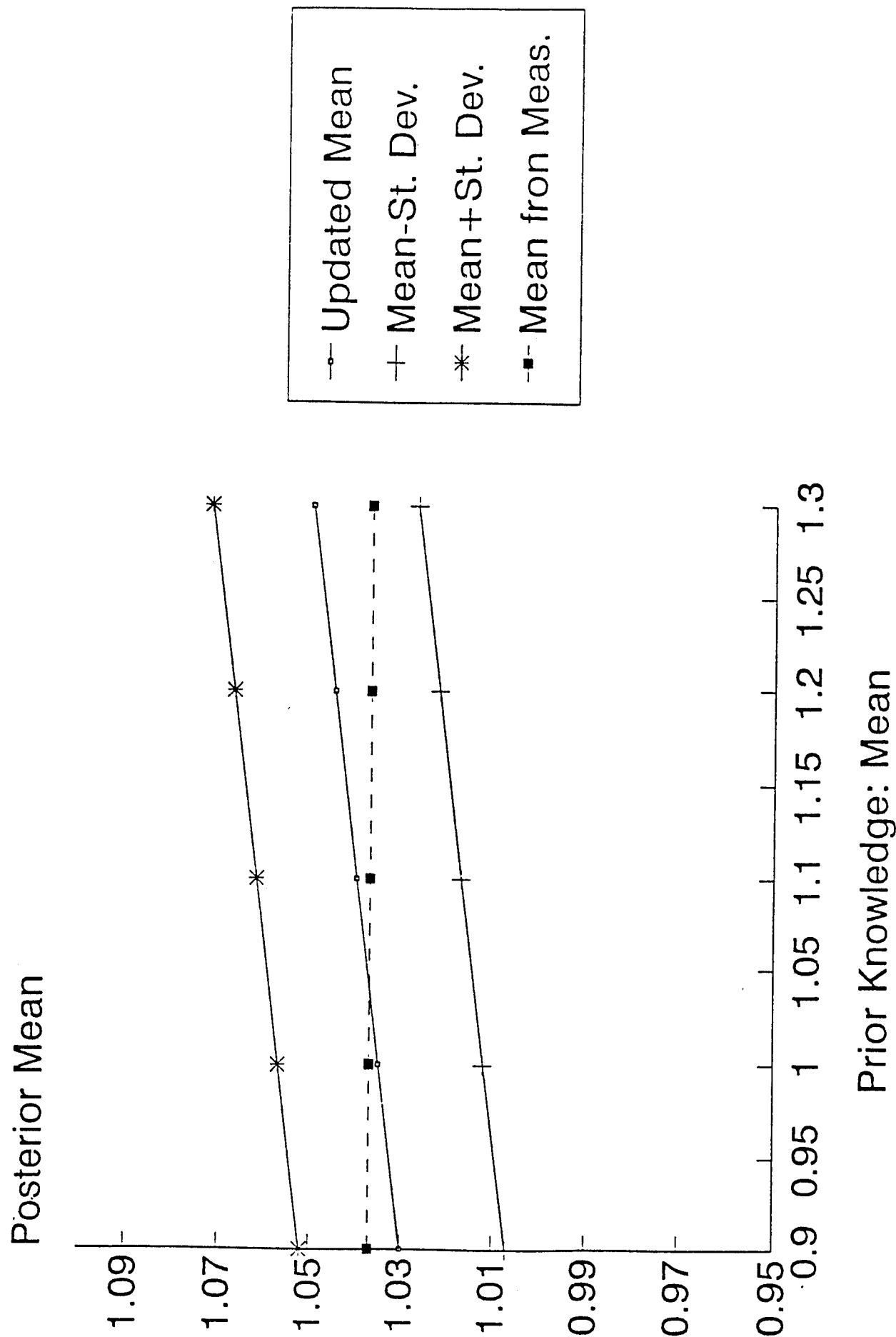

Prior Knowledge: Mean

Figure 6-13. Bayesian Estimation of Mean Bias Using Results from
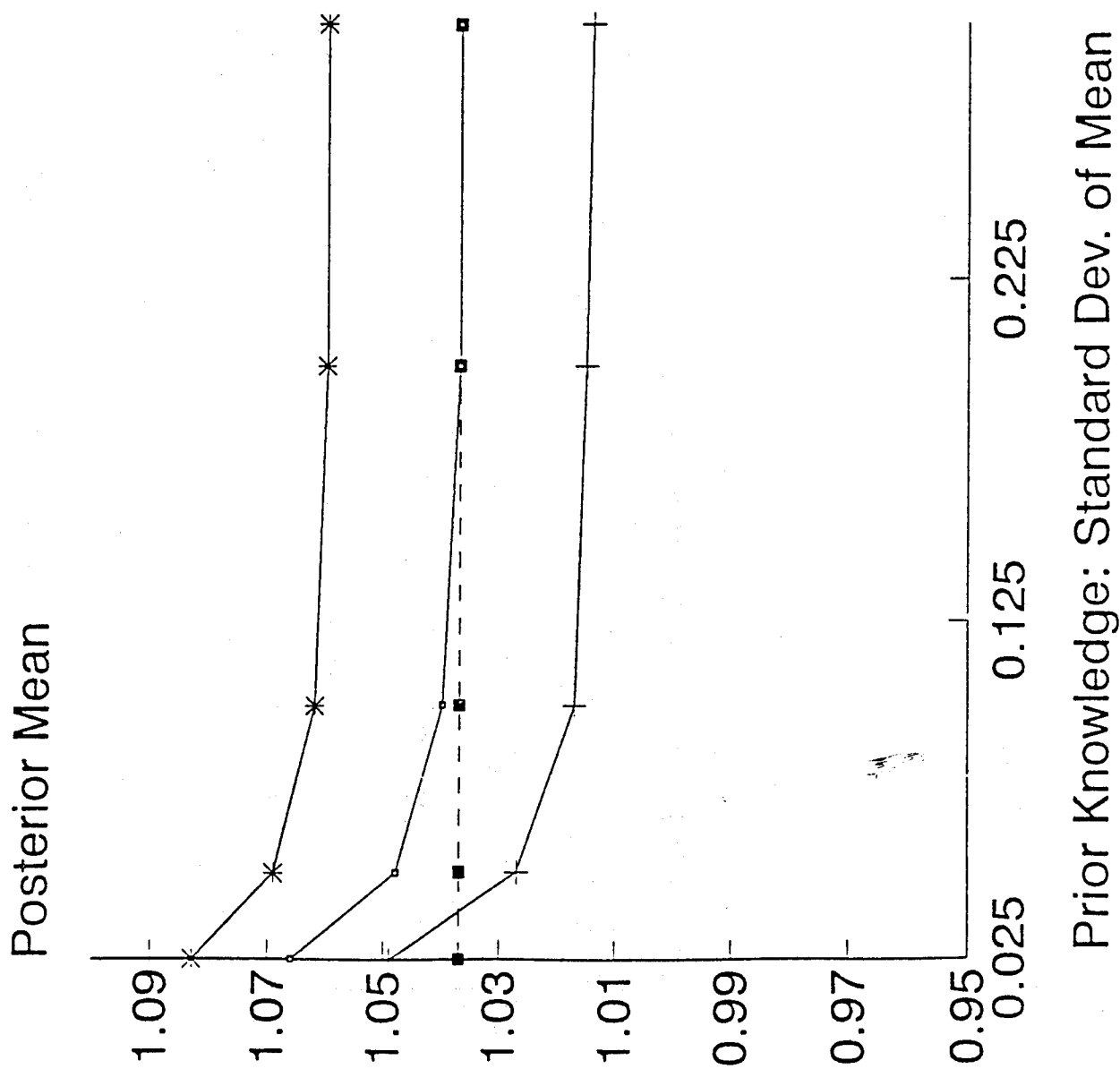Parametric Series: Posterior Mean vs. Prior Estimate of Mean

Figure 6-14. Bayesian Estimation of Mean Bias Using Results from Parametric Series: Posterior Mean vs. Prior Estimate of Standard Deviation of Mean

Figure 6-15. Bayesian Estimation of Mean Bias Using Michelutti's Results:
Posterior Mean vs. Prior Estimate of Mean

Figure 6-16. Bayesian Estimation of Mean Bias Using Michelutti's Results: Posterior Mean vs. Prior Estimate of Standard Deviation of Mean

94

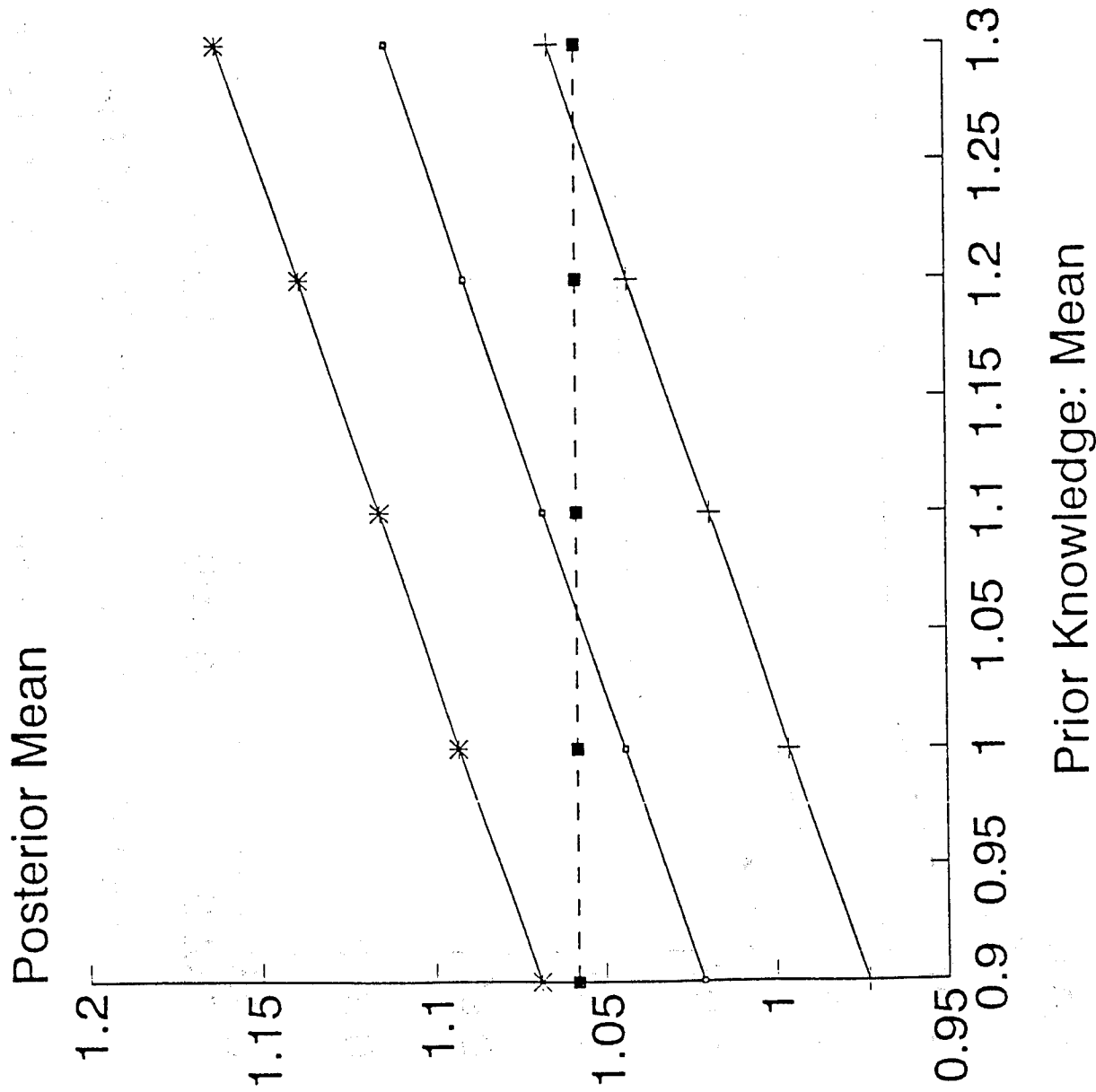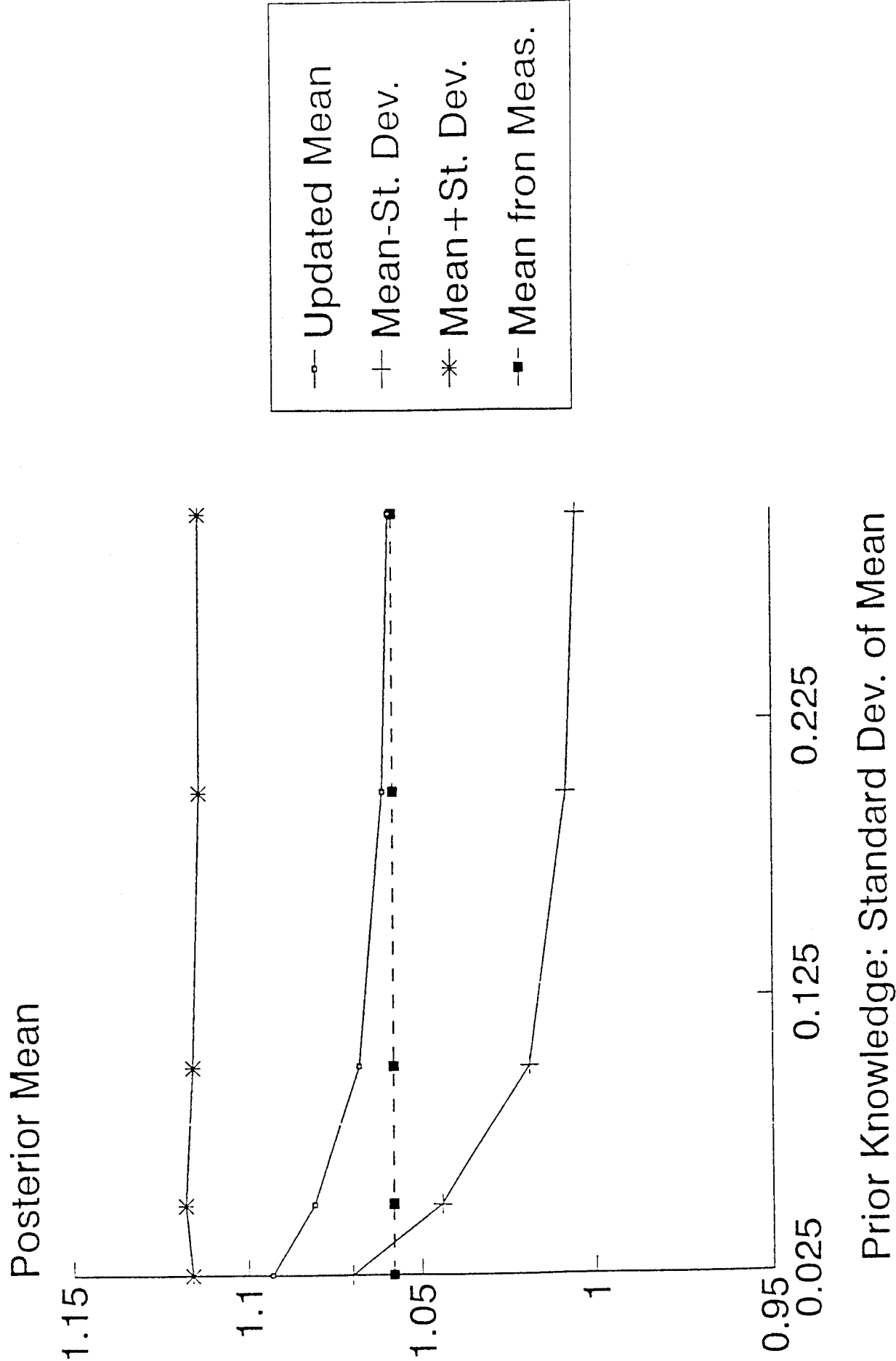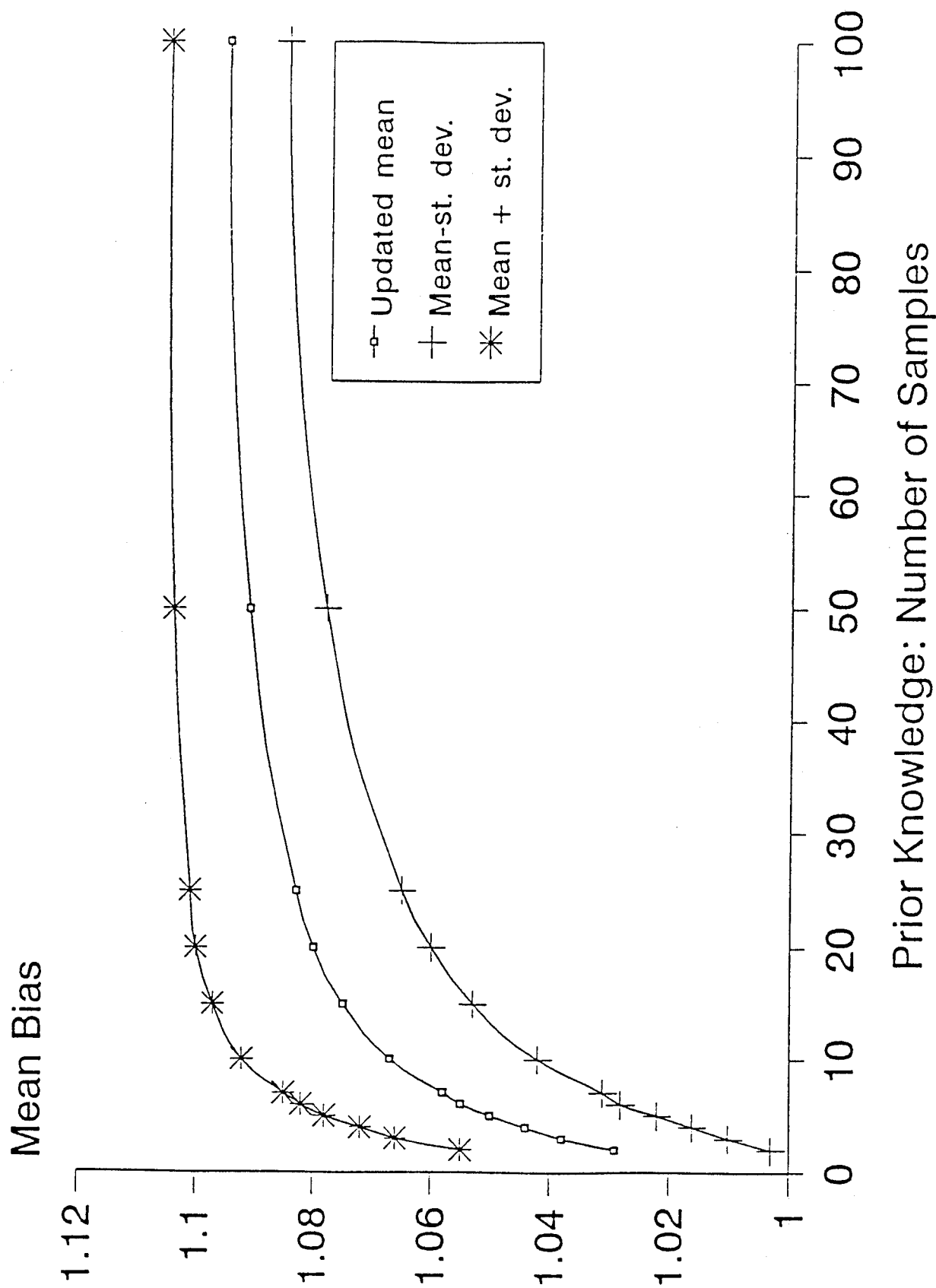Figure 6-17. Bayesian Method for Mean and Standard Deviation of Bias: Posterior Mean Bias vs. Number of Samples
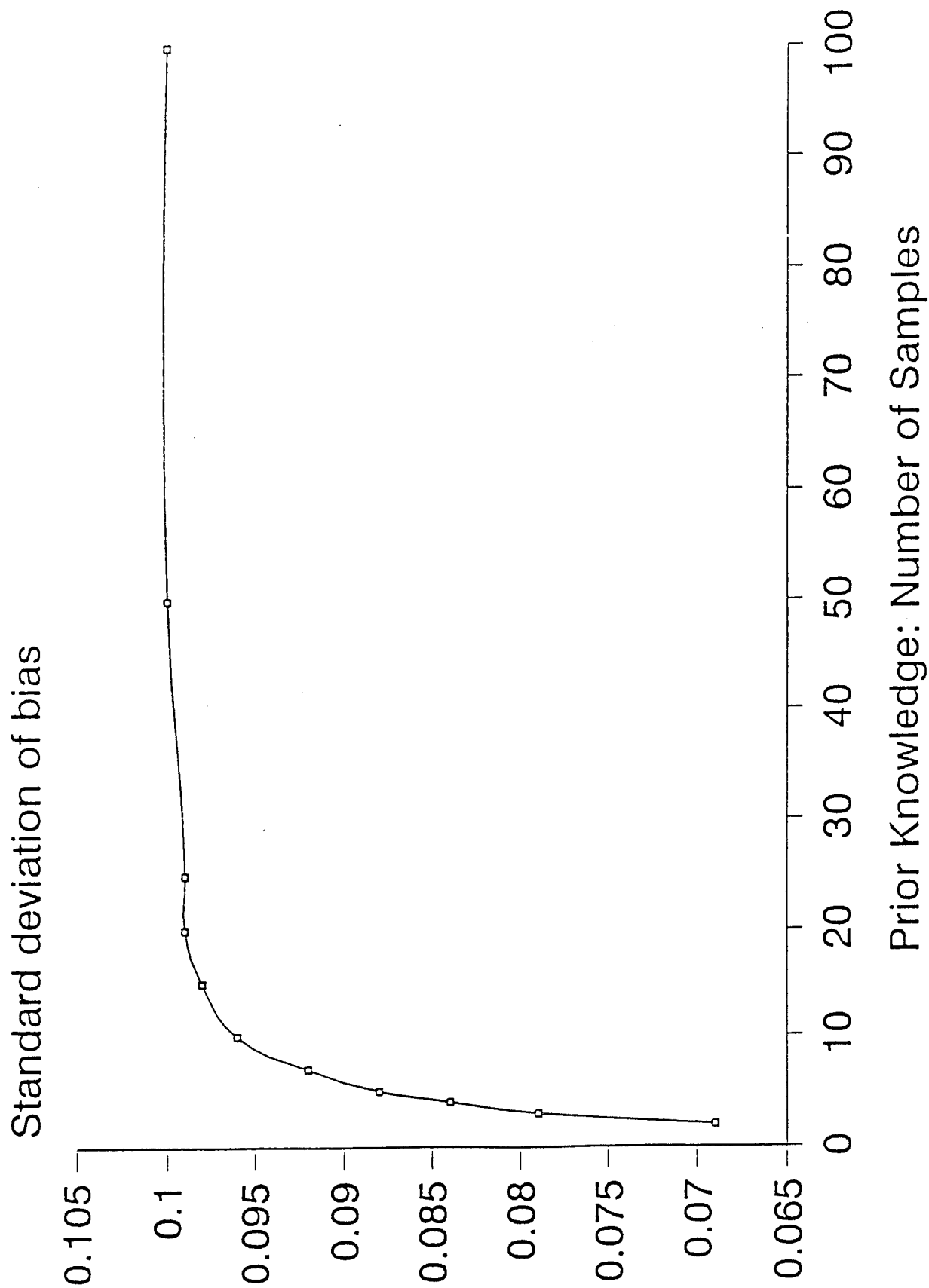
Figure 6-18. Bayesian Method for Mean and Standard Deviation of Bias: Posterior Standard Deviation vs. Number of Samples

APPENDIX A: REVIEW OF STIFFENER TRIPPING

APPENDIX A: REVIEW OF STIFFENER TRIPPING

A.1 Basic Theory of Elastic Tripping

When a stiffener is subjected to axial compression there are a number of ways for it to fail, including tripping. Tripping, or torsional buckling, differs from the buckling of a column in three ways: first, because the rotation occurs about the line of attachment between the plating and the stiffener; second, because the plating offers some resistance to the rotation; and third, because the stiffener itself may deflect and distort - it isn't rigid body rotation. For the case of typical ship structures the dimensions of the beams are such that we can consider the problem to be one of torsion of thin-walled members. As such, the governing differential equation for the rotation ϕ is (Hughes, 1988, also referred to as SSD)

$$EI_{sz}d^2\frac{d^4\phi}{dx^4}-\left(GJ-\sigma_aI_{sp}\right)\frac{d^2\phi}{dx^2}+K_\phi\phi = 0 \qquad (A-1)$$

where
- I_{sz} = moment of inertia of the stiffener only about an axis through the centroid of the stiffener and parallel to the web.
- $2d$ = stiffener web height.
- I_{sp} = polar moment of inertia of the stiffener about the center of rotation.
- K_ϕ = distributed rotational restrain which the plating exerts on the stiffener.

If the ends of the stiffener are regarded as simply supported, the solution for $\phi(x)$ is a buckled shape in which the rotation ϕ varies sinusoidally in m half-waves over the length a of the stiffener. The value of the applied in-plane stress which causes tripping according to elastic theory is denoted as $\sigma_{a,T}$. The solution to the above differential equation is the minimum value for the applied in-plane stress σ_a, that satisfies the following

$$EI_{sz}d^2\frac{m^4\pi^4}{a^4}+(GJ-\sigma_aI_{sp})\frac{m^2\pi^2}{a^2}+K_\phi(\sigma_a,m) = 0 \qquad (A-2)$$

The critical mode for tripping corresponds to whichever integer value of m gives the minimum value of σ_a. Note that the expression for K_ϕ is written as a function of both the number of half-waves m and the critical stress σ_a. It is dependent on the applied stress because if the stress is high enough to cause local plate buckling, the value of K_ϕ can go to zero or even become negative. The dependence on m is because the amount the value of K_ϕ diminishes with σ_a depends on whether the number of half-waves in the stiffener matches the number in the buckled plating. The other major contributor to the rotational restraint provided by the plating is the flexural rigidity of the plating.

The above discussion serves to show that the tripping of a stiffener involves three important variables which interrelate in a rather complex fashion: σ_a, m, and K_ϕ. The critical value of σ_a depends on K_ϕ and m, the value of m depends on the magnitude of K_ϕ relative to EI_{sz}, and K_ϕ depends on both σ_a and *m*.

A.2 AISC Approach to Tripping

The AISC Code looks at tripping as part of the special case of I-shaped beams subjected to strong axis bending. This sort of loading is considered in the marine industry to be a case of *flexural-torsional buckling* rather than lateral torsional buckling. In the flexure case the flange of the beam is put in compression due to the out-of-plane load causing a large bending moment. This is of great concern to bridge and building structural engineers because for these structures the predominant loads are out-of-plane loads which produce bending. They do not generally experience the very large in-plane types of loads that a ship's designer must be concerned with. However, the basic analysis procedure is the same and the LRFD approach adopted by the AISC should be carefully considered.

The strength requirement for tripping is considered to be a part of the overall strength requirement of the stability of I-shaped beams. The AISC procedure considers the full range of strength from laterally stable beams to situations where tripping causes considerable strength reduction. According to LRFD-F2, the strength requirement may be stated as

$$\phi_b M_n \geq M_u \tag{A-3}$$

where
ϕ_b = strength reduction factor for flexure = 0.90
M_n = nominal moment strength.
M_u = factored service load, typically given as a linear combination of Dead Load, Live Load and Wind or Snow Load, e.g. 1.2D + 1.6L + 0.5S.

Figure A.1, taken from Salmon and Johnson (1990), shows the effect of laterally unbraced length L_b on the flexural torsional buckling strength. The cases indicated as number 1 and 2 are not of direct interest. They represent situations where the beam reaches its full plastic moment, and other methods must be used for analysis. The last three cases are of more concern.
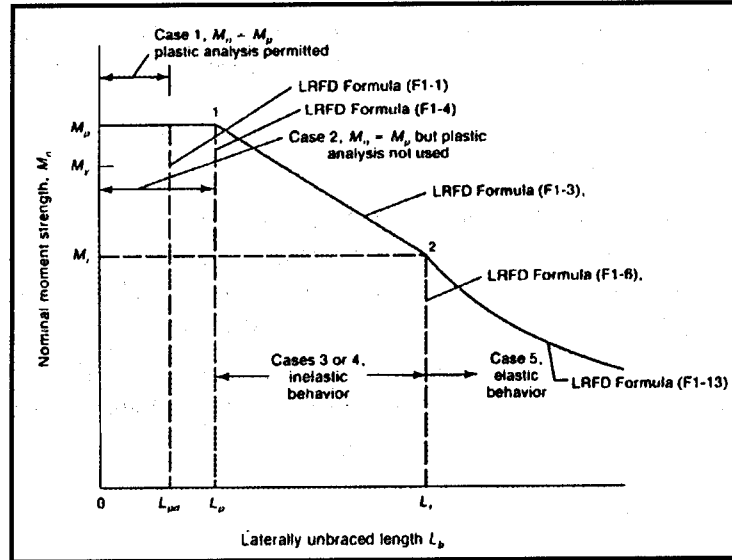
Figure A.1   AISC Nominal Strength of Compact Sections

Cases 3 and 4 are for the situation where the nominal moment strength, M_n, occurs in the inelastic region. The difference between the two cases is that case 3 is for "compact" sections. Most rolled shapes are compact sections, or sections whose flange dimensions preclude local buckling of the compression flange.

Of more concern, particularly for a comparative analysis is case 5. This is the case where the nominal moment strength M_n is the elastic buckling strength. Here the value of the nominal moment strength is given as

$$M_n = M_{cr} = C_b \frac{\pi}{L_b} \sqrt{\left(\frac{\pi E}{L_b}\right)^2 C_w I_y + E I_y GJ} \qquad (A-4)$$

where
C_b = factor to account for moment gradient.
L_b = laterally unbraced length.
C_w = torsional warping constant = $I_f d^2/2$.
I_f = moment of inertia of one flange about the y-axis.
I_y = moment of inertia about the y-axis.

The major difference between the AISC formula and the case for ships is that typical ship structure is stiffened plating. With stiffened plating the restraint caused by the plating must be included in the analysis, and for this reason the expression for M_n in equation (A-4) is not applicable. However, the form of the strength requirement in equation (A-3) is of interest. The AISC LRFD has cast the basic equation in the form which is consistent across the spectrum of column collapse mechanisms. The LRFD format allows for a constant load reduction factor and a consistent means for applying loading (factored loads). Using the combination of the two factors allows the code developers to control

100

the level of safety implied in the equations. What is hidden is all of the work that went into calibration of the code for the types of variables and their levels of uncertainty.

A.3 AASHTO Approach to Tripping

The AASHTO approach to tripping analysis is very simple. It consists of using the AISC Working Stress Design approach for what naval architects consider to be flexural-torsional buckling. The AASHTO LRFD code is expected to be very much like the AISC LRFD except that the load factors will be more specific to the typical highway bridge loading (i.e. average daily truck traffic). Because there is little difference with the AISC code and due to the non-applicability to a majority of typical ship structures, the AASHTO code will not be considered further.

A.4 API Approach to Tripping

The American Petroleum Institute guidelines does much the same as the AASHTO code does in regards to tripping; it defers to the AISC approach. However, the API guidelines specifically state not to use the AISC LRFD approach because the load and resistance factors have been calibrated for typical building practice, not for the harsher offshore environment.

A.5 U.S. Navy Design Data Sheets Approach to Tripping

The U.S. Navy DDS 100-4 addresses lateral torsional buckling in terms of providing support for the stiffener flange at some intermediate points along its span. There is no specific design check on the likelihood of tripping. Figure A.2 is taken from DDS 100-4 to show the relationship between material type, flange breadth, and stiffener depth.

A. MAXIMUM PERMISSIBLE RATIO OF SPAN TO FLANGE WIDTH FOR TEE STIFFENER WITHOUT INTERMEDIATE LATERAL SUPPORT
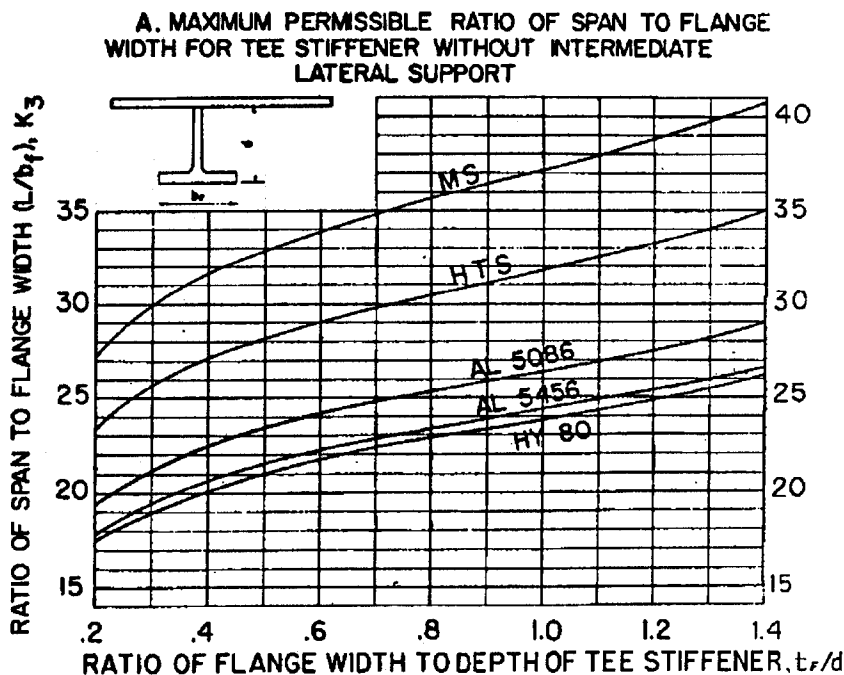
Figure A.2   Maximum Permissible Ratio of Span to Flange Width for Tee Stiffener without Lateral Support (DDS 100-4)

If the actual stiffener span to flange breadth ratio is greater than the value of K_3 found in figure A.2 but less than 1.75 K_3, then a support must be provided to the flange at the midpoint of the span. If the ratio is greater than 1.75 K_3, support must be provided at distances of not more than 0.75 $K_3 b_f$. This is all based on the assumption that the ratio of the stiffener web thickness to flange thickness is about 0.6 and that the sections are compact.

The problem with an approach like this is that there is no way to incorporate different geometries or materials. The designer is stuck with a cook book approach which offers no means of allowing innovation. While this approach has thus far produced safe designs, no one really knows what level of safety is provided.

<u>A.6   ABS Approach to Tripping</u>

The American Bureau of Shipping 1991 Rules for Building and Classing Steel Vessels has an even more basic approach to preventing tripping. In Section 9.3.5, Web Frames - Stiffener and Tripping Brackets, the rules require the flanges of the deep webs to be supported at intervals of "about" 10 feet when the flange breadth on either side of the web exceed 8 inches. The same requirement appears in Section 9.5.3, Side Stringers, and Section 11.7.4, Deck Girders. The only place in the Rules where those values differ significantly is in Section 29B.15.1b for slanted frames on Ice Class 1AA ships. Then the spacing is to be not more than 51 inches.

102

Again, no specific accounting for tripping is provided. This is probably due to ABS's experience with typical ship structures which has shown tripping not to be a failure problem. But once again, there is no flexibility in these rules for innovation in concepts or materials. There is also no means of determining the level of safety implied.

A.7 Proposed Model for Tripping

In order to develop a probabilistic approach to ship structural design, an explicit model needs to be developed for each failure mode. These models can then be used as limit-states to determine the levels of safety implied. The AISC LRFD approach to developing a design code is a sound one. The limit state can be expressed in terms of moments or stresses and can be a simple equation similar to equation (A-3). In the case of ship structures the proposed approach is to have the limit state expressed in terms of applied in-plane stress. Then one only needs to compare the critical buckling stress for tripping to the applied stress.

SSD presents a model for tripping that consists of a two step solution. Because of the interdependence of the three important variables as shown in Section A.1 of this report, m the number of half-waves in which the stiffener will trip, needs to be determined. A (non-integer) approximate value for m, denoted as r, is given by

$$r = \frac{a}{\pi} \sqrt[4]{\frac{4DC_r}{EI_{sz}d^2b}} \tag{A-5}$$

where
a = span length of the stiffener.
b = breadth of the stiffener flange
D = plate flexural rigidity, $Et^3/(12(1-\upsilon^2))$.
C_r = factor by which the plate rotational restraint is reduced by web bending which is given by

$$C_r = \frac{1}{1 + \frac{2}{3}\left(\frac{t}{t_w}\right)^3 \frac{d}{b}}$$

t = thickness of the plating.
t_w = thickness of the stiffener web

For each of the integer values of m above and below r, the following equation is used for determining $\sigma_{a,T}$.

$$\sigma_{a,T} = \begin{matrix} \text{Min} \\ m=1,2,\ldots \end{matrix} \left\{ \cfrac{1}{I_{sp} + \cfrac{2C_r b^3 t}{\pi^4}} \left[GJ + \frac{m^2 \pi^2}{a^2} EI_{sz} d^2 + \frac{4DC_r}{\pi^2 b} \left(\frac{a^2}{m^2} + b^2 \right) \right] \right\} \qquad \text{(A-6)}$$

where

I_{sp} = polar moment of inertia of the stiffener.

When the value for *r* found from equation (A-5) is very close to 1, a simpler form of equation (A-6) can be used

$$\sigma_{a,T} = \cfrac{1}{I_{sp} + \cfrac{2C_r b^3 t}{\pi^4}} \left[GJ + \frac{\pi^2 EI_{sz} d^2}{a^2} + \frac{4DC_r}{\pi^2 b} \left(a^2 + b^2 \right) \right] \qquad \text{(A-7)}$$

APPENDIX B: EXPLANATION AND VALIDATION OF THE STANDARD ALGORITHM FOR PANEL COLLAPSE

APPENDIX B: EXPLANATION AND VALIDATION OF THE STANDARD ALGORITHM FOR PANEL COLLAPSE

(Chapter 14 of *Ship Structural Design*)

ULTIMATE STRENGTH OF STIFFENED PANELS

As explained at the beginning of Chapter 12, the stiffened panels in ship structures are usually sufficiently sturdy that $(\sigma_a)_{cr} > \sigma_Y$. Hence the mode of compressive collapse is not elastic panel buckling, but rather a more complicated inelastic process, for which we use the words "failure" or "collapse" instead of buckling. Nevertheless, there are several aspects of elastic buckling which have their counterpart in the inelastic compressive collapse of plating. For example, in parallel with elastic buckling there are several possible levels and modes of inelastic plate collapse. If the panel is transversely stiffened, then plate failure by itself constitutes collapse, and the theory and methods of Section 12.7 are sufficient. If the panel is cross-stiffened there are two possible levels of collapse:

1. Interframe collapse, that is, collapse of stiffened panels between transverse frames.
2. Gross panel collapse, involving both longitudinal and transverse stiffeners.

In general, cross-stiffened panels should be designed such that interframe collapse occurs before gross panel collapse because the latter involves a larger portion of structure and is likely to be more catastrophic. Also, the structural proportions of ship panels are usually such that gross panel collapse is inelastic, and therefore it is an extremely difficult and complex task to calculate the collapse load with sufficient accuracy for design purposes. Therefore the best procedure is to design the panel such that gross panel collapse cannot occur before interframe collapse. This can be achieved by ensuring that the elastic gross panel buckling stress calculated by the discrete beam method of Section 13.6 is substantially larger than the elastic interframe buckling stress given by (13.1.8), and that both of these buckling stresses are substantially larger than the yield stress.

In practice the scantlings that a panel must have in order to satisfy the requirements of other modes of failure are usually sufficient to meet both of these requirements, but they should always be checked nonetheless. With this design philosophy it is not necessary to consider inelastic gross panel collapse and therefore this chapter deals only with inelastic interframe collapse.

14.1 BOUNDARY CONDITIONS, LOAD TYPES, AND COLLAPSE MODES

Boundary Conditions for Ultimate Strength Analysis

In a deck or side it is clear that the rotational restraint provided to the panels by the transverse frames is relatively small and is best ignored. In the bottom and in other regions having a large lateral load each panel receives some rotational restraint from the adjacent panel, and in principle this would give a larger ultimate compressive strength than if the panel were simply supported. However, in most cases it is possible for the compressive load to occur with little or no lateral load. Also there are many situations in which a bottom panel is far from being clamped. Figure 14.1 shows a common example, in a tanker the end panel of an empty cargo tank adjacent to a full cargo tank has only moderate rotational restraint at one end and is subjected to a destabilizing moment at the other end.
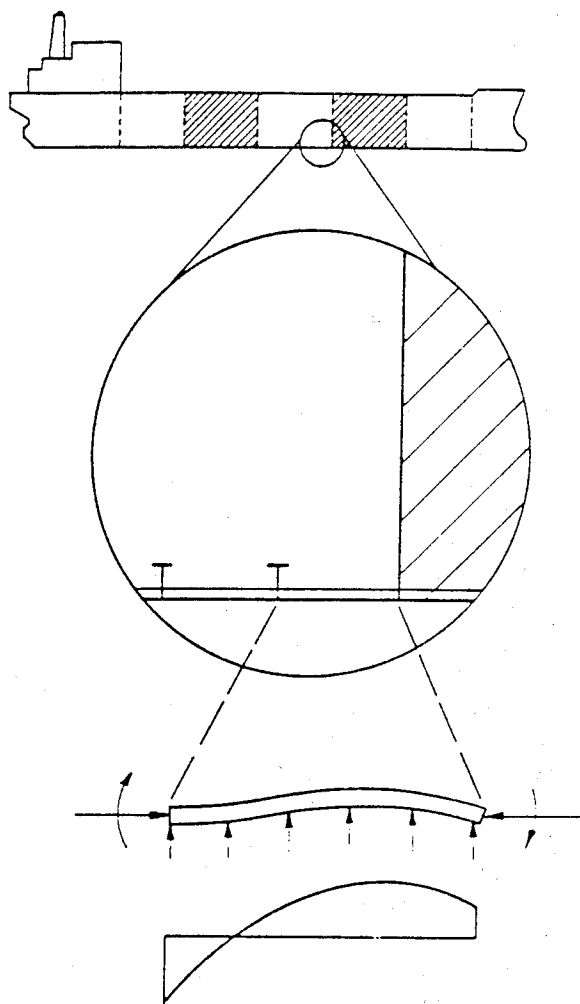
Figure 14.1 Occurrence of nonclamped conditions in bottom panels.

Although other panels may have more rotational restraint, it is obvious that this panel will govern the design of the bottom structure; it would be uneconomical and impractical for the panels to differ from one frame to another. In other ship types the same situation arises if a cargo hold is flooded due to underwater damage. It also arises in a double bottom in which one compartment is filled with fuel or ballast and the adjacent compartment is empty. Therefore unless a panel's rotational restraint is guaranteed to be permanently present under all conditions (which is quite rare) it should not be counted when calculating the ultimate strength of the panel. In general the safest and best procedure is to regard the panel as simply supported. However, the other effects of the lateral load—the maximum deflection and the maximum bending moment—should not be ignored since they decrease the panel's ultimate compressive strength. In

this chapter the deflection and the bending moment due to the lateral load (acting alone) are denoted by δ_0 and M_0. Although the panel ends are being taken as simply supported the theory presented in this chapter does not require that δ_0 and M_0 be the simply supported values. They can be either these values or, if desired and if it is practicable to calculate them, they can be the largest values which will occur, allowing for the actual amount of rotational restraint that is present in that worst case.

Although simply supported boundary conditions generally correspond to small or moderate values of lateral load, this chapter covers the simply supported case over the full range of lateral loads, from zero up to the plastic hinge value, and acting on either side of the plating.

Basic Load Types and Associated Mechanisms of Collapse

For longitudinally stiffened panels with simply supported edges there are three basic types of loads:

1. Lateral load causing negative bending of the panel (i.e., of the plate-stiffener combination).
2. Lateral load causing positive bending of the panel.
3. In-plane compression.

Throughout this chapter, bending moment in the panel is positive when it causes compression in the plating, and in-plane loads are positive if compressive.

Each of these three basic loads has associated with it one or more possible mechanisms of collapse. Whenever in-plane compression occurs in combination with one of the first two load types there is interaction between the specific mechanisms of collapse. As we shall see, the various interactions give rise to three distinct modes of collapse. The specific collapse mechanisms associated with each of the basic load types follow (see Fig. 14.2).

NEGATIVE BENDING

With this type of load the plating is in tension and hence cannot buckle. Also, since the neutral axis is close to the plating, it is the stiffener flange which first reaches yield (point A in Fig. 14.2). As the bending moment increases, yielding spreads through the stiffener. The plating then begins to yield in tension and, if there is no instability in the stiffener, collapse eventually occurs when the bending moment reaches M_P.
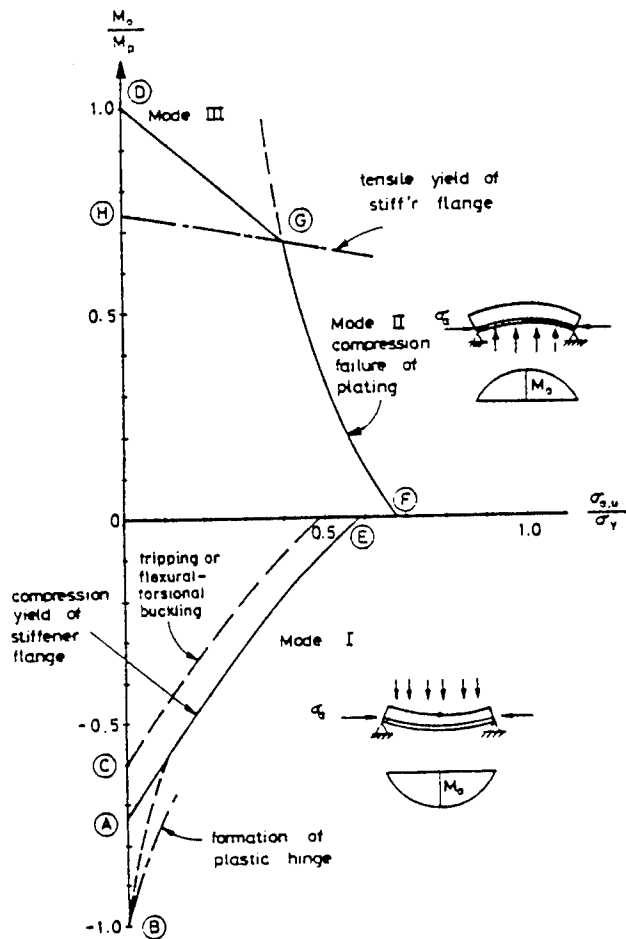
108

Figure 14.2 Collapse mechanisms in a stiffened panel under lateral and in-plane loads.

the value at which a plastic hinge is formed (see Section 16.1). This corresponds to point B in Fig. 14.2. However, since the stiffener is in compression it is possible that stiffener buckling might occur. Thus, for a negative bending load the plate-stiffener combination may not be capable of withstanding the full value of M_P for the section (point C in Fig. 14.2).

POSITIVE BENDING

With this type of load the plating is in compression, but since the neutral axis is very close to the plating the plate will not be heavily stressed until the load becomes very large, by which time the entire stiffener has yielded in tension and collapse is imminent. The plate then begins to yield in compression, and collapse finally occurs as the result of a plastic hinge, with the plate reaching compressive yield. In fact, for most ship panels the plastic neutral axis lies within the plat-

ing thickness, and so some portion of the plate's thickness is in tension. This stabilizes the plate and prevents it from buckling and hence for most ship panels the plate-stiffener combination is capable of absorbing almost the full value of the plastic bending moment M_P (point D in Fig. 14.2).

UNIFORM IN-PLANE COMPRESSION

By "uniform compression" we mean an applied load which causes a uniform shortening of the panel, and it is assumed that the load is not (directly) influenced by the panel's response. The most common example is the hull girder stress. Strictly speaking, the loading on the panel is an *applied uniform strain* ε_a, but for the present we shall deal with the *average applied stress* σ_a (or average distributed load N).

Under this type of load the panel is essentially a group of identical (and almost independent) unsymmetric columns, each consisting of a stiffener and a plate flange of effective width b_e. If the panel is sufficiently slender these columns will buckle elastically and the ultimate strength of the panel can be calculated by the methods of Chapter 13. But for typical ship panels the plate's response becomes inelastic prior to collapse because the plate's load versus end shortening curve is the σ_a versus ε_a curves of Fig. 12.24. This makes the collapse mechanism decidedly more complicated, but a method is presented in this chapter which overcomes the complications and gives an accurate prediction of the collapse value of this type of load. Basically the method consists in regarding the plate portion of the column as being made of a different material, having a reduced elastic modulus, and then using the basic column approach of Section 11.2 to calculate the collapse load, making careful allowance for initial eccentricity. In this approach, "collapse" is considered to occur when the stress in the extreme fiber of the compression flange of the column reaches the failure value for the material of that flange. For the stiffener flange this is simply the yield stress, but for the plate flange it is some other value which allows for the nonlinearity of the σ_a versus ε_a curve. Thus there are two different values of in-plane collapse load, depending on which flange is the compression flange, that is, depending on the direction of the buckling. These two collapse loads correspond to points E and F on the interaction diagram of Fig. 14.2. In general these two loads are not the same and either of them can be the smaller. Since almost any panel can be in a zero lateral load condition, both values must be

109

calculated and the lower value taken as the collapse load.

Combined Loads

In ship structures the stiffened panels are usually subjected to a combination of bending and in-plane loads. Also, in many ship panels the lateral bending can be either positive or negative. For example, a bottom panel in a tanker is subjected to an upward or a downward pressure, depending on the depth of cargo oil in that space relative to the draft. With combined loads there is an interaction among the three basic mechanisms outlined above. This interaction is rather complex and will be discussed fully in the next three sections. But at this point it will be helpful to present at least a qualitative overall view of the situation, and this will now be done with the aid of Fig. 14.2.

The first and most basic point is that with a lateral load the plate-stiffener "column" becomes a "beam column," and the basic column ultimate strength theory of Section 11.2 is replaced by the beam column theory of Section 11.3. In other words, collapse still occurs as the result of "failure of a flange," but the bending moment and deflection caused by the lateral load must be taken into account. Because of the bending, either flange could be the failure flange, depending on the sign of the bending moment, and the failure could be either tensile or compressive. Thus, in principle, there are four modes of collapse; in practice, one of the four—tensile failure of the plating—never occurs because the neutral axis is so close to the plating. Among the other three modes, the precise nature of the collapse mechanism differs, depending on which flange is the compression flange, that is, depending on the sign of the bending moment.

For greater generality we shall allow for the possibility of the stiffeners having a different value of yield stress from the plating. For this purppose we shall use the symbols σ_{Ys} and σ_{Yp}. We will also need to refer to the mean value of yield stress for the entire section, which is

$$\bar{\sigma}_Y = \frac{\sigma_{Ys}A_s + \sigma_{Yp}bt}{A_s + bt} \qquad (14.1.1)$$

Since the in-plane load usually arises from hull girder bending, it is usually more fundamental and more variable than the lateral load. Hence it is customary to define "ultimate strength" in terms of σ_a and to treat the value of the lateral load as an independent parameter. That is, the ultimate strength of a panel is the value of σ_a that causes collapse, in the presence of a specified value of lateral load. In an interactive collapse diagram such as Fig. 14.2 the ultimate strength is the horizontal distance to the curve at the height corresponding to the lateral load. Obviously this convention is not appropriate for panels in which the lateral load is always the dominant load. For such panels the ultimate strength is defined in terms of the lateral load and can be calculated by the plastic hinge theory of Section 16.1* But for the general case of a panel subjected to combined loads the ultimate strength theory must be sufficiently general to handle any combination of load. The theory presented in this chapter meets this requirement.

COMPRESSION PLUS NEGATIVE BENDING (FIG. 14.3)

Mode I: Compression Failure of the Stiffener. With this combination of loads the stiffener flange is the compression flange; therefore collapse occurs as the result of compressive failure of the stiffener flange, either by compressive yield or by buckling. Let us first consider compressive yield. When there is any appreciable amount of axial compressive stress σ_a, it directly increases the compressive bending stress in the stiffener and decreases the tensile bending stress in the plating. Therefore compressive yielding in the stiffener commences sooner and progresses more rapidly, whereas plate yielding is delayed. The result is that the section can no longer achieve a plastic hinge condition, as it could when the load was purely lateral (point B in Fig. 14.2). Instead, the stiffener reaches its limit of stress absorption soon after the yielding has penetrated through the stiffener flange, and when the stiffener is thus "neutralized" the effective moment of inertia of the section becomes very small, since only the plating is effective. The result is that once the stiffener flange is fully yielded collapse occurs soon afterward. Moreover, this mode of collapse is generally quite sudden. In most cases the precise cause of the failure is the formation of a local plastic mechanism in the flange such as that shown in Fig. 14.4. It is quite local because the flange becomes fully plastic at the point where the bending moment is a maximum. This mechanism involves large local sideways deflection and rotation, permitting the stiffener to shorten and thereby

---

*A cross-stiffened or gross panel subjected to lateral loads is termed a *grillage*. This type of structure can be designed in isolation, separate from the hull module, and is therefore not particular to ship structural design.
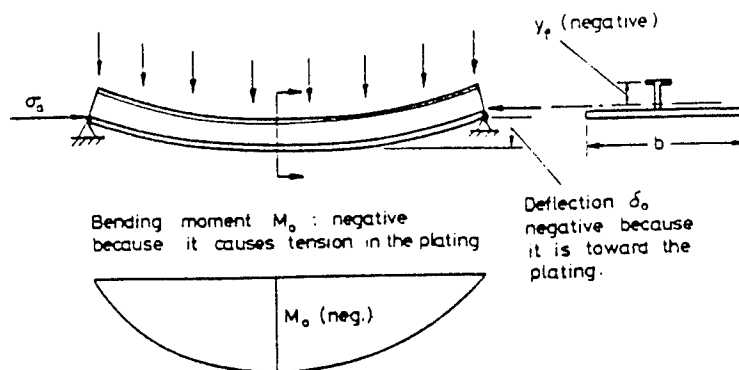
Figure 14.3 In-plane compression and negative bending.

escape from carrying the axial compressive load. The local sideways deflection of the flange is combined with rotation about the line of attachment and hence this type of failure is sometimes taken to be tripping, but this is not correct since the cause of the sideways deflection is a local plastic mechanism rather than overall flange buckling.

As noted earlier, when the loading is purely lateral the plate-stiffener combination can reach a plastic hinge condition before collapse occurs. Hence for load combinations which involve only a small amount of in-plane compression the collapse curve can depart from the "stiffener flange yield" curve and eventually, at zero axial load, it can reach the plastic hinge collapse point. However, the curve in this region is very steep, such that a small underestimate of the axial load would cause a serious overestimate of the collapse value of the lateral load. For this reason the plastic hinge mechanism of collapse should only be used when it is certain that in-plane compression cannot occur (e.g., platforms, ramps, machinery flats, and other laterally loaded stiffened panels). The calculation of ultimate strength under this type of loading is dealt with in Chapter 16. Therefore, for stiffened pan-

els which are subject to in-plane compression it is best to use the "stiffener flange yield" mechanism for all of the Mode I region, even though for very small in-plane loads this approach is conservative. Hence the Mode I collapse curve begins at point A in Fig. 14.2.

Alternatively, the stiffener may fail by tripping. If the amount of bending is small the elastic tripping stress $\sigma_{a,T}$ is given by the formulas of Section 13.1. If it is not small then the stiffener may undergo flexural-torsional buckling, and providing the stiffener remains elastic the value of $\sigma_{a,T}$ may be calculated by elastic nonlinear frame analysis, which is presented in Section 15.5. The analysis is simple and rapid because the buckling is of bifurcation type and requires only an eigenvalue analysis. However, as mentioned earlier, for most ship panels, buckling is not purely elastic and the simple bifurcation/eigenvalue approach cannot provide the true collapse value, $\sigma_{a,u}$, either with or without M_0. To obtain an accurate value of $\sigma_{a,u}$ would require the fully nonlinear finite element method (incremental and iterative), which is discussed in Section 15.6, but this involves too much computation for such a local and frequently occurring calculation (every panel) especially in a design procedure. Instead, there is a simple alternative suggested by Smith [1]. Since the maximum compressive stress in the flange must be kept below σ_{Y_s} in order to avoid a local plastic mechanism, stiffener buckling can be avoided simply by requiring that the value of $\sigma_{a,T}$ obtained from the elastic theory (Section 13.1 or 15.5, as appropriate) must be well above σ_{Y_s}.

Since collapse occurs when the stiffener flange stress reaches yield (or earlier if $\sigma_{a,T} < \sigma_{Y_s}$) the beam-column remains fully elastic prior to collapse. Therefore the combination of compression and negative bending is relatively straightforward to analyze, requiring only the ordinary beam column theory of Section 11.3.
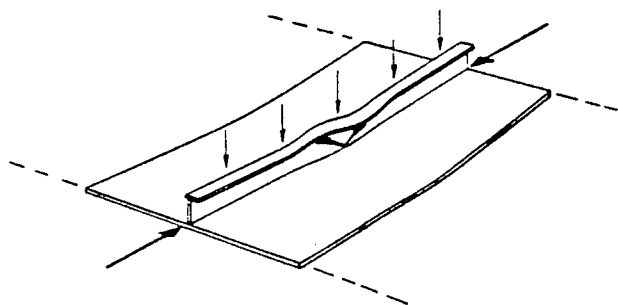

Figure 14.4 Local plastic collapse mechanism in a stiffener flange.

111

COMPRESSION PLUS POSITIVE BENDING (FIG. 14.5)

With this combination of loads the plating is the compression flange and there are two distinct modes of collapse, depending on the relative magnitude of the bending and the in-plane loads:

Mode II: Compression Failure of the Plating. With small and moderate lateral loads, collapse occurs when the stress in the plating reaches the failure value for the "special material" which is used to represent the plating. As will be shown, the use of a secant modulus to represent the plate's stress-strain relationship allows the beam-column to be treated as if it remained entirely elastic prior to collapse.

Mode III: Combined Failure of Stiffener and Plating. With large positive lateral loads the bending causes large tensile stresses in the stiffener. These are reduced by the in-plane applied compressive stress, but for larger and larger lateral loads the stiffener undergoes more and more tensile yielding, and collapse, when it finally occurs, is due to a combination of compressive failure of the plating material and tensile yielding of the stiffener.

In the next section we investigate each of these three modes of collapse.

14.2 MODES OF COLLAPSE

Mode I Collapse: Compression Failure of the Stiffener

The combination of in-plane compression and negative bending is illustrated in Fig. 14.3. With this com-

bination, collapse occurs due to compression failure of the stiffener flange. That is. collapse occurs when the total stress (σ_a plus the magnified bending stress) throughout the thickness of the flange has reached the "failure value" σ_F. The failure value is either the yield stress σ_{Ys} or the elastic tripping stress $\sigma_{a,T}$, whichever is less. Stated mathematically

$$\sigma_F = \text{MIN}\{\sigma_{Ys}, \sigma_{a,T}\} \qquad (14.2.1)$$

where $\sigma_{a,T}$ is obtained from the method of Section 13.1 or 15.5.

Strictly speaking, as the yield zone penetrates from the outer surface to the midthickness of the flange there is some nonlinearity, but since the half-thickness is small relative to the web depth the effect is negligible. Therefore, the failure process can be regarded as entirely elastic and can be completely described by the beam-column theory of Section 11.3. Accordingly, the total stress in the midthickness of the flange is

$$\sigma_f = \sigma_a + \frac{M_0 y_f}{I} + \frac{\sigma_a A (\delta_0 + \Delta) y_f}{I} \phi \qquad (14.2.2)$$

in which A and I = cross-sectional area and moment of inertia of the beam-column. (Note: Since the plating is in tension the plate flange is assumed to be of full width b. Therefore $A = A_s + bt$.)

M_0 and δ_0 = maximum bending moment and maximum deflection due to the lateral load acting alone. It is assumed that these maximum values occur at the midlength of the beam-column.
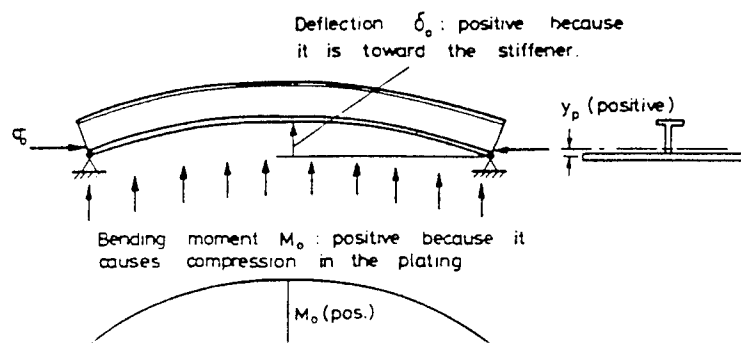

Figure 14.5 In-plane compression and positive bending.

Δ = initial eccentricity of the beam-column; a typical maximum permissible value for welded panels is $a/750$, where a is the length of the panel.

y_f = distance from the centroidal axis of the cross section to the mid-thickness of the stiffener flange.

ϕ = magnification factor due to the axial compressive stress σ_a:

$$\phi = \frac{1}{1 - \dfrac{\sigma_a}{\sigma_E}}$$

where σ_E is the Euler buckling stress for the beam-column:

$$\sigma_E = \frac{\pi^2 EI}{Aa^2}$$

The collapse or "ultimate" value of applied stress $\sigma_{a,u}$ is the value of σ_a at which $\sigma_f = \sigma_F$, and so we now proceed to make these substitutions and solve for $\sigma_{a,u}$. As in Section 11.3, we make use of the following nondimensional parameters:

$$\left.\begin{aligned}
R &= \frac{\sigma_{a,u}}{\sigma_F} \\[2mm]
\lambda &= \frac{a}{\pi\rho}\sqrt{\frac{\sigma_F}{E}} \qquad \text{where } \rho = \sqrt{\frac{I}{A}} \\[2mm]
\eta &= \frac{(\delta_0 + \Delta)y_f}{\rho^2} \\[2mm]
\mu &= \frac{M_0 y_f}{I\sigma_F}
\end{aligned}\right\} \quad (14.2.3)$$

In terms of these parameters the magnification factor is

$$\phi = \frac{1}{1 - \lambda^2 R}$$

Equation 14.2.2 becomes

$$(1 - R - \mu)(1 - \lambda^2 R) = \eta R \quad (14.2.4)$$

and the solution for the strength ratio R is

$$R = \frac{\zeta}{2} - \sqrt{\frac{\zeta^2}{4} - \frac{1 - \mu}{\lambda^2}}$$

where $\qquad \zeta = 1 - \mu + \dfrac{1 + \eta}{\lambda^2}$ $\qquad (14.2.5)$

Therefore, if $\sigma_F = \sigma_{Ys}$ the equation for the interactive collapse curve in the Mode I collapse region of Fig. 14.2 is

$$\left(\frac{\sigma_{a,u}}{\sigma_{Ys}}\right)_I = R \qquad (14.2.6a)$$

with R as given previously. The influence of M_0 is contained in the bending parameter μ. If $\sigma_F = \sigma_{a,T}$ then the equation becomes

$$\left(\frac{\sigma_{a,u}}{\sigma_{Ys}}\right)_I = R\frac{\sigma_{a,T}}{\sigma_{Ys}} \qquad (14.2.6b)$$

This equation is based on the following sign convention, which is used throughout this chapter.

Stress: Positive if compressive.

Bending moment: Positive when the plating is in compression.

Lateral deflection ⎫
Eccentricity ⎬ : Positive toward the stiffeners
⎭ (i.e., positive upward in Fig. 14.3). Note: For a simply supported panel, positive bending causes positive lateral deflection.

Distance from neutral axis: Positive toward the plating.

In simply supported panels that are subjected to negative bending, the collapse mode is always Mode I for any significant amount of negative bending, that is, throughout the lower half of the interaction diagram of Fig. 14.2. To make the diagram more useful the loads are nondimensionalized: values of maximum bending moment are normalized by dividing by M_P, and values of applied in-plane compressive stress are divided by $\bar{\sigma}_Y$. Thus the point corresponding to collapse under a pure bending load is the point -1 on the bending moment axis, providing that buckling does not precede flange yield. As the amount of in-plane compression increases, the amount of bending which is required to cause collapse is lessened. The exact shape of the interactive collapse curve depends on the scantlings and geometry of the panel. If the failure mechanism is buckling, the ultimate strength will be less than it

113

would be for failure by yielding, and the entire curve will lie closer to the origin, as shown by the dashed line in Fig. 14.2.

Mode II Collapse: Compression Failure of the Plating

We next consider the combination of in-plane compression σ_a and positive bending moment M_0 as shown in Fig. 14.5. If the bending is small or moderate in magnitude, collapse occurs due to compression failure of the plate flange. If the plating remained perfectly elastic, with no buckling or nonlinearity, the total applied stress acting on the plating, σ_{pa}, would be given by the usual beam-column formula

$$\sigma_{pa} = \sigma_a + \frac{M_0 y_p}{I} + \frac{\sigma_a A (\overset{\Delta}{\Phi} + \delta_0) y_p}{I} \phi \qquad (14.2.7)$$

As shown in Section 12.6, the compressive collapse of welded plating is a complex inelastic process. The relationship between load and end shortening, that is, between the applied stress σ_{pa} and the average strain ε_a, is described by the curves of Fig. 12.24. For our present application the applied stress in the plating is σ_{pa} and so this symbol replaces σ_a of Fig. 12.24. As an illustration, and for later reference, a typical curve of σ_{pa} versus ε_a from Fig. 12.24 is reproduced in Fig. 14.6. The earlier figure showed that for most plates ($\beta > 1$) the relationship between σ_{pa} and ε_a becomes nonlinear well before collapse. Both figures also illustrate what we mean by "plate failure," namely, the point in the σ_{pa} versus ε_a curve at which the plating has lost most of its in-plane stiffness. In geometric terms it is the point at which the tangent of the curve has become significantly less than the original value, E. Strictly speaking, the failure point is the peak of the curve. However, for plates of low and intermediate slenderness there is a discernible knee in the curve (unless the initial distortion δ_p is very large) and this is the simplest and safest choice of the failure point. For very slender plates the failure point is either the peak of the curve or the point at which the slope has decreased to some specified value (e.g., $\frac{1}{3}E$).

Since the plating is actually being subjected to an imposed uniform strain, collapse is, strictly speaking, measured by the value of average strain corresponding to this loss of stiffness: $\varepsilon_a = \varepsilon_{ult}$, as shown in Fig. 14.6. However, it is more convenient to deal in terms of stress. For later use we define σ_F as the equivalent elastic failure stress, that is, the value of σ_{pa} which
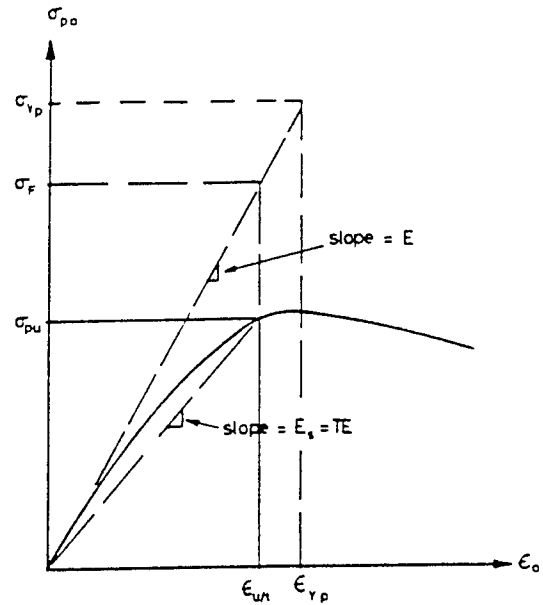

Figure 14.6 Typical curve of load versus end shortening for welded steel plating.

would correspond to ε_{ult} if the plate maintained a linear relationship between σ_{pa} and ε_a.

For most plates the slope of the curve begins to decrease well before the point of "plate failure." Therefore σ_{pu}, the true value of applied stress which corresponds to plate failure, is significantly less than σ_F. This also means that during the load sequence that leads to plate failure, the average plate stiffness is significantly less than the elastic or material stiffness E. The average stiffness over the entire range of loading is given by the secant modulus $E_s = TE$, which is the slope of the line joining the origin to the point of plate failure, as shown in Fig. 14.6. For our purpose this straight line can be used in place of the actual curve because we simply want to be able to predict plate failure, and we are not interested in the detailed plate response prior to that. With this approach we are, in effect, representing the plating as if it were made of a different material which has a smaller value of Young's modulus, and for which the *curve of σ_{pa} versus ε_a is perfectly linear, right up to failure.* As we shall see, the latter property is of very great advantage.

The mathematical expression for the secant modulus was given in (12.6.4) which for convenience is reproduced here

$$T = \frac{E_s}{E} = 0.25 \left(2 + \xi - \sqrt{\xi^2 - \frac{10.4}{\beta^2}} \right)$$

$$(14.2.8)$$

where

$$\xi = 1 + \frac{2.75}{\beta^2}$$

Also, it was noted in Section 12.6 that the ultimate strength curve has the same shape as the curve for T and can be represented sufficiently accurately by simply subtracting 0.1 from T. That is

$$\frac{\sigma_{pu}}{\sigma_{Yp}} = T - 0.1$$

$$= 0.25\left(1.6 + \xi - \sqrt{\xi^2 - \frac{10.4}{\beta^2}}\right)$$

with ξ again given by (14.2.9)

$$\xi = 1 + \frac{2.75}{\beta^2}$$

We now consider the composite beam column comprised of a stiffener and a plate flange of width b, as shown in Fig. 14.7. The total cross-sectional area is $A = A_s + bt$. The loads are an applied compressive stress σ_a and a lateral load which causes a positive. bending moment of maximum value M_0. The plate flange has a different elastic modulus than the stiffener and hence, before we can apply beam theory, we must

Figure 14.7 Use of transformed section to represent combined stiffener-and-plate as an equivalent elastic beam column.

transform this composite section into an equivalent section which has a uniform elastic modulus, as was done for the hull girder in Section 3.6. We choose the stiffener as the reference material, and hence the cross-sectional area of the plating is multiplied by the transformation factor T. In the present application, to avoid any confusion about plate thickness we apply T to the flange width b instead of to the plate thickness. Therefore, in the transformed section the plate flange has a transformed width $b_{tr} = Tb$. The total area is now $A_{tr} = A_s + b_{tr}t$, the neutral axis is at the centroid of the transformed section, and the effective moment of inertia of the beam-column is I_{tr}, which is the second moment of the transformed section. The strain distribution is linear and continuous but the stress distribution is discontinuous because in the plating the stress is $\sigma_{pa} = T\sigma_{pa}^*$, where σ_{pa}^* is the stress obtained by applying ordinary beam theory to the transformed section (see Fig. 14.7). It should be noted that σ_{pa}, the actual value of stress in the plating, acts across the entire width of the plate flange; the transformed width b_{tr} is merely a device for obtaining the neutral axis position and moment of inertia of the composite section.

The axial stress in the transformed section is

$$\sigma_{a,tr} = \sigma_a\frac{A}{A_{tr}} = \sigma_a\frac{A_s + bt}{A_s + b_{tr}t} \quad (14.2.10)$$

and this is the value of stress at the neutral axis of the section. If we now apply the ordinary beam column theory as in (14.2.7) to the transformed section we obtain the uncorrected plate stress σ_{pa}^*

$$\sigma_{pa}^* = \sigma_{a,tr} + \frac{M_0y_{p,tr}}{I_{tr}} + \frac{\sigma_{a,tr}A_{tr}(\Delta + \delta_0)y_{p,tr}}{I_{tr}}\phi$$

$$(14.2.11)$$

and the true value of σ_{pa} is then

$$\sigma_{pa} = T\sigma_{pa}^* \quad (14.2.12)$$

From beam-column theory we know that collapse of the beam-column occurs when the stress in the compression flange (here σ_{pa}) reaches the failure value for that material (σ_{pu}, as shown in Fig. 14.6). The ultimate strength of the beam-column is defined as the value of applied axial stress in the beam-column ($\sigma_{a,tr}$) which is sufficient to cause the above collapse condition. That is, $(\sigma_{a,tr})_{ult}$ is defined as the value of $\sigma_{a,tr}$

115

which satisfies

$$\sigma_{pu} = \sigma_{pa}$$

or $$\sigma_{pu} = T\sigma_{pa}^{*} \qquad (14.2.13)$$

where σ_{pa}^{*} is as given previously. Rather than multiplying every term of σ_{pa}^{*} by T, it will be more convenient to bring T to the left-hand side and define an equivalent plate failure stress σ_F:

$$\sigma_F = \frac{\sigma_{pu}}{T}$$

as was foreshadowed earlier (see Fig. 14.6).

Thus far we have considered only longitudinal stress in the plating. If there is a transverse stress σ_{ay} (positive compressive) and shear stress τ, the ultimate strength of the plating is less than the uniaxial value σ_{pu}. If these other two stresses are not large (less than, say, $0.3\ \sigma_{ax}$) the value of σ_{pu} can be corrected by applying a reduction factor to σ_{pu}. The reduction factor to account for τ is given by (12.6.3)

$$r_{\tau} = \sqrt{1 - 3\left(\frac{\tau}{\sigma_{Yp}}\right)^2}$$

The interaction between σ_{ax} and σ_{ay} is discussed in Section 12.6, and is shown to depend on the plate slenderness β and aspect ratio a/b. The interaction is quite complex, being actually beneficial in the case of sturdy plates ($\beta < 1$) and becoming linear, and detrimental, in the case of slender plates. For design purposes we want a simple relationship which covers the worst cases without being unduly pessimistic in other cases. The worst case is the linear interaction given by (12.6.16) corresponding to slender plates. If we adopt this then the reduction factor to be applied to σ_{pu} is

$$r_{ay} = 1 - \frac{\sigma_{ay}}{\sigma_{ay,u}}$$

in which $\sigma_{ay,u}$ is given by (12.6.12) assuming that $a/b \geq 1$. We now apply these two reduction factors to σ_{pu}, and for simplicity of notation we do so by redefining σ_F, the equivalent failure stress for the plating, such that it includes these factors. We also take advantage of the fact that σ_{pu} can be represented in terms of T, as in (14.2.9): $\sigma_{pu} = (T - 0.1)\sigma_{Yp}$. The definition of σ_F becomes

$$\sigma_F = \frac{T - 0.1}{T}\sigma_{Yp}\sqrt{1 - 3\left(\frac{\tau}{\sigma_{Yp}}\right)^2}\left(1 - \frac{\sigma_{ay}}{\sigma_{ay,u}}\right)$$
$$(14.2.14)$$

and σ_F is an artificial or equivalent failure stress for the plating, such that the plate fails when the uncorrected plate stress σ_{pa}^{*} reaches σ_F. Substituting for σ_{pa}^{*} from (14.2.11) we obtain the equation governing the collapse condition:

$$\sigma_F = (\sigma_{a,rr})_{ult} + \frac{M_0 y_{p,rr}}{I_{rr}} + \frac{(\sigma_{a,rr})_{ult} A_{rr}(\Delta + \delta_0)y_{p,rr}}{I_{rr}}\phi$$
$$(14.2.15)$$

In parallel with the procedure adopted for Mode I collapse, we define the following nondimensional parameters

$$R = \frac{(\sigma_{a,rr})_{ult}}{\sigma_F}$$

$$\lambda = \frac{a}{\pi\rho_{rr}}\sqrt{\frac{\sigma_F}{E}} \qquad \text{where } \rho_{rr} = \sqrt{\frac{I_{rr}}{A_{rr}}}$$

$$\eta = \frac{(\Delta + \delta_0)y_{p,rr}}{\rho_{rr}^2} \qquad (14.2.16)$$

$$\mu = \frac{M_0 y_{p,rr}}{I_{rr}\sigma_F}$$

$$\phi = \frac{1}{1 - \lambda^2 R}$$

In terms of these parameters, (14.2.15) reduces to the same nondimensional beam-column equation as for Mode I, given in (14.2.4)

$$(1 - \mu - R)(1 - \lambda^2 R) = \eta R$$

and the solution for the strength ratio R or (R_{II}, to indicate the collapse mode) is

$$R_{II} = \frac{\zeta_{II}}{2} - \sqrt{\frac{\zeta_{II}^2}{4} - \frac{1 - \mu}{\lambda^2}}$$
$$(14.2.17)$$

where $$\zeta_{II} = 1 - \mu + \frac{1 + \eta}{\lambda^2}$$

This equation is based on the sign convention defined earlier and hence $y_{p,rr}$, δ_0, and Δ are all positive quantities.

INDUCED LOAD ECCENTRICITY DUE TO DECREASED PLATE STIFFNESS

In investigating panel collapse of a stiffened panel structure we usually wish to find and analyze the first panel to collapse. Hence the panels which are immedi-

116

ately adjacent in the direction of the load should be treated as fully effective. But the main reason for treating them as such is that this is a more severe condition for the subject panel. The reduced stiffness of the plating has been allowed for by defining a transformed section in which the neutral axis is displaced slightly further from the plating. By definition the neutral axis is the line of action, within the cross section of the beam column, of the total axial force $P(P = A\sigma_a = A_{tr}\sigma_{a,tr})$ which is transmitted by the cross section. But the line of action of the externally applied force is the centroid of the total area A, which means that the applied load has a slight positive eccentricity, and this creates an extra positive moment in the section and therefore decreases the ultimate strength. The eccentricity is equal to the distance moved by the neutral axis, which is

$$\Delta_p = hA_s\left[\frac{1}{A_{tr}} - \frac{1}{A}\right] \qquad (14.2.18)$$

where h is the distance from the midplane of the plating to the centroid of the stiffener, and A_s is the sectional area of the stiffener.

The effect of Δ_p is to add another term to the right-hand side of (14.2.15). Unlike other forms of eccentricity, Δ_p does not undergo magnification since it is the final value of the neutral axis eccentricity, at the instant of failure. Therefore the additional term is

$$\frac{(\sigma_{a,tr})_{ult}A_{tr}\Delta_p y_{p,tr}}{I_{tr}}$$

Accordingly, we define an additional nondimensional parameter η_p, analogous to the geometric eccentricity parameter η

$$\eta_p = \frac{\Delta_p y_{p,tr}}{\rho_{tr}^2} \qquad (14.2.19)$$

The nondimensional equation governing collapse becomes

$$[1 - \mu - R(1 + \eta_p)](1 - \lambda^2 R) = \eta R$$

for which the solution is

$$R_{II} = \frac{\zeta_{II}}{2} - \sqrt{\frac{\zeta_{II}^2}{4} - \frac{1 - \mu}{(1 + \eta_p)\lambda^2}}$$

$$(14.2.20)$$

where

$$\zeta_{II} = \frac{1 - \mu}{1 + \eta_p} + \frac{1 + \eta_p + \eta}{(1 + \eta_p)\lambda^2}$$

NONUNIFORM APPLIED COMPRESSIVE STRESS

If the panel forms part of a hull girder the overall depth of the hull girder is sufficiently large that the hull girder stress σ_a can be regarded as constant over the height of the panel. If, however, the overall structure is a shallower box girder, such as a double bottom or a barge or a simple box girder beam, then the applied stress σ_a has a trapezoidal distribution over the height of the panel and this also induces some additional eccentric bending. The eccentricity is again positive (providing that the stiffeners are on the inside of the box girder flanges) and is given by

$$\Delta_H = \frac{I}{AH} \qquad (14.2.21)$$

where A and I refer to the total panel cross section (not the transformed section) and H is the distance from the centroidal axis of the total panel cross section to the neutral axis of the overall box girder, that is, to the axis of zero stress in the box girder, taking into account any axial stress which may be present in it. Since Δ_H is an initial eccentricity it may simply be added to Δ, and there is no need for a new term as there was for Δ_p.

The steps in calculating the Mode II ultimate strength may be summarized as follows:

1. For the given lateral load, calculate M_0 and δ_0.
2. From (14.2.8) calculate T and then calculate σ_F from

$$\sigma_F = \frac{T - 0.1}{T}\sigma_{Yp}\sqrt{1 - 3\left(\frac{\tau}{\sigma_{Yp}}\right)^2}\left(1 - \frac{\sigma_{av}}{\sigma_{ay,u}}\right)$$

with $\sigma_{ay,u}$ given by (12.6.12).

3. For a transformed section having a plate flange of width Tb, calculate A_{tr}, $y_{p,tr}$, I_{tr}, ρ_{tr}, and Δ_p. (Note: Eqs. 8.3.6 are helpful for this task.
4. Using (14.2.16) and (14.2.19) calculate the parameters λ, η, η_p, and μ.
5. Calculate the strength ratio R_{II} from (14.2.20).
6. Calculate the collapse load $\sigma_{a,u}$ from (14.2.10)

$$\sigma_{a,u} = (\sigma_{a,tr})_{ult}\left(\frac{A_{tr}}{A}\right)$$

117

which is, in terms of R_{II}

$$\sigma_{a,u} = \sigma_F R_{\mathrm{II}} \left(\frac{A_{tr}}{A} \right) \qquad (14.2.22\mathrm{a})$$

or in nondimensional terms

$$\left(\frac{\sigma_{a,u}}{\bar{\sigma}_Y} \right)_{\mathrm{II}} = \frac{\sigma_F}{\bar{\sigma}_Y} R_{\mathrm{II}} \left(\frac{A_{tr}}{A} \right) \qquad (14.2.22\mathrm{b})$$

R_{II} is a function of M_0 through the medium of μ

$$\mu = \frac{M_0 y_{p,tr}}{I_{tr} \sigma_F}$$

and therefore (14.2.22) is the equation for the Mode II interactive collapse curve of Fig. 14.2.

Mode III Collapse: Combined Failure of Stiffener and Plating

If the positive bending moment M_0 is large it creates a large tensile stress in the stiffener. This is partly canceled by the applied compressive stress, but if the bending moment is sufficiently large there will be tensile yielding in the stiffener flange as well as compressive failure of the plating. This further reduces the effectiveness of the section, and so the plate failure analysis of the previous section is no longer sufficient. The point on the Mode II curve where this simultaneous failure begins to occur is labeled G on the interaction diagram of Fig. 14.2. This simultaneous failure occurs in all combinations of collapse loads in which the bending moment exceeds $(M_0)_G$. Therefore in this region of the interaction diagram there is a new mode of collapse—Mode III—and a new segment of the collapse curve extending from point G up to point D, where the load is a pure bending load. For this loading, the stiffener can achieve full yield and as this occurs the effective neutral axis moves toward the plating. For most panel proportions it eventually enters the plating, putting it partly in tension. This stabilizes the plating such that it can absorb almost the full value of compressive yield stress. Hence for a purely lateral load collapse does not occur until the panel has reached a plastic hinge condition.

A precise calculation of the collapse loads for Mode III collapse would be extremely difficult because of the complicated interaction between the simultaneous stiffener tensile yielding and plate compressive failure. Experiments [2] show that the interaction curve

for this collapse mode is convex upward and that it always intersects the Mode II curve at some distance above point G. That is, the Mode II collapse analysis becomes inaccurate only gradually, in proportion to the extent to which M_0 exceeds $(M_0)_G$, such that the collapse involves some yielding of the stiffener flange. Therefore we choose a straight line between points D and G as the interaction curve for Mode III collapse. This choice is safe since the actual collapse points always lie slightly above this line, and it greatly simplifies the analysis of Mode III collapse. The analysis only requires finding point G, the load combination which causes simultaneous compression failure of the plating and tensile yield of the stiffener flange. The latter occurs when the total flange stress reaches the tensile yield stress, which in the sign convention of this chapter is $-\sigma_{Ys}$. Therefore the condition for flange yield is

$$-\sigma_{Ys} = (\sigma_{a,tr})_{\mathrm{ult}} + \frac{M_0 y_{f,tr}}{I_{tr}} + \frac{(\sigma_{a,tr})_{\mathrm{ult}} A_{tr} (\delta_0 + \Delta) y_{f,tr}}{I_{tr}} \phi$$
$$+ \frac{(\sigma_{a,tr})_{\mathrm{ult}} A_{tr} \Delta_p y_{f,tr}}{I_{tr}}$$
$$(14.2.23)$$

This equation corresponds to the curve GH in Fig. 14.2. To facilitate the solution for the value of $(\sigma_{a,tr})_{\mathrm{ult}}$ we again define a set of nondimensional parameters. These differ from those of Mode II in that the flange distance $y_{f,tr}$ replaces $y_{p,tr}$, which means that both η and η_p will have negative values. Also, since the failure stress is now negative $(\sigma_F = -\sigma_{Ys})$ the strength ratio R will likewise have a negative value, and this means that the expression for the magnification factor must be altered to

$$\phi = \frac{1}{1 + \lambda^2 R}$$

In order to distinguish the nondimensional parameters which correspond to the curve GH from those of Mode II, we shall use a subscript GH. Accordingly, the parameters are

$$R_{GH} = \frac{(\sigma_{a,tr})_{\mathrm{ult}}}{-\sigma_{Ys}}$$

$$\lambda_{GH} = \frac{a}{\pi \rho_{tr}} \sqrt{\frac{\sigma_{Ys}}{E}}$$

$$\eta_{GH} = \frac{(\Delta + \delta_0) y_{f,tr}}{\rho_{tr}^2}$$

$$\eta_{p.GH} = \frac{\Delta_0 y_{f.tr}}{\rho_{tr}^2} \qquad (14.2.24)$$

$$\mu_{GH} = \frac{M_0 y_{f.tr}}{I_{tr}(-\sigma_{Ys})}$$

$$\phi_{GH} = \frac{1}{1 + \lambda^2 R_{GH}}$$

The condition for flange yield (i.e., the equation of curve GH) is then

$$[1 - \mu_{GH} - R_{GH}(1 + \eta_{p.GH})](1 + \lambda_{GH}^2 R_{GH})$$
$$= \eta_{GH} R_{GH}$$

and solving for R_{GH} gives*

$$R_{GH} = \frac{\zeta_{GH}}{2} \pm \sqrt{\frac{\zeta_{GH}^2}{4} + \frac{1 - \mu_{GH}}{(1 + \eta_{p.GH})\lambda_{GH}^2}}$$

where

$$\zeta_{GH} = \frac{1 - \mu_{GH}}{1 + \eta_{p.GH}} - \frac{1 + \eta_{p.GH} + \eta_{GH}}{(1 + \eta_{p.GH})\lambda_{GH}^2}$$

The other condition defining point G is the Mode II condition. Therefore, from (14.2.20) the second equation for determining point G is

$$R_{II} = \frac{\zeta_{II}}{2} - \sqrt{\frac{\zeta_{II}^2}{4} - \frac{1 - \mu_{II}}{(1 + \eta_{p.II})\lambda_{II}^2}}$$

where $\qquad\qquad\qquad\qquad\qquad$ (14.2.26)

$$\zeta_{II} = \frac{1 - \mu_{II}}{1 + \eta_{p.II}} + \frac{1 + \eta_{p.II} + \eta_{II}}{(1 + \eta_{p.II})\lambda_{II}^2}$$

in which the nondimensional parameters are those of (14.2.16) and (14.2.19). From these expressions for R_{GH} and R_{II} we can obtain two equations for $(\sigma_{a.u})_G$ as a function of $(M_0)_G$. For the stiffener tensile yield condition the equation for $(\sigma_{a.u})_G$ in terms of R_{GH} is similar to (14.2.22), namely

$$\left(\frac{\sigma_{a.u}}{\overline{\sigma}_Y}\right)_G = \frac{-\sigma_{Ys}}{\overline{\sigma}_Y}\left(\frac{A_{tr}}{A}\right)R_{GH} \qquad (14.2.27)$$

*We here indicate both roots of the quadratic because the solution for point G can involve either root, depending on M_0 and the panel proportions.

The result will be positive since R_{GH} is negative. R_{GH} is a function of $(M_0)_G$ since

$$\mu_{GH} = \frac{(M_0)_G y_{f.tr}}{I_{tr}(-\sigma_{Ys})}$$

The second equation for $(\sigma_{a.u})_G$ and $(M_0)_G$ comes from the plate failure condition, for which (14.2.22) gives

$$\left(\frac{\sigma_{a.u}}{\overline{\sigma}_Y}\right)_G = \frac{\sigma_F}{\overline{\sigma}_Y}\left(\frac{A_{tr}}{A}\right)R_{II} \qquad (14.2.28)$$

in which R_{II} is a function of $(M_0)_G$, since

$$\mu_{II} = \frac{(M_0)_G y_{p.tr}}{I_{tr}\sigma_F}$$

The required collapse loads $(\sigma_{a.u})_G$ and $(M_0)_G$ are obtained by solving (14.2.27) and (14.2.28) simultaneously, using an appropriate numerical technique. By equating the right-hand sides of these equations we obtain a single implicit equation for $(M_0)_G$:

$$R_{II}\sigma_F = -R_{GH}\sigma_{Ys} \qquad (14.2.29)$$

The solution must be performed iteratively, and the best approach is to begin with a trial value of $(M_0)_G$, calculate the corresponding value of $(\delta_0)_G$ (which depends on the type of lateral load), then evaluate R_{II} and R_{GH}, and hence the left and right sides of (14.2.29). In general these will not agree and it will be necessary to choose another value of $(M_0)_G$ and repeat until the agreement is satisfactory. Some numerical technique (Newton's method, Secant method, etc.) may be used to obtain each new value of $(M_0)_G$.

Since the other end-point of the Mode III collapse line is $(\sigma_{a.u}/\overline{\sigma}_Y = 0; M_0/M_P = 1)$ the equation for the ultimate strength of a panel in the Mode III collapse regime is

$$\left(\frac{\sigma_{a.u}}{\overline{\sigma}_Y}\right)_{III} = \frac{M_P - M_0}{M_P - (M_0)_G}\left(\frac{(\sigma_{a.u})_G}{\overline{\sigma}_Y}\right)$$
$$(14.2.30)$$

in which $(\sigma_{a.u})_G$ is obtained from either of two expressions:

$$(\sigma_{a.u})_G = \sigma_F\left(\frac{A_{tr}}{A}\right)R_{II}$$

$$(14.2.31)$$

119

or

$$(\sigma_{a,u})_G = -\sigma_{Ys}\left(\frac{A_{tr}}{A}\right)R_{GH}$$

Effect of Initial Eccentricity

If there is no lateral load the initial eccentricity Δ becomes the crucial factor in determining which mode of collapse occurs. The load eccentricity Δ_p which is induced by the shift of the neutral axis at plate failure is always positive: that is. it is always such as to encourage a Mode II collapse. Therefore if the initial geometric eccentricity Δ is positive, then the theory necessarily predicts a Mode II collapse because both of the eccentricities, Δ and Δ_p, are positive. Of course there are other possible factors. such as stiffener imperfections and eccentricity of applied load, which can override this tendency and cause a Mode I collapse. But it is a fact that panels which have a positive initial eccentricity and are subjected to a purely in-plane load usually collapse in Mode II. The converse is not true; that is, a panel with a purely axial load and with a small or moderate negative initial eccentricity may collapse in either Mode I or Mode II. This is because

Figure 14.8 Effect of initial eccentricity.

the induced load eccentricity Δ_p is always positive, and hence it may eclipse a negative value of Δ.

Also, a negative initial eccentricity can give an apparent strengthening against a Mode II collapse. A negative deflection relieves the plate of some compression, and therefore a small or moderate negative initial eccentricity (not large enough to cause a Mode I collapse) may delay plate failure and hence give a small but measurable increase in the Mode II collapse strength.

This strengthening effect is not restricted to the case of pure in-plane loading. For any lateral load it will occur whenever Δ is of opposite sign to δ_0, whether positive or negative. However, the effect is significant only for small lateral loads, when δ_0 is of the same order of magnitude as Δ. In this case η is very small since it is proportional to the sum of these two eccentricities. The effect which this has on the collapse curves is shown in Fig. 14.8. exaggerated for clarity. Some examples of this effect in actual panels are presented in Section 14.4.

14.3 ULTIMATE STRAIN OF STIFFENED PANELS

As mentioned earlier, in overall structural collapse due to hull girder bending the loading condition on each plate panel is actually a uniform applied strain. ε_a. rather than a uniform applied stress. and it is more correct to express plate collapse in terms of the value of strain in the plate when it collapses, $\varepsilon_{a,u}$. The same is true for the stiffener-plate combination and so it is necessary to have an expression for $\varepsilon_{a,u}$ for this type of member. The expression depends on the degree of yielding in the cross section. which in turn depends on the collapse mode. For Mode I the cross section is still elastic and so the ultimate strain is

$$\epsilon_{a,u} = \frac{\sigma_{a,u}}{E} \qquad (14.3.1)$$

with $\sigma_{a,u}$ given by (14.2.6).

For Mode II the stiffener is again elastic since the upper end of the Mode II range is stiffener tensile yield. The plating is inelastic but it has been replaced by a pseudoelastic plate. having an effective elastic modulus E_r. Thus the stiffener and the plate are like two parallel elastic rods for which the axial stiffnesses are EA_s/L and E_rA_p/L. Since they are in parallel and must have the same axial shortening, the total stiffness
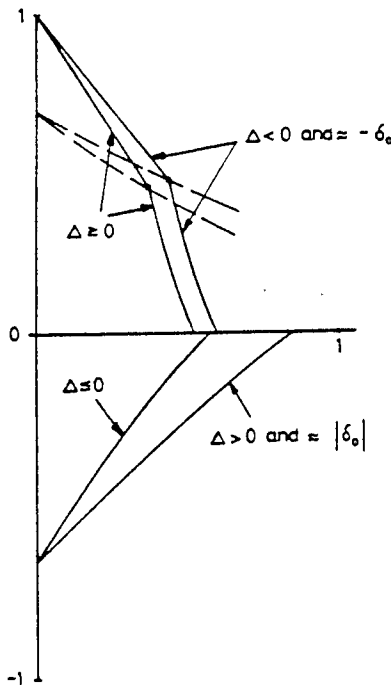
120

is the sum of the individual stiffnesses. Expressing the total stiffness in terms of the total area $A = A_p + A_s$ and a mean value of secant modulus $\bar{E}_s$ gives

$$\frac{\bar{E}_s A}{L} = \frac{EA_s}{L} + \frac{E_S A_p}{L}$$

and by noting that $A_{tr} = A_s + TA_p$ we have

$$\bar{E}_s = \frac{A_{tr}}{A} E \qquad (14.3.2)$$

The ultimate strain is then

$$\varepsilon_{a,u} = \frac{A}{A_{tr}} \frac{\sigma_{a,u}}{E} \qquad (14.3.3)$$

in which $\sigma_{a,u}$ comes from the procedure given at the end of the discussion of Mode II collapse, during which A_{tr} is also evaluated.

For Mode III the degree of yielding in the stiffener is not known precisely and the safest and easiest course is to regard the stiffener as being fully yielded, with an effective tangent modulus of zero. The mean value of secant modulus for the panel is then

$$\bar{E}_s = \frac{A_p}{A} E_s \qquad (14.3.4)$$

and the ultimate strain is

$$\varepsilon_{a,u} = \frac{A}{A_{p,\sigma}} \frac{\sigma_{a,u}}{E} \qquad (14.3.5)$$

14.4 COMPARISON OF THEORY AND EXPERIMENT

Single Span Panels

In order to verify the beam column approach presented in the previous sections, we now compare the collapse loads predicted by this method with the measured collapse loads of a series of fifteen panels which were tested to destruction under various combinations of lateral and in-plane load by Michelutti and Murray at Monash University in Melbourne [2,3,4]. The experimental setup is shown in Fig. 14.9. The bending moment was provided by two point loads W applied to
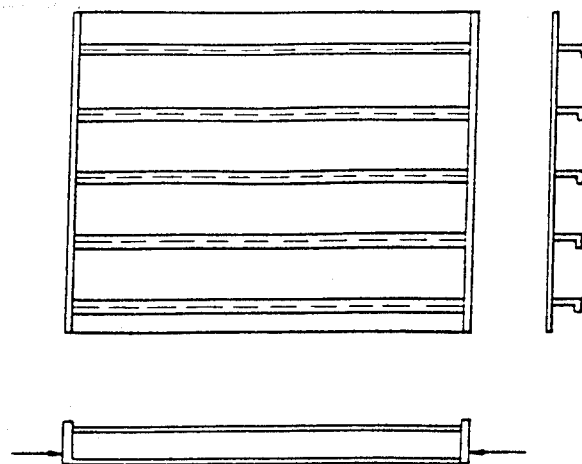
(a) Panel Geometry
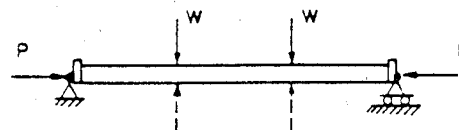
(b) Loading

Figure 14.9 Experimental setup of Monash tests.

each stiffener at the $a/3$ positions, giving a bending moment $M_0 = Wa/3$ which is constant over the middle one-third of the panel. For this load the maximum deflection is

$$\delta_0 = \frac{23Wa^3}{648EI} \qquad (14.4.1)$$

Also the plastic hinge load W_P is related to M_P by

$$M_P = \frac{W_P a}{3} \qquad (14.4.2)$$

Thirteen of the panels were of the same (nominal) overall dimensions, namely:

$a = 3.20$ m, $\qquad B = 2.44$ m, $\qquad b = 0.533$ m,

$h_w = 0.152$ m, $\qquad t_p = 9.7 \pm 0.3$ mm,

$t_w = 7.3 \pm 0.2$ mm

121

One panel (panel A4 in the terminology of Ref. 2) was slightly shorter ($a = 3.05$ m) but was geometrically similar to the others. Only one panel (panel A6) had any significant difference in geometry; panel A6 was 54% longer, having $a = 4.93$ m.

The principal difference among the panels was in regard to yield stress. Within each panel the stiffeners and plating had different yield stresses, and the ratio varied from panel to panel. In nine panels σ_{Ys} exceeded σ_{Yp}, the three largest ratios being 1.25 (panel Q) and 1.19 (panels A5 and N) and in six panels σ_{Ys} was less than σ_{Yp}, the two smallest ratios being 0.86 (panel L) and 0.91 (panel A3). Details are given in Table 14.1, including the value of initial eccentricity Δ/a and the values of various parameters. The table gives the experimental collapse loads and the corresponding normalized values $\sigma_{a.u}/\overline{\sigma}_Y$ and W_{ult}/W_P. This is followed by the theoretical normalized values obtained from the theory of the preceding sections.

Although fourteen of the panels were virtually identical in geometry, the variation in the ratio of yield stress means that each panel has a different collapse curve. For each panel the complete curve was calculated using the particular values of plate and stiffener thickness and of initial eccentricity of that panel, in order to make the comparison of theory and experiment more precise. Some examples are shown in Fig. 14.10. These have been chosen to cover the full range

of collapse load combinations and to illustrate the variety among the curves. For clarity most of the curves are not plotted in full but only in the vicinity of the experimental collapse load for that panel.

Panel Q is one of the panels with a large value of σ_{Ys}/σ_{Yp} and hence its Mode III curve is higher. Panels A2, H, and Z are typical of most of the panels, with a yield stress ratio close to unity. Panels H and A6 were subjected to pure in-plane compression and they collapsed due to plate failure (Mode II). The behavior of stiffened panels that are subjected to a purely axial load is an important aspect of stiffened panel response and merits some discussion. Therefore we shall use these two panels as examples to illustrate and explain this behavior.

When the loading is pure in-plane compression the initial eccentricity has a strong influence on whether collapse occurs in Mode I or Mode II. Also, as discussed in the previous section, a negative initial eccentricity can give an apparent strengthening against a Mode II collapse. This phenomenon occurred in panel H. Unfortunately, neither the direction nor the magnitude of the initial eccentricity were recorded for panel H. However, it appears clear from the test results that the initial eccentricity was negative because the measured values of lateral deflection are negative at all stages of the loading, until just before collapse. At an applied load of $\sigma_a = 232$ MPa ($\sigma_{a.u}/\overline{\sigma}_Y =$

TABLE 14.1 COMPARISON OF THEORY AND EXPERIMENT

	Panel Characteristics						Experiment				Theory[a]		Discrepancy		Coll-apse Mode
Panel	σ_{yp}	σ_{Ys}	$\dfrac{\sigma_{Ys}}{\sigma_{Yp}}$	$\overline{\sigma}_Y$	a/Δ	$\lambda_{I,II,GH}$	$\sigma_{a.u}$	W_{ult}	$\dfrac{\sigma_{a.u}}{\overline{\sigma}_Y}$	$\dfrac{W_{ult}}{W_P}$	$\dfrac{\sigma_{a.u}}{\overline{\sigma}_Y}$	$\dfrac{W_{ult}}{W_P}$	Value	%	
L	315	270	0.86	305	−3150	0.79 (I)	0	−39.0	0	−0.89	0	−0.72	0.17	19.1	I
L1	396	379	0.96	391	1600	0.94 (I)	0	−39.6	0	−0.71	0	−0.71	0	0	I
Y	363	378	1.04	367	1580	0.94 (I)	62	−29.8	0.17	−0.65	0.15	−0.58	0.08	11.9	I
Z	367	370	1.01	368	6300	0.93 (I)	123	−14.6	0.33	−0.31	0.31	−0.30	0.02	4.4	I
N	332	396	1.19	346	930	0.97 (I)	184	−9.0	0.53	−0.19	0.51	−0.18	0.02	3.5	I
J	370	381	1.03	374	−1200[b]	0.95 (I)	235	0	0.63	0	0.64	0	0.01	1.6	I
H	378	389	1.03	381	not given	0.80 (II)	253	0	0.66	0	0.59	0	0.07	10.6	II
A6[c]	368	383	1.04	372	530	1.21[c] (II)	153	0	0.41	0	0.39	0	0.02	4.9	II
Q	318	397	1.25	335	890	0.75 (II)	172	11.1	0.51	0.24	0.51	0.24	0	0	II
A5	324	385	1.19	338	970	0.75 (II)	170	22.8	0.50	0.49	0.46	0.45	0.06	8.6	II
A4	372	361	0.97	369	1330	0.76 (II)	154	36.4	0.42	0.65	0.38	0.59	0.07	9.6	II
A3	370	338	0.91	363	1150	0.82 (GH)	139	37.0	0.38	0.69	0.33	0.59	0.12	15.2	III
A2	383	354	0.92	378	1050	0.84 (GH)	139	38.4	0.37	0.71	0.31	0.60	0.12	15.1	III
A1	378	371	0.98	376	1400	0.85 (GH)	93	42.0	0.25	0.79	0.24	0.74	0.05	6.1	III
P	324	369	1.14	334	800	0.88 (GH)	0	46.8	0	1.02	0	1.00	0.02	2.0	III

[a]All theoretical results are for $a/\Delta = \pm750$ (− for Mode I; + for Modes II and III).
[b]In this panel the eccentricity was in the axial load, and was equivalent to $\Delta = -a/1200$.
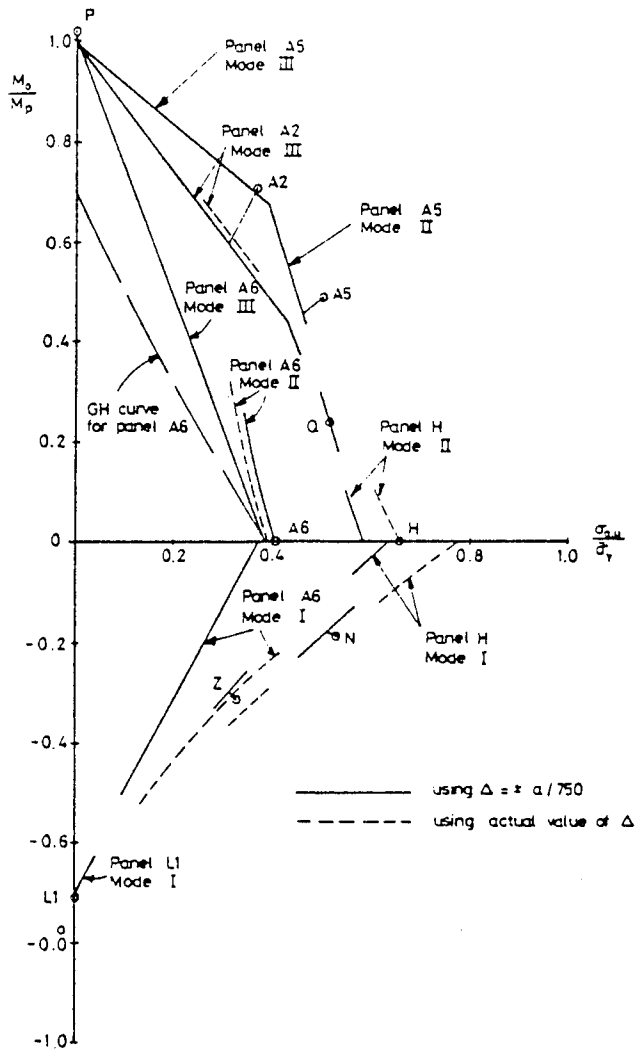[c]Long panel ($a = 4.93$ m); therefore λ is large.

Figure 14.10 Comparison of theory and experiment for sample panels.

(with a small negative value of Δ, both equations have solutions). The resulting values of $\sigma_{a.u}/\overline{\sigma}_Y$ were 0.77 and 0.67 for Modes I and II, as shown in Fig. 14.10. Thus when the negative initial eccentricity which appears to have been present is represented by a typical value, the theory correctly predicts that Mode II is the collapse mode, and the predicted value agrees closely with the experimental value of 0.66. For comparison. Fig. 14.10 also shows the collapse curves corresponding to the standard design values of initial eccentricity ($-a/750$ for Mode I and $+a/750$ for Mode II). These are the curves which would in practice be taken as the predicted capability of the panel. Since they are design curves they must always give a predicted collapse load which is less than the actual collapse load for any panel whose initial eccentricity is within the permissible range: $-a/750 < \Delta < a/750$. At the same time they should not be excessively conservative. As shown in the figure, the curves for panel H fulfill both of these requirements.

Panel A6 is the long panel and consequently it has a much larger slenderness parameter: $\lambda_I = 1.46$ and $\lambda_{II} = 1.21$, compared to typical values of 0.95 and 0.75 for the other panels. This causes a substantial decrease in ultimate strength in both modes. In fact, the stiffener tensile yield curve for panel A6 (the curve GH in Fig. 14.10) is so close to the origin that it does not intersect the Mode II curve, and the Mode III collapse curve is a straight line from the point $M_0/M_P = 1$ to the point where the GH curve crosses the horizontal axis. As noted earlier, this is conservative because in such cases the collapse load combinations would follow the Mode II collapse curve upward for some distance (i.e., up to moderate values of M_0). But the conservativism is not excessive and it emphasizes the fact that such a panel does have generally low values of nondimensional collapse loads.

Panel A6 also provides another illustration of the crucial influence which the initial eccentricity has when there is no lateral load. For this panel, when the standard design value of $-a/750$ is assumed for Mode I and $+a/750$ for Mode II, the two values of $\sigma_{a.u}/\sigma_Y$ are 0.376 and 0.405 respectively, as shown in the figure. Thus if we were considering this panel in an objective design context, in which both positive and negative eccentricity must be allowed for, the panel could be said to be weaker in Mode I than in Mode II. But in this specific case the panel had a relatively large positive initial eccentricity ($+a/530$) and therefore Mode I collapse could not and did not occur. For a Mode I collapse to occur, Δ would have to be negative (and sufficiently negative to overcome the induced

$232/381 = 0.61$) the plating began to fail and the panel immediately deflected in the positive direction (i.e., toward the stiffeners). On further increase of load, the positive deflection grew rapidly and a Mode II collapse occurred soon after, at $\sigma_{a.u}/\overline{\sigma}_Y = 0.66$. With a positive eccentricity (e.g., the standard design value of $+a/750$) the beam column theory for Mode II, as outlined previously, gives a collapse load ratio of 0.59. Therefore it appears that the panel had a negative initial eccentricity which artificially strengthened it. Obviously, one must ignore such strengthening when designing, but in comparing theory and experiment it is important to model the actual situation as closely as possible. Therefore a small negative initial eccentricity ($-a/2000$) was assumed and the theoretical collapse loads were calculated for Mode I and Mode II

123

eccentricity effect). When the measured value of $+a/530$ is used for the Mode II calculation. the predicted collapse strength is 0.390, which agrees well with the experimental result: the panel in fact underwent a Mode II collapse at an applied load ratio of 0.41.

Since the tests covered a full range of load combinations, including purely lateral loads and purely inplane loads, the discrepancy between theory and experiment is best measured along a radial line from the origin as shown for panels A2. A5, N, and Z in Fig. 14.10. The relative error is then obtained by dividing this radial discrepancy by the length along the radial line from the origin to the experimental collapse point. This has been done for all fifteen cases and the results are given in Table 14.1. Also, to give a clearer overall comparison, Fig. 14.11 contains all of the radial discrepancies plotted in their correct positions relative to a single typical collapse curve. The calculations were performed using the standard design values of initial eccentricity, $\pm a/750$. The results indicate that the beam column equations presented in the previous sections are of satisfactory accuracy, and that the value of $\pm a/750$ for the initial eccentricity is suitable for design. In all panels except A6 (the long panel) the design value of eccentricity exceeded the actual value (see Table 14.1). The design value of $\pm a/750$ is a maximum permissible value; panels with larger eccentricity would either be forbidden by the fabrication specifications or would be designed as curved panels. For all panels in which the initial eccentricity was within these permissible limits the actual value of ultimate strength was never less than the design value, and the design value was never excessively conservative. Moreover, even in panel A6, in which the initial eccentricity was slightly over the permissible value, the collapse load was still slightly above the design value. These results demonstrate that the beam column approach is well suited for the design of stiffened panels, since it gives an accurate estimate of strength for all load combinations and for any typical amount of initial eccentricity.
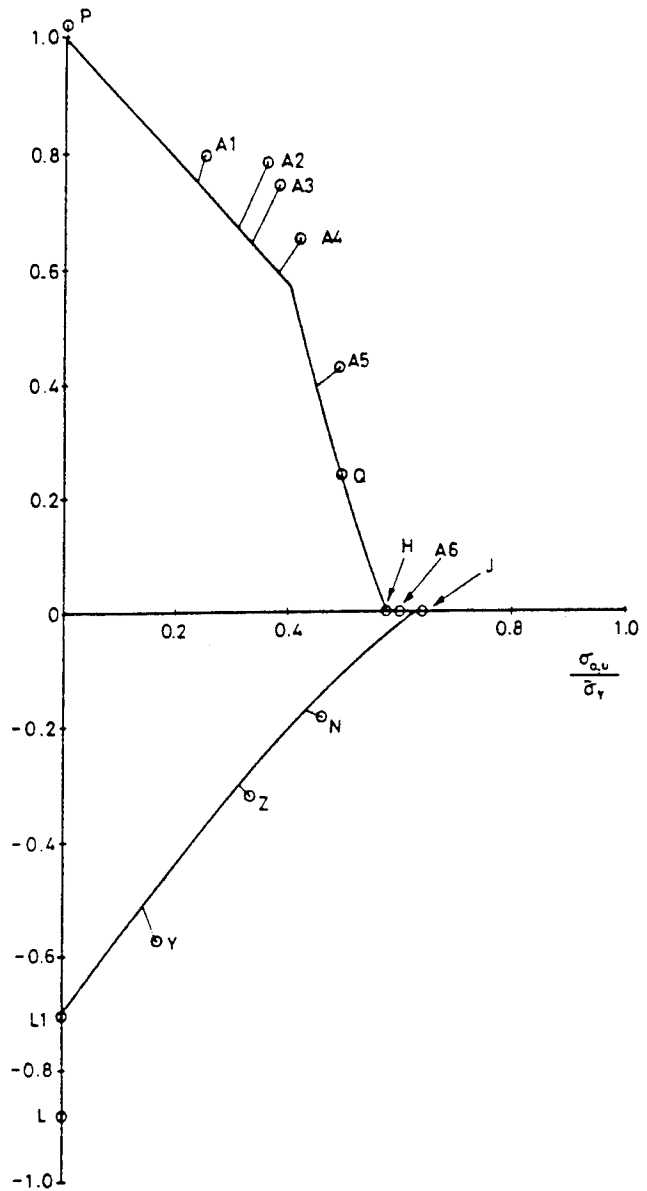
Figure 14.11 Composite plot of results.

Multispan Panels Without Lateral Load

To demonstrate the validity of the method for multispan panels we next compare its predicted values of $\sigma_{a,u}$ and $\varepsilon_{a,u}$ with the measured values obtained by Dowling et al. [5] in a test of a 3.9-m long box girder subjected to a sagging bending moment (model no. 2 in the terminology of Ref. 5). The cross section is shown in Fig. 14.12. The upper flange (the "strength
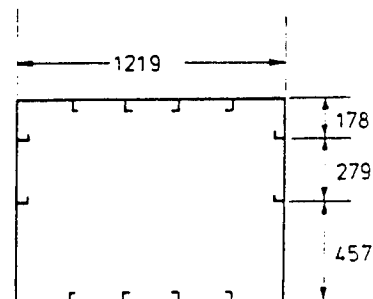

Figure 14.12 Box girder model section.

124

deck") consisted of five in-line panels 787 mm in length. The panels were typical in all respects to ship panels; details are given in the figure and in Table 14.2. From Ref. 5, in the bay where the collapse occurred the conditions before loading were:

maximum initial deflection of stiffeners:

upward (towards plating)

$$\Delta = -0.010 \text{ in.} = -0.25 \text{ mm} \quad (a/3100)$$

downward (towards stiffener)

$$\Delta = 0.055 \text{ in.} = 1.40 \text{ mm} \quad (a/563)$$

average longitudinal residual stress:

$$\sigma_r = 0.18 \, \sigma_Y$$

Since there is no lateral load, both Mode I and Mode II collapse must be investigated. In order to provide a worked example of the method some details of the calculation will be given.

Mode I collapse

Beam-column parameters:

from (8.3.6): $C_1 = 0.083$, $I = 326700 \text{ mm}^4$,

$$\rho = 14.65 \text{ mm}$$

$$C_2 = 0.8775, \, y_f = -44.6 \text{ mm}$$

from (14.2.3): $\lambda = 0.623$, $\eta = 0.052$

from (14.2.5): $R = 0.925$

and hence the value of $\sigma_{a,u}$ for a Mode I collapse is $0.925\sigma_{Ys} = 255.8 \text{ N/mm}^2$. From (14.3.1) the value of $\varepsilon_{a,u}$ is 1.226×10^{-3}.

Mode II collapse

Plate slenderness: $\beta = 1.89$

from (14.2.8): $T = 0.825$,

TABLE 14.2 PROPERTIES OF BOX GIRDER MODEL

Component	Dimensions (mm)	σ_Y (N/mm²)	E (N/mm²)
Compression flange	4.88	298.0	208,500
Tension flange	4.88	298.0	208,500
Web	3.38	211.6	216,200
Stiffeners	50.8 × 15.9 × 4.8L	276.5	191,500

$$\sigma_F = \frac{T - 0.1}{T} \sigma_{Yp} = 262 \text{ N/mm}^2$$

from (8.3.6): $C_1 = .096$, $I_{tr} = 352000 \text{ mm}^4$,

$$\rho = 15.73 \text{ mm}$$

$$C_2 = 0.854, \, y_{p,tr} = 7.41 \text{ mm}$$

from (14.2.18):
$$\Delta_p = hA_s\left(\frac{1}{A_{tr}} - \frac{1}{A}\right)$$

$$= (29.5)297\left(\frac{1}{1279} - \frac{1}{1487}\right)$$

$$= 0.958 \text{ mm}$$

from (14.2.21):
$$\Delta_H = \frac{I/A}{H} = \frac{\rho^2}{H} = \frac{(15.73)^2}{457 - 8}$$

$$= 0.55 \text{ mm}$$

from (14.2.16): $\lambda = 0.63$, $\eta = 0.060$

from (14.2.19): $\eta_p = .0287$

from (14.2.20): $R_{II} = 0.899$

from (14.2.22): $\sigma_{a,u} = 202.3 \text{ N/mm}^2$

and from (14.3.3): $\varepsilon_{a,u} = 1.128 \times 10^{-3}$

Since the Mode I value of $\sigma_{a,u}$ was larger than this Mode II value the latter is selected as the predicted value of ultimate strength.

As shown in Fig. 14.13 this predicted result is in quite good agreement with the experimental results:
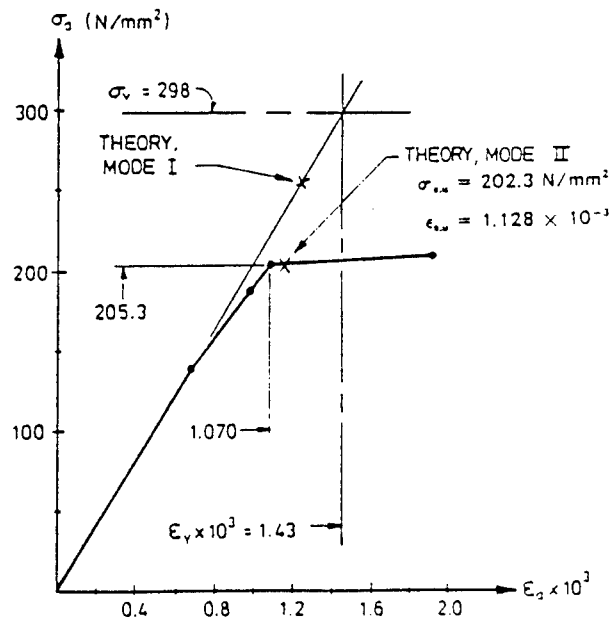

Figure 14.13 Collapse of upper flange of box girder model.

125

Mode II collapse at an average applied stress of 205.3 N/mm^2 and a strain of 1.070×10^{-3}.

It should be noted that the selection of the predicted mode of collapse must be based on $\sigma_{a.u}$ and not on $\varepsilon_{a.u}$. A smaller value of $\varepsilon_{a.u}$ for Mode I does not mean that Mode I collapse would occur first, because the Mode II collapse actually begins much earlier, when the plate begins to fail, and from this point onward the beam-column undergoes ever-increasing positive bending, opposite to that of Mode I. Thus a Mode I collapse can only occur if the value of $(\sigma_{a.u})_I$ is smaller than the load which initiates plate failure. Hence we are being conservative in saying that a Mode I collapse only requires that $(\sigma_{a.u})_I$ be less than $(\sigma_{a.u})_{II}$, and then taking this smaller value to be the ultimate strength of the panel. But as mentioned earlier, whenever the lateral load is small or is absent the occurrence of Mode I or Mode II depends not only on the properties and proportions of the panel but also on the particular circumstances and details such as initial deflections, load sequence, and residual stress, which cannot be known or predicted by the designer. Hence the designer must always be conservative and assume the worst, which means choosing whichever mode gives the lower value of strength.

Multispan Panels With Lateral Load

We next compare the method's predictions with the results of tests by Smith [6] on multispan panels subjected to a uniform lateral pressure in addition to axial compression. In comparing theory and experiment it is necessary to have full information about the initial conditions (residual stress, preload deflections, and the values of δ_0 and M_0 due to the lateral load) for the particular stiffener-plate combination which triggered the collapse. Of the 11 panels tested in Ref. 6 panels 3a and 3b are chose for the comparison because for these panels all of the required information was recorded and presented. Also these two panels provide valuable information about the effect of lateral pressure because they were a matching pair and one of them (3a) had a lateral pressure of 3 psi whereas the other had no lateral load.

PANEL 3a

This panel was subjected to a constant lateral pressure of 3 psi. The panel collapsed when the applied axial stress reached $0.69\,\overline{\sigma}_Y$, where $\overline{\sigma}_Y$ is the mean value of

yield stress of the stiffeners and plating, averaged over the panel cross section.

This case is worth examining in some detail, especially in regard to the causal sequence of failures, because it provides an example of how a laterally loaded multispan panel, in spite of the rotational restraint at the ends of each span, can undergo the same type of collapse as a laterally loaded pinned panel.

As shown in Fig. 14.14 the collapse involved upward flexural buckling in one of the central bays and downward bucking of an adjacent bay, together with a stiffener flange mechanism of the type shown in Fig. 14.4, close to the central transverse frame. All three failures occurred more or less simultaneously, and to determine the precise interactions and the causal relationships we must examine the state of loading just prior to failure. Figure 14.15 illustrates the bending moment distribution in the stiffeners due to the lateral pressure. This was not given in Ref. 6 but was calculated by the author by a nonlinear finite element analysis of the gross panel. The total compressive stress in the stiffener flange is a maximum at the midlength of the gross panel, because of the peak value of bending moment there. The finite element analysis showed that when the applied axial stress reached the experimental collapse value the total stress in the stiffener flange at the midlength had just slightly exceeded the yield stress of the stiffener. At this time yield had not occurred anywhere else and all of the panels were still stable. This shows clearly that it was the stiffener

Figure 14.14 Panel 3a after collapse. (Photo courtesy of Admiralty Marine Technology Establishment, Dunfermline, Scotland).
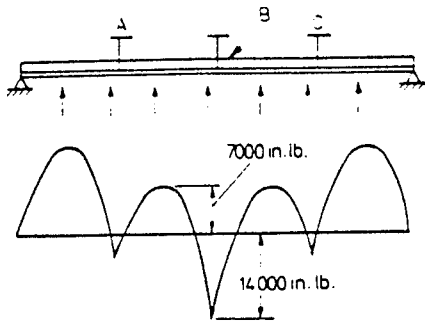
Figure 14.15 Bending moment in panel 3a.

flange mechanism which triggered the collapse, and also provides the explanation as to why the panels buckled at the same time as the formation of the stiffener flange mechanism. Such a mechanism is virtually the same as a hinge (an ordinary hinge, not a plastic hinge) because the flange has lost nearly all of its axial stiffness. Therefore the stiffeners rotated about this point and transferred the bending moment into the spans. The new bending moment in each span is approximately that for a beam which is pinned at one end and clamped at the other, with a midspan value of $pba^2/12$. The increased bending stress in the plating was sufficient to cause a Mode II collapse of span AB, and so this span collapsed immediately after the flange mechanism had occurred, with no further increase in axial load. Since the transverse frame provides very little rotational restraint and also permits at least a small lateral deflection, it is the hinge rather than the frame which constitutes the endpoint of the two beam-columns, and since AB is longer than BC the Mode II collapse occurred in the former.

This case demonstrates that in spite of the rotational restraint which exists at the ends of each span in a laterally loaded multispan panel, collapse can still occur in a manner very similar to that of a panel with pinned ends. Therefore the pinned beam-column approach, with allowance for the values of M_0 and δ_0 which exist within the span, is directly relevant to such panels.

In the rationally-based design process of Fig. 2.19, the hull module analysis, member limit analysis and constraint evaluation of the panels (steps 3, 4, and 5) will indicate if a stiffener flange mechanism can occur, and if so the use of any reasonable estimates of the post-mechanism values of M_0 and δ_0 will give a good estimate of $\sigma_{a.u}$. For example, using the approximate post-mechanism values of $pba^2/12$ for M_0 and $\frac{1}{2}(5pba^4)/384EI$ (half of the simply supported value) for δ_0, together with a typical design value of $a/750$

for Δ, gives a value of $0.658\overline{\sigma}_Y$ for $\sigma_{a.u}$, which differs from the actual value by only 5%, and on the conservative side.

The actual measured value of Δ for the span where the collapse occurred was $\Delta = 0.03$ in. ($a/2000$) and when this value is used the predicted value of $\sigma_{a.u}$ is $0.69\overline{\sigma}_Y$, the same as the experimental value.

PANEL 3b

A second panel which was virtually identical to panel 3a collapsed at an applied stress of $\sigma_{a.u} = 0.61\overline{\sigma}_Y$. Fig. 14.16 shows the panel after collapse. Since there is no lateral load, a Mode II collapse would also have been possible and one of the requirements of any method for estimating ultimate strength is that it should correctly identify the critical mode, that is, the mode with the lower value of $\sigma_{a.u}$. For this panel the initial deflection of the collapsed span was approximately 0.15 in. toward the plating ($\Delta = -a/400$). With the method presented herein the predicted values of $\sigma_{a.u}$ for Modes I and II are $0.57\overline{\sigma}_Y$ and $0.69\overline{\sigma}_Y$.[*] Thus the method correctly identifies the collapse mode and predicts a value for $\sigma_{a.u}$ which differs from the experimental value by only 7% on the conservative side. This 7% margin comes mainly from the conservative assumption that a stiffener flange mechanism forms as soon as the stress in the midthickness of the stiffener flange reaches yield, whereas in reality it forms only after the flange is fully yielded.
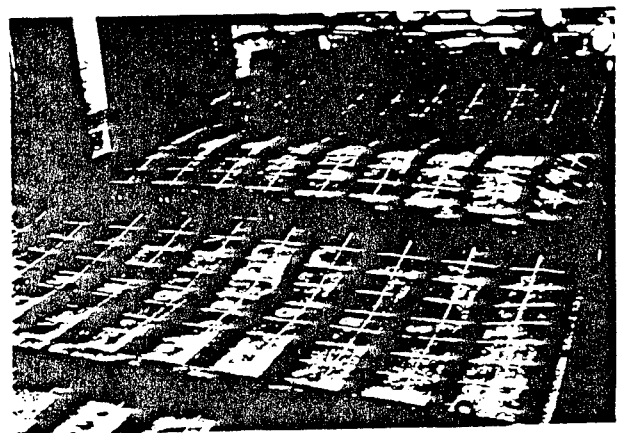

Figure 14.16 Panel 3b after collapse. (Photo courtesy of Admiralty Marine Technology Establishment, Dunfermline, Scotland).

[*] The latter is obtained using the largest positive value of Δ, which was 0.22 in. ($a/270$).

In the previous multispan examples the collapse has been Mode II, and hence this example demonstrates the accuracy of the method for a Mode I collapse of a multispan panel.

CONCLUSIONS

The analysis of panel 3b shows that when a multispan panel has no lateral load the ultimate strength is basically that of a simply supported subpanel. For reference purposes we shall denote this value as $(\sigma_{a,u})_0$. It is always the lesser of two values: either the Mode I value from (14.2.6) or the Mode II value from (14.2.22). If the lateral load is above a certain magnitude, each subpanel is effectively clamped and if this remains true then the ultimate strength is larger than for a simply supported panel. For panels 3a and 3b the increase was from $0.61\bar{\sigma}_Y$ to $0.69\bar{\sigma}_Y$, or 13%. But it is extremely difficult to predict the magnitude of lateral load that is required to constrain all subpanels to behave as clamped, first, because the behavior of each subpanel is strongly influenced by local factors (eccentricity, residual stress, nonuniformity of lateral load, etc.) and, second, because each subpanel interacts with its neighbors. Moreover, although the lateral load may be sufficient to keep each subpanel rotationally restrained for a time, such that the value of σ_a can exceed $(\sigma_{a,u})_0$, there is always the possibility of a stiffener flange mechanism, whereupon two or more of the subpanels suddenly change to the alternating wave shape and immediately undergo collapse, because σ_a already exceeds $(\sigma_{a,u})_0$. We thus have four factors to consider:

1. The possibility that the lateral load may become small.

2. The difficulty of calculating the magnitude of the lateral load which would guarantee end clamping.

3. The possibility of a stiffener flange mechanism, which becomes more likely with increasing lateral load.

4. The undesirability of sudden collapse.

For all of these reasons, any value of ultimate strength larger than $(\sigma_{a,u})_0$ should not be used for design purposes, even though larger values may in fact be achieved when there is a lateral load. That is, $(\sigma_{a,u})_0$ is an upper limit or "cutoff" value. In a rationally-based design process it is necessary to calculate $\sigma_{a,u}$ for each load case. For the various load cases involving a lateral load it would be possible to calculate accurate values

of $\sigma_{a,u}$ by using the information from steps 3, 4, and 5 of the overall design procedure, as discussed previously. But for design purposes this is not necessary because these values will nearly always exceed the cutoff value, $(\sigma_{a,u})_0$. Hence for design purposes it is sufficient to use the simple and conservative pinned beam-column approach, with M_0 and δ_0 equal to their simply supported values, for estimating the values of $\sigma_{a,u}$ for the various load cases involving a lateral load. Although the true ultimate strength would be larger than this value it would usually be ruled out because it exceeded $(\sigma_{a,u})_0$. Therefore the value obtained by the pinned beam-column approach will not be unduly conservative. For example, for the load case involving lateral pressure (panel 3a) the use of the simply supported values of M_0 and δ_0 and a typical value of Δ $(a/750)$ gives a value of $0.56\bar{\sigma}_Y$. For this load case the true ultimate strength is $0.69\bar{\sigma}_Y$, but this cannot be used for design purposes because it exceeds the value for zero lateral load, $(\sigma_{a,u})_0 = 0.61\bar{\sigma}_Y$. Hence, taking $0.56\bar{\sigma}_Y$ as the ultimate strength for the laterally loaded case is not overly conservative since it is only 8% below the experimentally obtained value of $(\sigma_{a,u})_0$.

REFERENCES

1. C. S. Smith, "Influence of Local Compressive Failure on Ultimate Longitudinal Strength of a Ship's Hull," Proc. Int'l. Symp. on Practical Design in Shipbuilding (PRADS), Tokyo, October 1977.

2. N. W. Murray, "Analysis and Design of Stiffened Plates for Collapse Load," Struct. Eng., 53 (3), March 1975, pp. 153–158.

3. W. M. Michelutti, Stiffened Plates in Combined Loading, Ph.D. thesis, Dept. of Civil Engineering, Monash University, Melbourne, 1976.

4. W. M. Michelutti and N. W. Murray, "The Collapse Behaviour of Stiffened Plates under Combined Axial and Bending Loads," 6th Australasian Conference on the Mechanics of Structures and Materials, Univ. of Canterbury, Christchurch, N. Z., 1977.

5. P. J. Dowling, S. Chatterjee, P. A. Frieze, and F. M. Moolani, "The Experimental and Predicted Collapse Behaviour of Rectangular Stiffened Steel Box Girders," Int'l. Conference on Steel Box Girder Bridges, Institute of Civil Engineers, London, 1973.

6. C. S. Smith, "Compressive Strength of Welded Steel Ship Grillages," Trans. RINA, 117, 1975, pp. 325–359.

Project Technical Committee Members

The following persons were members of the committee that represented the Ship Structure Committee to the Contractor as resident subject matter experts. As such they performed technical review of the initial proposals to select the contractor, advised the contractor in cognizant matters pertaining to the contract of which the agencies were aware, and performed technical review of the work in progress and edited the final report.

Mr. Rickard Anderson–Chairman Military Sealift Command

Mr. Stephen Yang	Directorate Naval Architecture and Specialty Engineering– Canada
Mr. Natale Nappi	Naval Sea Systems Command
Mr. Robert Sedat	U. S. Coast Guard
Dr. Paul H. Wirshing	University of Arizona
Mr. William Siekierka	Naval Sea Systems Command, Contracting Officer's Technical Representative
Mr. Alex Stavovy Dr. Robert Sielski	National Academy of Science, Marine Board Liaison
CDR Mike Parmelee CDR Steve Sharpe	U.S. Coast Guard, Executive Director Ship Structure Committee

SHIP STRUCTURE COMMITTEE PUBLICATIONS

SSC–356　Fatigue Performance Under Multiaxial Load by Karl A. Stambaugh, Paul R. Van Mater, Jr., and William H. Munse　1990

SSC–357　Carbon Equivalence and Weldability of Microalloyed Steels by C. D. Lundin, T. P. S. Gill, C. Y. P. Qiao, Y. Wang, and K. K. Kang　1990

SSC–358　Structural Behavior After Fatigue by Brian N. Leis　1987

SSC–359　Hydrodynamic Hull Damping (Phase I) by V. Ankudinov　1987

SSC–360　Use of Fiber Reinforced Plastic in Marine Structures by Eric Greene 1990

SSC–361　Hull Strapping of Ships by Nedret S. Basar and Roderick B. Hulla　1990

SSC–362　Shipboard Wave Height Sensor by R. Atwater　1990

SSC–363　Uncertainties in Stress Analysis on Marine Structures by E. Nikolaidis and P. Kaplan　1991

SSC–364　Inelastic Deformation of Plate Panels by Eric Jennings, Kim Grubbs, Charles Zanis, and Louis Raymond　1991

SSC–365　Marine Structural Integrity Programs (MSIP) by Robert G. Bea　1992

SSC–366　Threshold Corrosion Fatigue of Welded Shipbuilding Steels by G. H. Reynolds and J. A. Todd　1992

SSC–367　Fatigue Technology Assessment and Strategies for Fatigue Avoidance in Marine Structures by C. C. Capanoglu　1993

SSC–368　Probability Based Ship Design Procedures: A Demonstration by A. Mansour, M. Lin, L. Hovem, A. Thayamballi　1993

SSC–369　Reduction of S–N Curves for Ship Structural Details by K. Stambaugh, D. Lesson, F. Lawrence, C–Y. Hou, and G. Banas　1993

SSC–370　Underwater Repair Procedures for Ship Hulls (Fatigue and Ductility of Underwater Wet Welds) by K. Grubbs and C. Zanis　1993

SSC–371　Establishment of a Uniform Format for Data Reporting of Structural Material Properties for Reliability Analysis by N. Pussegoda, L. Malik, and A. Dinovitzer　1993

SSC–372　Maintenance of Marine Structures: A State of the Art Summary by S. Hutchinson and R. Bea　1993

SSC–373　Loads and Load Combinations by A. Mansour and A. Thayamballi　1994

SSC–374　Effect of High Strength Steels on Strength Consdierations of Design and Construction Details of Ships by R. Heyburn and D. Riker　1994

None　Ship Structure Committee Publications – A Special Bibliography